KTH

DEPARTMENT OF AERONAUTICS

Fatigue Behaviour of Welded High-Strength Steels

by

Luis Lopez Martinez

Report No. 97-30

KUNGLIGA TEKNISKA HÖGSKOLAN
STOCKHOLM SWEDEN

Department of Aeronautics
The Royal Institute of Technology
SE-100 44 Stockholm
Sweden

Fatigue Behaviour of Welded High-Strength Steels

by

Luis Lopez Martinez

Report No. 97-30

Preface

The research presented in this thesis has mainly been carried out under the NordList research programme started in October 1993 and to be officially ended on December 31, 1997. Under these years I have been working as Application Research Engineer at SSAB Oxelösund AB. This work was jointly financed and supported by SSAB Oxelösund AB, Nordic Industrial Fund and NUTEK. Their support is gratefully appreciated.

I am grateful to Dr. Anders F. Blom the project leader, supervisor and friend, for his confidence in me, guidance and support during difficult moments and situations during these years. I also wish to express my sincere appreciation to Prof. Jan Bäcklund, head of the department, for accepting me as a Ph.D. Candidate. Further, my gratitude goes to all co-authors of the papers appended in this thesis.

I owe many thanks to my colleagues at the research laboratories of SSAB Oxelösund AB and all the colleagues within the Nordic project for the stimulating and friendly contacts over the years. All the people working in a number of laboratories, which have been involved in experimental work are also acknowledged.

Sincere thanks to Peter Westman, General Manager Research and Quality of SSAB Oxelösund AB, for his support under these last few very hectic years.

Stockholm, October 1997

Luis Lopez Martinez

Abstract

The present thesis is concerned with "Fatigue Behaviour of welded High-Strength Steels". This is due to the increased interest in higher pay loads in machinery such as earth moving equipment, which has focused on a more widespread use of high-strength steels. High-strength steel should allow, at least under static loading, an increase in design stresses so that the plate thickness and the weight can be reduced.

However, the design stresses are always limited by the fatigue strength of welded joints subjected to fluctuating loads. It is a well known fact that this fatigue strength is more or less independent of parent plate mechanical properties in the as-welded condition. The only remedy to this appears to be applying post weld treatment in order to increase the fatigue lives of high-strength steels.

Since almost all engineering components and structures are subjected to spectrum loading during their service live, the main challenge is to combine the benefit of the fatigue life improvement methods and these loading conditions.

These aspects are treated in detail in the appended papers. However, an extensive amount of work performed within the NordList programme and independently by SSAB Oxelösund AB is documented also in additional papers/reports not included in the thesis, see Refs. [1-14].

The research that has been carried out, may be divided into four areas, namely:

- Weld process and weld imperfections — Paper [A] and Ref. [7, 11,13]
- Residual Stresses and relaxation — Papers [B, C] and Ref. [1, 2]
- Spectrum loading of improved weldments — Papers [D] and Ref. [6, 8, 10]
- Fatigue crack growth modelling — Papers [E] and Ref. [8, 9,10]

In the following, the introduction and the appended five papers are summarised as follows.

Introduction

An overview of the major reasons for the reduced fatigue strength in welded joints is presented. These problems must be overcome, e.g. by fatigue life improvement techniques, to improve the fatigue resistance of welded joints so that high-strength steels can be used more effectively.

Paper A

Characterisation of initial defect distribution and weld geometry in welded fatigue test specimens, ***Lopez Martinez L.*** *and Korsgren P., SSAB Tunnplåt AB.*

The paper consists of two parts. The first part is a comprehensive weld defect comparison between different weld methods and different filler metals and was carried out using specially manufactured test coupons. The second part deals with the

measurements of local weld geometry parameters on fatigue test specimens. After the fatigue testing the fractured surfaces have been analysed.

Paper B

Spectrum fatigue testing and residual stress measurements on non-load carrying fillet welded test specimens. Bogren J., FFA, and ***Lopez Martinez L.***

The aim of this paper was to study the influence of various spectrum parameters on fatigue life. These parameters were irregularity factor I and stress ratio, R.. The influence of these parameters on relaxation of welding induced residual stresses during spectrum loading was also studied.

Paper C

Investigation of Residual stresses in As-Welded and TIG-Dressed specimens Subjected to Static/Spectrum Loading, ***L. Lopez Martinez****, R. Lin and D. Wang, Studsvik and A. F. Blom, FFA.*

This paper deals with residual stresses in welded fatigue test specimens. By neutron diffraction and χ-ray diffraction, residual stress distributions in as-welded and TIG-dressed specimens were non-destructively measured. In addition, the effects of both static and spectrum fatigue loading were evaluated. Results are also compared to ultrasonic 3-D measurements.

Paper D

Fatigue behaviour of Steels with Strength levels Between 350 and 900 MPa- Influence of Post Weld Treatment under Spectrum Loading, ***L. Lopez Martinez****, A. F. Blom, FFA; H. Trogen, SSAB Tunnplåt AB and T. Dahle ABB Corporate Research.*

In this paper fatigue data for a range of materials are presented, obtained both under constant amplitude loading as well as under different types of load spectra. It is shown that the use of improvement techniques on welds subjected to spectrum loading may allow an increase in admissible stresses. This increase is found to be larger for higher strength steels.

Paper E

Fracture Mechanics Modelling of FCG in Welded Joints, G.S. Wang, A. F. Blom, FFA and ***L. Lopez Martinez***

This paper addresses fracture mechanics modelling of certain chosen experimental combinations of the parameters involved in the overall fatigue behaviour under complex loading. The model accounts for local stress concentration, residual stresses distribution, residual stress relaxation, applied stress level, spectrum shape and weld-induced defect distribution.

Contents

Dissertation

The dissertation consists of the following five papers:

Paper A

L. Lopez Martinez and Korsgren P., "Characterisation of initial defect distribution and weld geometry in welded fatigue test specimens", Proceedings of the Nordic Conference on Fatigue. Edited by A.F. Blom, EMAS Publishers, West Midlands, England 1993.

Paper B

Bogren J., FFA, and **Lopez Martinez L.**, "Spectrum fatigue testing and residual stress measurements on non-load carrying fillet welded test specimens". Ibidem.

Paper C

L. Lopez Martinez, R. Lin and D. Wang, Studsvik and A. F. Blom, FFA. "Investigation of Residual Stresses in As-Welded and TIG-Dressed specimens Subjected to Static/Spectrum Loading". Proceedings of the Conference on Welded High-Strength Steel Structures, Stockholm, October 1997.

Paper D

L. Lopez Martinez, A. F. Blom, FFA; H. Trogen, SSAB Tunnplåt AB and T. Dahle ABB Corporate Research. "Fatigue behaviour of Steels with Strength Levels Between 350 and 900 MPa- Influence of Post Weld Treatment under Spectrum Loading". Ibidem.

Paper E

G.S. Wang, A. F. Blom, FFA and **L. Lopez Martinez** , "Fracture Mechanics Modelling of FCG in Welded Joints". Ibidem.

Division of Work Between Authors

Paper A

"Characterisation of initial defect distribution and weld geometry in welded fatigue test specimens" by **Lopez Martinez L.** and Korsgren P.

The paper was planned and written by L. Lopez Martinez. Experiments were performed by L. Lopez Martinez. P. Korsgren helped with evaluation of results and derived the distributions shown in Table 5.

Paper B

"Spectrum fatigue testing and residual stress measurements on non-load carrying fillet welded test specimens" by Bogren J. and **Lopez Martinez L.**

The paper was planned by L. Lopez Martinez and A. F. Blom. J. Bogren helped with the experimental programme and evaluated all fatigue data. L. Lopez Martinez performed the other experimental work and wrote the paper.

Paper C

"Investigation of Residual stresses in As-Welded and TIG-Dressed specimens Subjected to Static/Spectrum Loading" by **Lopez Martinez**, R. Lin, D. Wang and A. F. Blom.

The idea for the paper was made jointly by L. Lopez Martinez and A. F. Blom. All the planning of fatigue testing was made jointly by L. Lopez Martinez and A.F. Blom. The measurements were carried out by Dr. Lin. The plots of residual stresses were made by Dr. Wang. The fatigue testing and planning of relaxation studies were carried out by L. Lopez Martinez. The paper was written jointly by L. Lopez Martinez, R. Lin and A. F. Blom.

Paper D

"Fatigue behaviour of Steels with Strength levels Between 350 and 900 MPa- Influence of Post Weld Treatment under Spectrum Loading" by **L. Lopez Martinez**, A. F. Blom, H. Trogen and T. Dahle.

The idea for the paper was made jointly by L. Lopez Martinez and A. F. Blom. All the planning of fatigue testing was made jointly by L. Lopez Martinez and A.F. Blom. The fatigue testing was the responsibility of L. Lopez Martinez. Mr. T. Dahle has done the input of test results for evaluation. Mr. H. Trogen was responsible for constant amplitude fatigue testing. The paper was written by L. Lopez Martinez and A. F. Blom.

Paper E

"Fracture Mechanics Modelling of FCG in Welded Joints" by G.S. Wang, A. F. Blom and **L. Lopez Martinez**.

The idea for the paper was made jointly by L. Lopez Martinez and A. F. Blom. All the fracture mechanics calculations were made by Dr. Wang. The fatigue testing and residual stress measurements were the responsibility of L. Lopez Martinez. The paper was written by A. F. Blom.

References

1) Effects of residual stress fields on the brittle fracture of high strength structural steels. Lopez Martinez L., Pereira M. V. University of Kassel, Wohlfarhrt, Technical University of Braunschweig. Int. Conference on Materials Development in Rail, Tire Wing, Hull Transportation 22-24 Sept. 1992. Associazione Italiana di Metalurgia, Milano, Italy.

2) The influence of various spectrum parameters on fatigue life and residual stress relaxation. Lopez Martinez L., SSAB Oxelösund AB and Bogren J., FFA, MAT-TEC 92. Fracture and Fatigue, Ed. L. Castex, G. Pluvinage, L. Vincent. IITT-international Technology Transfer Series, ISBN 2-907669-24-9.

3) Fatigue life of high strength steel plate elements with welded attachments, Petersen R.I., Agerskov H., Askegaard V. and Lopez Martinez L. Proceedings of the Nordic Conference on Fatigue. Edited by A.F. Blom, EMAS Publishers, West Midlands, England 1993.

4) Fatigue life of high strength steel tubular joints. Lopez Martinez L., Petersen R.I., DTH and Agerskov H., DTH, Ibìdem.

5) SN-curves for low cycle region in high strength steels, Lopez Martinez L. Proceedings of Fatigue Design 95. Helsingfors Sept. 1995.

6) Influence of life Improvement Techniques on different steel grades under spectrum loading. Lopez Martinez L. and Blom A., FFA, Ibìdem.

7) The influence of welding parameters on the size and distribution of weld defects for various weld methods. Hedegård J. KTH, Lopez Martinez L, Morasdaskafti N., KTH, and Trogen H. SSAB Tunnplåt AB, Ibìdem.

8) Fatigue behaviour of TIG improved welds, Lopez Martinez L., Blom A. and G. S. Wang, FFA, FATIGUE 96, Berlin 6-10 May 1996.

9) Spectrum Fatigue of Improved Welded joints- Modelling and Experiments, Lopez Martinez L., G. S. Wang and Blom A. FFA, International Conference on Fatigue of Welded Components and Structures, Senlis, France June 12-14, 1996.

10)Influence of Spectrum Loading on the Fatigue Strength of Improved Welds, Lopez Martinez L. and Blom A., FFA, IIW Conference "Performance of Dynamically Loaded Welded Structures", 14-15 July 1997, San Francisco, USA.

11)High Productive MAG Welding- Fatigue Properties of Weldments, M. Lundin, KTH; Lopez Martinez, J. Hedegård, KTH; K. Weman KTH and ESAB. Welded High-Strength Steel Structures; Stockholm October 8-9, 1997.

12)Guidelines for Optimum Design of Load-Carrying Fillet Welds under Fatigue Loading, H. Spennare, VCE; G.S. Wang, FFA and L. Lopez Martinez, Ibìdem.

13)Weld Defects Before and After Post Weld Treatment for MAG and High-Productivity MAG Welding, L. Lopez Martinez, A. F. Blom, FFA and J. Samuelsson, VCE, Ibìdem.

14)Swedish Contribution to IIW-programme on Post Weld Treatment Evaluation, L. Lopez Martinez, S. Bodin, KTH; A. F. Blom FFA and J. Samuelsson, VCE, Ibìdem.

Introduction

It is widely accepted that the fatigue strength of a welded joint is essentially independent of the yield strength of the parent steel. Consequently, in all the current fatigue design standards, Ref. [1-4] no account is taken of the parent steel material and the design classification is based only on the geometric characteristics of the weld detail, the likely site of fatigue initiation, and orientation of the welds with respect to the loading direction.

With the increasing use of high-strength steels in applications involving fatigue loading it may be helpful to highlight two important points.

First, there is no evidence to suggest that welded joints in high-strength steels are any worse than the corresponding details made in medium or mild steel grades. Indeed test results show that welded joints in higher strength steels are at least as good as similar details involving lower strength steels which were used in generating the underlying data for the current fatigue design rules.

Secondly, there is ample evidence to show that the use of high-strengths tells in welded joints treated by fatigue life improvement techniques is positively beneficial. The extent of benefit achieved by TIG dressing, toe burr grinding, hammer peening, needle peening, etc. increases with the parent steel strength. The influence of steel strength is particularly noticeable in the shorter life/higher stress regime. This is because the various fatigue life improvement techniques rely either on the introduction of beneficial (i.e. compressive) residual stresses near the joint, or the addition of a significant crack initiation phase to the overall fatigue life by removing all the pre-existing weld flaws such as slag intrusions, inclusions, undercuts, etc. which are normally present at the weld toes and act as sites for fatigue initiation.

Both of these factors are positively influenced by higher yield strength. Higher strength steels are capable of locking in larger compressive residual-stresses. Also, unlike fatigue crack growth properties which are essentially insensitive to steel strength, crack initiation takes longer in time in higher strength steels.

Fatigue Strength of Plain Unwelded Steel Plates

In absence of sharp crack-like defects (such as those associated with weld toes) the fatigue life of parent plate is spent predominantly in crack initiation. As stated previously, crack initiation properties of most steels are heavily influenced by their static strength. Indeed, as a general rule of thumb it can be stated that fatigue limit of plain unwelded steel (defined as the stress range below which no fatigue failure is expected) will be approximately 0.5 x UTS (ultimate Tensile Strength) [5]. However, this simple rule does not take into account other factors such as surface roughness, near-surface residual stresses, applied stress ratio, etc. which also influence fatigue initiation. In practice, these factors contribute to scatter in data when test results are expressed in terms of stress range. For instance, fatigue strength data (stress range) corresponding to fatigue life of $2x10^6$ cycles are shown in Figure 1 for different steel grades tested in the as delivered condition. The results clearly exhibit a degree of scatter resulting from different surface quality. Complete details of test data can be found in Ref. 6.

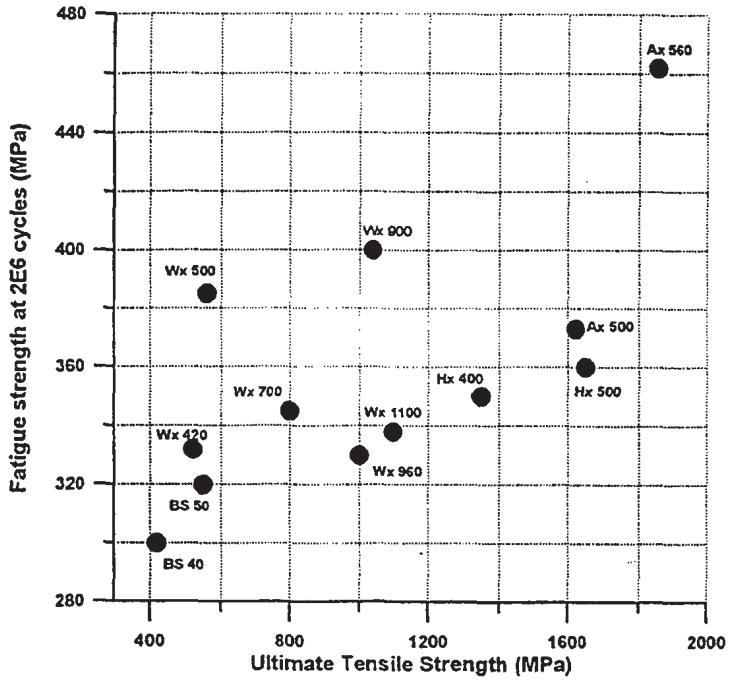

Figure 1 Fatigue strength vs. Ultimate Tensile Strength for various

The information presented above can be used to quantify the reduction in fatigue strength resulting from welding in a given grade of steel (e. g. Parent plate vs. butt weld, parent plate vs. fillet weld, etc.). Also, when joints are treated by fatigue life improvement techniques, the ultimate aim is to restore the original fatigue strength of the parent material. Therefore the fatigue strength values presented in Fig. 1 can be regarded as a ceiling to the amount of benefit that can be aimed for. The higher the grade, the higher the ceiling an therefore the greater is the potential benefit. However, caution is required because in most practical situations involving welded joints under fluctuating service load, the site of fatigue initiation is transferred to other (less severe) sources of stress concentration once the weld toes are treated by fatigue life improvement techniques. Therefore, the parent plate fatigue strength is seldom quite achieved in practice.

Fatigue Strength of Welded Joints

The allowable design stress in structures subjected to fluctuating service load is nearly always governed by the fatigue strength of the welded joints, particularly any fillet welds present. The poor fatigue strength of such joints, which in the as-welded condition is also independent of parent steel strength, can be attributed to the conjoint effect of three factors: local concentration of stress due to the geometric discontinuity at the joint; the presence of sharp crack-like flaws such as undercuts an slag intrusions introduced by the welding process; and the presence of large tensile residual stresses in the weld metal and the surrounding heat affected zone (HAZ).

Global Stress Concentration

Every welded joint gives rise to a geometric discontinuity associated with the change in section at the connection. When loaded, the discontinuity will result in stress concentration which increases the magnitude of local stresses. The extent of stress concentration will depend on how abrupt the change of section is: fillet welds with convex profile and small toe radii produce the largest stress concentration and butt welds with relatively flat overfills produce the smallest. However, as can be seen from Fig. 2, even in butt welds, the stress concentration resulting from the weld detail itself can be significant.

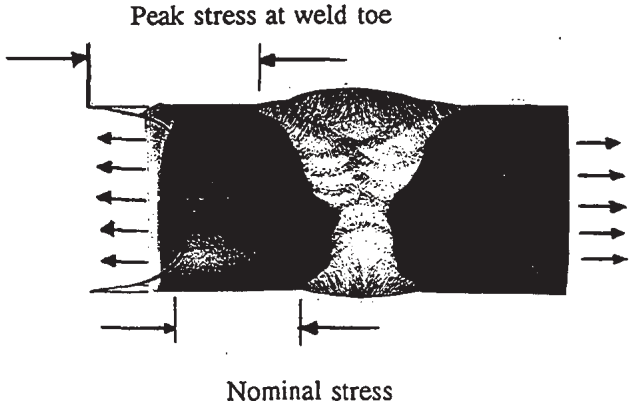

Figure 2 Nominal stress and stress concentration in a butt weld

Incidentally, the global stress concentration effect of the detail can explain why, other factors being the same, fillet welds behave generally worse than butt welds. Also it explains why some nominally "non-load-carrying" details have such poor fatigue strengths. A notable example is that of a longitudinal stiffener with fillet welds all round, which depending on stiffener length and its proximity to free edges can have a fatigue design classification as low as Class G, Ref. [2]. The reason for the low fatigue class is simply that the stiffener attracts and concentrate the load paths at its two ends and thus leads to highly localised and sharp stress gradients here.

Weld flaws

Undercutting of the plate surface often occurs at the toe of most welds, leading to a source of local stress concentration. Also, in most welds produced industrially and regarded as having acceptable quality, the presence of very sharp, almost crack-like, slag intrusions, inclusions, etc. cannot be ruled out, Ref. [7]. These weld flaws are normally too small to be detected by routine non destructive examination, see Fig. 3 and 4.

Nevertheless, by acting as ready sites for fatigue initiation they have a profound effect on the behaviour of welded joints. By removing any significant fatigue initiation, they ensure that the fatigue life of a welded joint is spent almost entirely in crack propagation. As

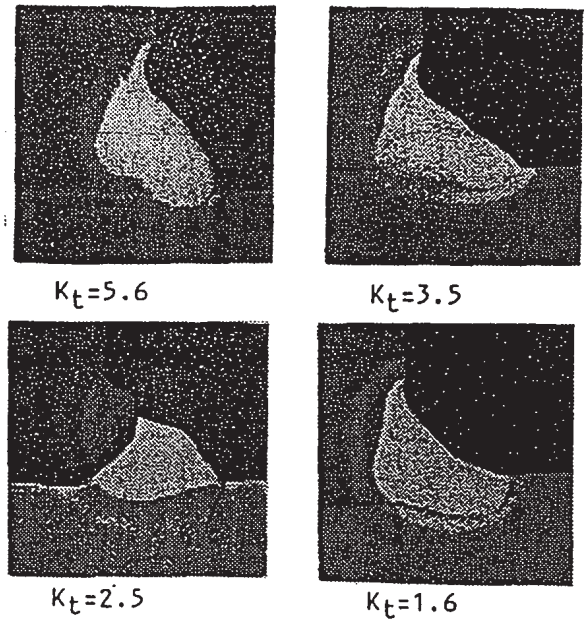

Figure 3 Various fillet weld geometries and the correspondent Stress Concentration, [10]

crack propagation properties of most steels are essentially similar, the presence of weld flaws results in fatigue behaviour of the detail being essentially independent of parent steel grade.

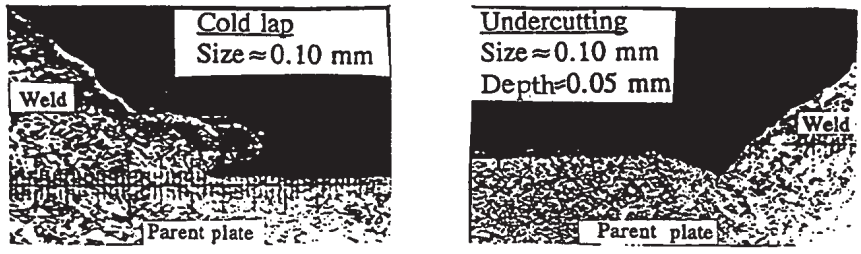

Figure 4 Typical weld imperfections at weld toe region

Residual stresses

In general, fatigue cracks will not propagate when the effective stress at the crack tip is compressive. Thus when considering the fatigue performance of plain steels it is conventional to ignore compressive components of applied stress. During, welding, high tensile residual stresses form in the weld metal and surrounding HAZ. These residual stresses arise primarily from differential contractions during cooling, but thermal gradients during cooling and a volume change associated with a phase transformation in some materials can also contribute to the total residual stress distribution, Ref. [8].

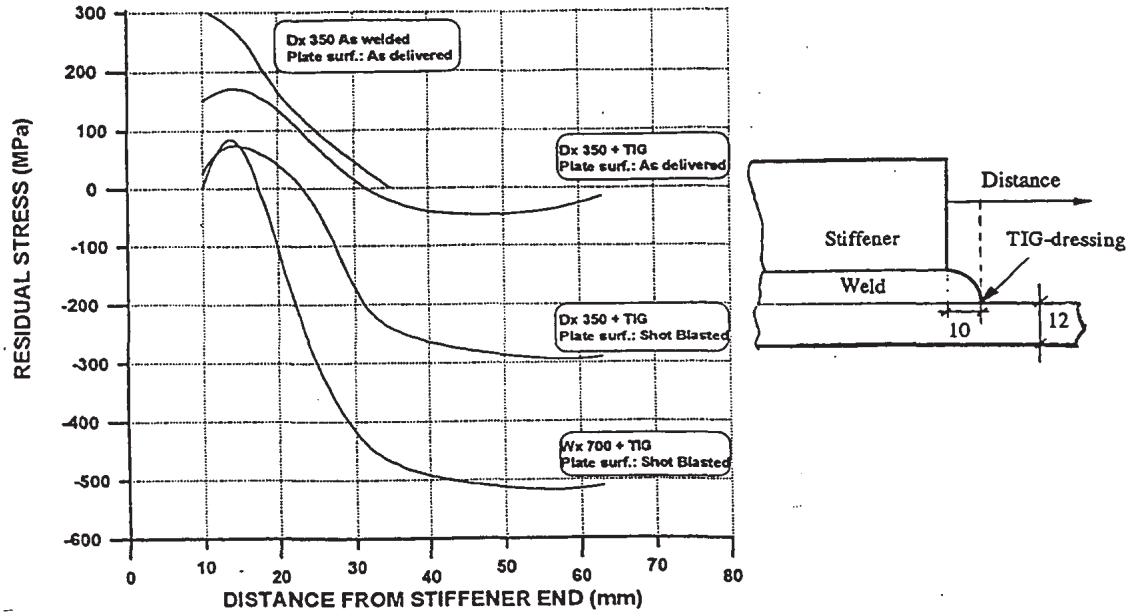

Figure 5 Distribution of residual stresses away from weld toe in a fillet weld, [11].

These residual stresses, see Fig. 5, combine with the applied stresses to increase the effective mean stress. Thus applied compressive stresses can be as damaging as applied tensile stresses and fatigue failure can occur even under fully compressive loading.

Incidentally, another important effect of welding residual stresses is that in fatigue design of welded joints only the stress range, that is the difference between the minimum and the maximum applied cyclic stress, needs to be taken into account. The applied mean stress, an important parameter in the fatigue design of unwelded components , plays no role in the design of welded components. This is because with large tensile residual stresses present, the weld experiences high mean stresses even when the applied mean stress is low.

Fatigue Design Standards

Fatigue design of welded joints has developed significantly over the past two decades and there now exist several codes regulating such design. However, still exists some discrepancies regarding the choice of safety factor, stress range for a specific detail classification and cut-off limit. These aspects have been studied in detail in Ref. 9. Here below we present a summary of that study.

Detail classification

The detail classification, stress range at $2x10^6$ cycles, differ for the non-load carrying fillet weld considered. BSK and Eurocode 3 assumes a stress range of 50 MPa, while BS and IIW assume 61MPa respective 71 MPa.

Failure risk

The failure risk for the considered fatigue design standards varies depending on the choice of partial coefficient. Fatigue design curve for BS 7608:1993 gives a failure risk of $2.3x10^{-2}$. The corresponding failure risk for BSK is $1.0x10^{-2}$ when partial coefficient is taken as 1.

Fatigue limit

Fatigue limit for constant amplitude is assumed to start at $5x10^6$ cycles, in Eurocode 3, in the IIW document and in BSK. In BS 7608:1993 the fatigue limit for constant amplitude is defined at 10^7 cycles.

Change of slope

The change of the slope in S-N curve due to the cut-off limit for variable amplitude is as follows:
Eurocode 3: $N>5.0x10^6$ then m=5 until 10^8cycles.
IIW Document: $N>5.0x10^6$ then m=5 until 10^8cycles.
BS 7608:1993: $N>1.0x10^7$ then m=m+2.
BSK: $N>5.0x10^6$ then m=5 until 10^8cycles.

Fatigue life improvement techniques

The situation is even more precarious when fatigue life improvement techniques are focused. Still, it is not possible to find fatigue design curves for any detail which has been treated by fatigue life improvement techniques. This is mostly due to a need for systematic experimental studies of improved welded joints behaviour under spectrum loading.

BS 7608:1993 and IIW Document mention the possibility of increasing the design stress level if a remedial treatment of the weld toe region by controlled machining or grinding is implemented. In the case of BS it is stated that such treatment leads to an increase in the allowed design stress range. The S-N curve can be then improved in strength by 30%. This is equivalent to a factor of 2.2 on life. Consequently the BS presents a clear description of the treatment that should be carried out regarding tools, machining deep and posterior control. The IIW document consider also the application of fatigue life improvement techniques. The IIW document goes further than BS and point bout a series of techniques to improve fatigue resistance. Nevertheless, the IIW document point out the necessity of fatigue test in order to verify the actual procedure for the specific stress range of interest and the fatigue life improvement used.

Scope of Thesis

The present thesis is directed to the above field on the general fatigue behaviour of steels subjected to spectrum loading. Specifically, the aim has been to investigate this behaviour of high-strength steels and to evaluate various life improvement techniques making the use of high-strength steels possible in welded structures subjected to fatigue loading.

Paper A introduces the test specimen used in subsequent papers and adresses the flaw population under different welding procedures.

Paper B focuses on residual stresses due to welding. In particular, the relaxation of residual stresses due to spectrum fatigue loading is assessed by χ-ray diffraction techniques.

Paper C looks further into the residual stress problem by investigating the full 3D-behaviour by means of neutron radiography. Also, the effect of post-weld treatment is adressed in this paper.

Paper D summarizes numerous spectrum fatigue test results and show the potential for high-strength steels in spectrum fatigue loaded structures after the application of suitable post-weld treatments.

Paper E correlates the interaction of all studied experimental parameters by fracture mechanics modelling of the entire fatigue process.

References

1. Swedish Regulations for Steel Structures, BSK. National Board of Physical Planning and Building. AB Svensk Byggtjänst, Stockholm 1987, Sweden.

2. British Standards BS 7608:1993. Code of practice for design and assessment of steel structures. BSI, Park Street, London W1A 2BS, UK.

3. IIW Document XII-1539-94/XV-845-94. Recommendations on Fatigue of Welded Components. Prof. Dr. A. Hobbacher, Fachhochaschule Wilhelmshaven, R. Paffrath-Str. 10, D-26389 Wilhelmshaven, Germany.

4. EUROCODE 3: Design of steel structures. Part 1-1: General rules and rules for buildings. ENV 1993-1-1:1992. European Committee for Standardisation, Rue de Stassart 36, B-1050, Brussels.

5. Maddox S.J.; "Fatigue Strength of Welded Structures", 2nd Ed. Abington Publishing. Cambridge CB1 6AH, UK.

6. Lopez Martinez L.; "Fatigue Strength in WELDOX", 5th Ed., April 1995. SSAB Oxelösund AB.

7. Lopez Martinez L., SSAB Oxelösund AB and Korsgren P., SSAB Tunnplåt AB; "Characterisation of initial defect distribution and weld geometry in welded fatigue test specimens". Proceedings of the Nordic Conference on Fatigue. Edited by A.F. Blom, EMAS Publishers, West Midlands, England 1993.

8. Macherauch E. and Wohlfahrt H.; "Different sources of residual stress as a result of welding", Welding Inst. Conf. Residual Stresses in Welded Constructions and their Effects, 1979.

9. Lopez Martinez L. "Correlation between some Fatigue Design Standards concerning safety factor, detail classification and cut-off limit", Materials Technology of Welding II, KTH, April 1997.

10. Samuelson J., "Fatigue design of vehicle components: methodology and applications", Report No. 8823, Department of Aeronautical Structures and Materials, KTH.

11. Lopez Martinez L. and Blom A. F.; "Influence of fatigue life improvement techniques on different steel grades under spectrum loading", Fatigue Design 95, VTT Finland, Sept. 1995.

PAPER A

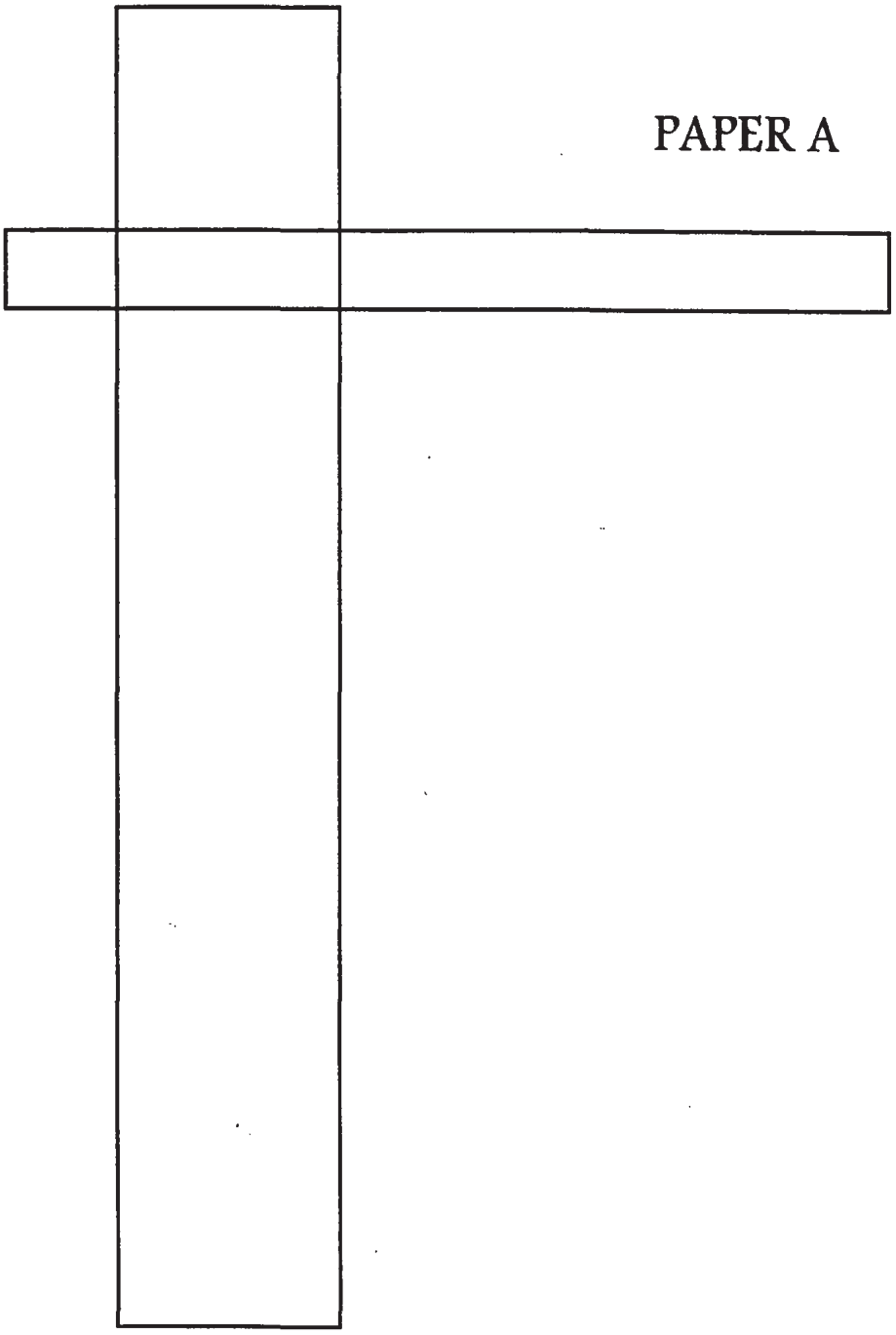

CHARACTERIZATION OF INITIAL DEFECT DISTRIBUTION AND WELD GEOMETRY IN WELDED FATIGUE TEST SPECIMENS.

L.Lopez Martinez [1] and P.Korsgren [2]

The presence of defects in non loaded weldements in cruciform sections were studied by microscop inspection. Weld method induced defects consisted mainly in cold laps or shrinkage cracks orientated parallel to the parent plate surface. Basic coated electrode and basic flux cored wire gave deeper cold laps than rutile flux cored wire and solid electrode. The last one showed most cold laps, dimension all less than 0.15 mm depth. An extensive documentation of fatigue specimens with non load carrying fillet weld was carried out. The local geometry, toe radius and toe angle have been documented by plastic replica technique. Calibration showed that the used measurement method gave reasonable accuracy only if weld toe area is clean enough.

INTRODUCTION

The influence of crack like weld toe defects on the fatigue strength of fillet welded joints has been studied in a series of papers (1)-(3). The stress intensity factor, K_I, for such weld defects can under certain premises be calculated by Linear Elastic Fracture Mechanics. For this purpose it is necessary to know the initial defect. The local geometry at the weld toe can be used to determine the stress concentration factor for the uncracked weld (4)-(5). This information, along with initial defect size and stress concentration, can be used to predict fatigue lifes, see (4).

The present paper consist in two parts. The first part of this investigation is a comprehensive weld defect comparison between different weld methods and

[1] Application Research and Development, SSAB Oxelösund AB, S-613 80, Oxelösund, Sweden.

[2] R. & D. and Customer Service, SSAB Tunnplåt AB, S-781 84, Borlänge, Sweden.

different filler metals and was carried out using specially manufactured test coupons. The second part is the measurements of the local weld geometry parameters on fatigue test specimens. After the fatigue testing the fracture crack surfaces of the specimens have been analyzed.

EXPERIMENTAL PROGRAM

General.

The experimental program consisted of two parts, separate test coupons and fatigue test specimens.

In the first part, test coupons were used in a comprehensive investigation to characterize both the welding method in terms of filler metal and type of weld defects and size distribution.

In the second part, fatigue test specimens were analyzed to characterize both weld defects and local weld geometry specially in regions of expected fatigue failure.

Measurement of weld toe radius. Several authors have reported measurements of weld toe radius (7),(2),(3),(6) but only one have reported in detail how the radius was defined (3). Due to lack of that information it is not possible to state whether the different radius measurements reported are strictly comparable. Neither the IIW-document "Fatigue testing of components" (10) gives any information regarding preferred ways to measure the radius on irregular transitions between the parent material and filler material.

Determination of initiation site. The aim was to measure the weld geometry at the crack initiation point. However the crack initiation point was not easily found in all specimens which was due to lack of distinct beach marks from the initial crack propagation stages. Furthermore it was difficult to find in any specimens initial defects on the fracture surface when studied in an optical microscope.

In these specimens (and specimens without cold-laps) the initiation point was determined as the centre of the elliptic beach marks that could be identified from the later stages of the crack propagation. As additional cuts and measurements on the replicas were made at approximately 1 mm on each side of the assumed initiation point, the initiation area was presumably covered.

Calibration of local weld geometry measurements. The basis of the geometry measurements were the plastic replicas. To check how well the shape of the replicas could represent the local shape of weld toe, a calibration exercise was

carried out. Three welds were chosen from the 3 mm thick specimens and seven replicas were made. Figure 1 shows the welds and the replicas.

The same magnification of the replicas were used to measure weld toe angle. The results from the calibration measurements carried out on these photos are given in Table 1.

The conclusion is that the weld toe area **should be** cleaned from slag to give a reasonable estimation of the weld toe-radius and -angle.

TABLE 1 - Calibration of weld geometry measurements.

Toe Angle (°)		Toe Radius (mm)	
Weld	Replica	Weld	Replica
53	66 (*)	0.03	0.5,0.87,0.44 (*)
47	50	0.05	0.63,0.03,0.10
63	65	0.03	0.23,0.23,0.18
62	60	0.25	0.15,0.10,0.20
55	56	0.06	0.03
52	51	0.03	0.10

(*) The weld toe region was obviously not "clean" enough.

Separate test coupons.

Test coupons according to fig. 2 were used for investigation of weld induced defects by weld method or by filler metal. In these specimens the defect size distribution and defect quantities have been documented.

Weld parameters for defect analysis specimens. The two weld methods which have been studied are: MMA, manual metal arc and GMA, gas metal arc. For GMA three different filler metals have been investigated.

For each of the two welding methods and/or the different filler metals a number of specimens have been prepared. The weld parameters are presented in Table 2.

The specimens were cut perpendicular to the longitudinal direction of the weld see, fig. 2. Thereafter they were milled, and wet polished using polishing compound with particle size 3 μm and finally etched in 3% NITAL.

In a microscope with magnification 50 to 200 the weld toe area was examined and searched for defects and undercuts. The depth (d) and orientation (φ°) of the observed defects were measured, see fig 3.

After observation in microscope the procedure (milling, polishing and etching) was repeated and new positions in the weld were investigated. A distance of 2 mm between each surface of examination was required in order to cover some significant weld length.

TABLE 2 - The weld parameters used for defect analysis test coupons.

Weld Method	MMA	GMA		
Filler Metal	OK48.00	PZ 6130	PZ 6111	OK12.51
Gas	------	Mison 25 15 l/min	Fogon 20 14 l/min	Mison 25 8 l/min
Welding Position	1G	1G	1G	1G
Throat Thickness	5 mm Nominal	5 mm Nominal	5.5 mm Measured	3-4 mm Nominal
Electrode Size (mm)	4	1.6	1.6	1.0
Current (A)	185	185	257	140
Voltage (V)	24	23	25	20
Heat Input (kJ/mm)	2.0	1.6	1.3	0.6
Interpass Temperature (° C)	25 110 125 130	25 125 135 80	20 20 20 20	20 20 20 20

Fatigue test specimens

Specimens according to fig. 4 have been used for fatigue testing, both in constant amplitude and spectrum loadning. In these specimens weld geometry parameter and a fracture surface investigation have been done.

Two different steel grades Domex 350 XP, produced at SSAB Tunnplåt, and Weldox 900, produced at SSAB Oxelösund AB, have been used for the fabrication of the fatigue test specimens.

The chemical composition and mechanical properties are presented in Table 3. Two different plate thicknesses have been tested, 12 mm and 3 mm. Table 4 shows the welding parameters for the three different specimen groups.

Local weld geometry. Plastic replicas were taken at all potential crack sites, four per specimen, before fatigue testing. After testing the crack initiation site was localized on the fracture surface and the corresponding position was sectioned on the replica. Two photographs were taken the replicas cross section. One was taken with magnification factor 4.5 used to measure the weld toe angle. The other magnification was 40, used to measure the weld toe radius.

TABLE 3 - Chemical composition and mechanical properties of the tested steels

	DOMEX 350 XP	DOMEX 350 XP	WELDOX 900
Thickness	3 mm	12 mm	12 mm
C	0.053	0.058	0.17
Si	0.20	0.02	0.22
Mn	0.51	0.62	1.40
P	0.006	0.009	0.025
S	0.003	0.010	0.010
Al	0.048	0.042	0.065
Nb	0.030	0.014	0.030
Ti	—	—	0.020
B	—	—	0.002
V	—	—	0.030
CE_{IIW}	0.15	0.18	0.56
R_{eH}(MPa)	366	371	1005
R_{eL}(MPa)	355	370	—
R_m(MPa)	457	471	1030
A_5 %	40	28	14

The weld toe angle was defined as the angle between the extension of the parent plate surface and the line representing the shape of the weld near the toe area. The weld toe radius was measured by fitting circles to the transition between the parent plate and the weld metal, see fig 5.

In many cases there were small irregularities sited on a "smooth" curved surface, leading to difficulties in determining how to measure the radius, see fig.6.

A very small radius would result in a negligible initiation phase. Therefore it was concluded that a radius smaller than 0.1mm was of no interest. Thus, in cases where the minimum local radius was less than 0.1 mm the "overall" radius - if it existed - was measured.

The measurements of local weld geometry were carried out at the crack initiation sites of the two specimens with the shortest and the longest life in each fatigue test series, see Table 7 and Table 8. The complete information about fatigue lifes are reported in references (8) and (9).

TABLE 4 - Chemical composition and mechanical properties of the filler metal used in fatigue test specimens.

	PZ 6130 Domex 350 XP 12 mm	OK 12.51 Domex 350 XP 3 mm	Fluxofil 45 Weldox 900 12 mm
Producer	Filarc	ESAB	Oerlikon
C	0.05-0.09	0.1	0.05
Si	0.2-0.5	0.8	0.45
Mn	1.0-1.3	1.5	1.7
P	0.025	—	—
Cr	—	—	1.0
S	0.025	—	—
Mo	—	—	0.4
Ni	—	—	2.2
R_{eL} (MPa)	420	470	890
R_m (MPa)	500-570	570	950-1100
A_5 (%)	26	25	14

Fatigue testing.

Fatigue testing was carried out under load control both for constant amplitude and spectrum loadning regime. The constant amplitude tests were run in a servohydraulic 500 kN, MTS testing machine at room temperature. The frequency

was approximately 10 Hz at variable R-ratios (0-0.9). The spectrum fatigue testing has been carried out for various spectrum types. A complete summary of all fatigue test results for the various spectra are presented in ref. (9).

RESULTS AND DISCUSSIONS

The results of the weld defect analysis are presented under subsidiary heading "Separate test coupons". The results of measurements of weld geometry parameter and fracture surface analysis of fatigue test specimens are presented under subsidiary heading "Fatigue test specimens".

Separate test coupons.

Weld defect analysis for different weld methods and filler metals This investigation has been carried out along with the documentation of the fatigue test specimens. The results should be representative for the defects existing in the welds of the fatigue test specimens. For practical reasons the weld defect analysis was carried out on the longitudinal part of the weld and not in the area at the end of the stiffener where the cracks, were expected to initiate. In these two different regions one may infer that differences in welding conditions exist which would influence the both local and global shape of the weld. However, the inspection of fracture surfaces in fatigue test specimens revealed a dominance of the same type of defects, cold laps, as found in the investigation presented below. It would indicate the results of weld defect analys carried out is representative for the weld defects localized in the crack site in fatigue test specimens.

Types of defects. The majority of the observed defects were defined as "cold laps", and their orientation were mainly parallel to the plane of parent metal plate surface. Some typical examples of the observed defects are show in fig. 7. In fig. 8 some defects are designed "unusual". Defects with depth greater than 0.01 mm were sampled and the maximum depth found was 1.4 mm. See Table 5 for details.

TABLE 5 - Defect distribution in non loaded fillets welds.

A: Filler metal.
B: Orientation (°) see figure 3.
C: Number of investigated points.
D: Number of spots where defects were found.
E: Percentage of inspected points where defects were found.
F: Mean distance between inspected surfaces (mm).
G: Mean value in mm.
H: Standard Deviation in mm.

A	B	C	D	E	F	G	H
OK 48.00	0	712	38	5.3	1.59-2.03	0.27	0.30
PZ 6130	0	720	83	12	1.59-2.10	0.25	0.25
PZ 6111	0	5824	112	1.9	2	0.047	0.050
OK 12.51	0	2896	475	35	0.37-2.15	0.13	0.15
PZ 6111	90	5824	49	0.84	2	0.10	0.19
OK 12.51	90	2896	66	4.3	0.37-2.15	0.24	0.0049
Ref.(3)	90	135	135	100	0.27	0.042	0.28

Comments to Table 5:

(i) There is a small difference when looking at all results from each electrode OK 48.00 (basic coated electrode) and PZ 6130 (basic flux core wire).
(ii) The 90° defects which were found almost only in PZ 6111(rutile flux cored wire) and OK 12.51(solid electrode), were rather small for OK 12.51 but deeper for PZ 6111. In the latter case they did not appear very often.
(iii) Smith et alt., (3), found defects at every investigated point when he studied 9 welds located at the end of a stiffener.

Fatigue test specimens

Fracture surface examination After fatigue testing the fracture surfaces were studied. The task was to locate the crack initiation sites and to determine the initial defects.

The crack initiation sites were seldom easy to localize exactly. The region where the crack was initiated could, however, always be identified as the centre of the crack propagation pattern that could be seen from the later part of the propagation stage. These patterns occurred typically 2-4 mm away from the initiation point and were often seen as just a slight shading on the surface. The results of fracture surface examinations are presented in Table 8 and Table 9. Illustrations of the findings on the fracture surfaces are shown in Figure 9.

For the detected cold laps we have defined two "dimensions", width or x-direction and length or y-direction. These are also ilustrated in Figure 9.

A clearly visible initial crack oriented normal to the plate surface was not observed on any of the fracture surfaces. In the majority of the localized initiation

areas there were instead the remaining of a local lap defect, or the estimated initiation site coincided with a local maximum in the x-direction of the cold lap defect .

Weld toe angle and weld toe radius. The weld toe angles were measured on the plastic replicas at crack initiation sites after fatigue testing. The results are presented in Figure 10 and Figure 11.

In addition to these figures the mean values and the corresponding scatter band for two standard deviations are presented in Table 6.

Weld geometry parameter; comparison with literature. Figure 9 presents the results from the present investigation together with results from references (1),(2),(3),(6). Different measurement techniques may affect the results, as well as the fact that the different investigations includes quite different weld sizes, from a=3 mm to a=25 mm.

In ref. (1) weld toe radius and angles has been determined from photographs of sawcut sections, taken in a microscope with magnification factor 5.12 and 2.8 respectively. The sections were end sections of 100 mm wide fatigue specimens. Eight sites were studied on each specimen.

In ref. (2) silicone rubber casting of the reinforcement was made before fatigue testing. After fatigue testing the castings were cut at the location of the crack initiation. Measurements were made by using a microscope with a magnification of 20. This method is rather similar to the one used in the investigation presented in this paper.

TABLE 6 - Characteristics of the geometry parameters

Thickness (mm)	Numb of meas.	Radius mean*	+2 sdev	-2 sdev	Angle mean (°)	+2 sdev	-2 sdev
12	27	0.14	1.0	0.019	43	60	27
3	23	0.067	0.47	.0096	38	61	16

* The statistics of the radius were calculated in $\log_e$-scale as the obtained distribution shapes are closer to $\log_e$-normal than to normal. The values above are then obtained by conversion from $\log_e$-scale to mm.

Fatigue lives vs. weld defect size/weld geometry parameters The results from constant amplitude fatigue testing are presented in Table 8. For every tested

specimen the weld toe radius and weld toe angle were measured. The results for fracture surface analys is also presented.

For the results from variable amplitude fatigue testing the same information is presented in Table 8. In this case only some "representative" specimens are presented.

No correlation has been found between defect size and fatigue lifes within the frames of this project. A versatile method to quantify the fatigue lifes of specimens having cold laps is lacking due to its complexity. Therefore an engineering approach is used, which is based on fracture mechanics, see (4).

TABLE 7 - Constant Amplitude Test Results and Local Weld Geometry

Specim. See Fig.11	Stress Range (MPa)	Cycles (E6)	Toe Radius (mm).	Toe Angle (°)	Type of Defect	Width/ Length See Fig.11
11	107	2.713	0.15	43	Cold lap.	0.15/0.8
13	107	1.144	0.1	44	Cold lap.	0.5/1.0
14	107	4.008	0.2	50	Geom.	---
16	250	0.075	0.23	48	Cold lap.	0.5/1.0
18	250	0.107	0.4	40	Cold lap.	0.4/1.5
21	175	0.280	0.23	52	Cold lap.	0.8/2.0
22	175	0.202	0.19	41	Cold lap.	0.4/1.5
33	175	0.214	0.23	39	Cold lap.	.125/.25
34	125	0.467	0.38	31	Cold lap.	0.05
43	125	1.158	--	--	Geom.	--
51	125	0.693	0.025	45	Geom.	--
60	125	5.667.	0.23	18	Geom.	--
60	175	0.769	0.23	18	Geom.	--
67	125	0.759	0.075	39	Cold lap.	0.1/0.1

TABLE 8 - Variable amplitude test results and local weld geometry

Spec./ Spectrum Ref. (9)	Stress Range (MPa)	Cycles (E6)	Toe Radius (mm).	Toe Angle (°)	Type of Defect	Width/ Length.
1B/R	210	10.7	1.0	32	Cold lap.	1.0/ 0.35
4C	210	8.7	0.1	32	Cold lap.	1.0/ 0.15
8D/R	350	1.7	0.2	33	Micro edge	—
17B/R	210	10.0	0.5	28	Cold lap.	0.6/0.3
26C	350	1.74	0.4	36	Geom.	—
27C/R	350	1.25	0.25	33	Geom.	—.
37C/R	350	2.09	0.1	32	Geom.	—
39C/SP2	350	1.74	0.2	33	Cold lap.	—
58C/R	230	33.7	1.0	32	Micro edge	—
59C/SP2	125	219.0	0.1	30	Cold lap.	1.0/0.5
66C/SP2	250	5.20	0.1	30	Cold lap.	0.3/0.1
73C	230	190.0	0.1	23	Cold lap.	0.4/0.2
75B/SP2	170	24.0	1.0	33	Cold lap.	1.0/0.5
76A/SP2	210	43.3	1.0	31	Geom.	—
77/SP2	210	16.4	0.1	31	Geom.	—
78/SP2	210	32.4	0.23	33	Cold lap.	0.7/0.3

CONCLUSIONS

Separate test coupons

Weld method induced defects. Cold laps or defects parallel to parent plate surface: OK 12.51 (solid electrode) gave the greatest number of small defects. PZ 6130 (basic flux cored wire) showed more small defects than OK 48.00 (basic coated electrode) and particulary than PZ 6111 (rutile flux cored wire).

For greater defects than 0.65 mm there was no significant difference between OK 48.00 and PZ 6130, while PZ 6111 and OK 12.51 clearly gave less number of defects.

Undercuts defect orientation 90° were almost only found in the welds of OK 12.51 and PZ 6111. The maximum depth found was 0.15 mm and most defects were found in OK 12.51.

Fatigue tests specimens

Local Weld Geometry 3 mm specimens showed smaller radius and angles, 0.07mm respective 38° than 12mm specimens, 0.14mm respective 43°. These mean values of the radius were calculated in $\log_e$-scale with the corresponding linear mean values of 0.11mm and 0.21 mm. The values of the radius and angles were in the same order of magnitude as reported by litterature.

To obtain accurate measurements of weld toe angles and weld toe radius by the plastic replica method a thorough cleaning of the studied area is required .

Fatigue lifes vs. weld defects weld geometry parameters The type of weld defects found and their orientation make it difficult to find a reasonable correlation between defect size and fatigue lifes due to its relative complexity.

ACKNOWLEDGEMENTS

This work was financially supported by NUTEK (Swedish National Board for Industrial and Technical Development), NI (Nordic Industrial Found), ABB, SSAB, SAAB-SCANIA and VME. All the personal of the laboratories involved in this investigation are greatfully acknowledged.

REFERENCES

(1) Engesvik K., Moan T. "Probabilistic analysis of the uncertainty in the fatigue capacity of welded joints", Engineering Fracture Mechanics,Vol 18.No.4,pp.743-762,1983.

(2) Nihei M., Sasaki E., Kanao M. and Inagaki M. "Statistical analysis on fatigue strength of arc-welded joints using covered electrodes under various welding conditions with particular attention to toe shape", Transactions of national research institute for metals, Vol.23, No.1(1981)

(3) Smith I.F.C. and Smith R.A. "Defects and crack shape development in fillet welded joint", Fatigue of Engineering Materials and Structures, Vol.5,No.2,pp.151-165, 1982.

(4) Dahle T. , Larsson B."Fatigue Life predictions of Longitudinal Non-Load-Carrying fillet Welded Specimens based on Current Flaw Distribution".Proceedings of the Nordic Conference on Fatigue. Edited by A. F. Blom, EMAS publishers, West Midlands, England, 1993.

(5) Samuelsson J."Fatigue Design of Vehicle Components:Methodology and Applications", Dept. of Aeronautical Structures and Materials, Report 88-23. The Royal Institute of Technology, Stockholm, Sweden, 1988.

(6) Berge S. "On the Effect of Plate Thickness in Fatigue of Weld", Engineering Fracture Mechanics, Vol 21. No. 2, pp. 423-435, 1985.

(7) Gurney T.R. "Fatigue of Welded structures", Second Edition, The Welding Institute Cambridge University Press 1979, Cambridge, England.

(8) Spennare H., Samuelsson J. "Spectrum Fatigue testing of a longitudinal non-load carrying fillet weld A Round Robin Exercise". Proceedings of the Nordic Conference on Fatigue. Edited by A. F. Blom, EMAS publishers, West Midlands, England, 1993.

(9) Bogren J., Lopez Martinez L. "Spectrum Fatigue Testing and Residual Stress Measurements on Non-load Carrying Fillet Welded Test Specimens".Proceedings of the Nordic Conference on Fatigue. Edited by A. F. Blom, EMAS publishers, West Midlands, England, 1993.

(10) "Fatigue Testing of Welded Components", IIW Document XIII-WGT1-24-90.Feb 1990.

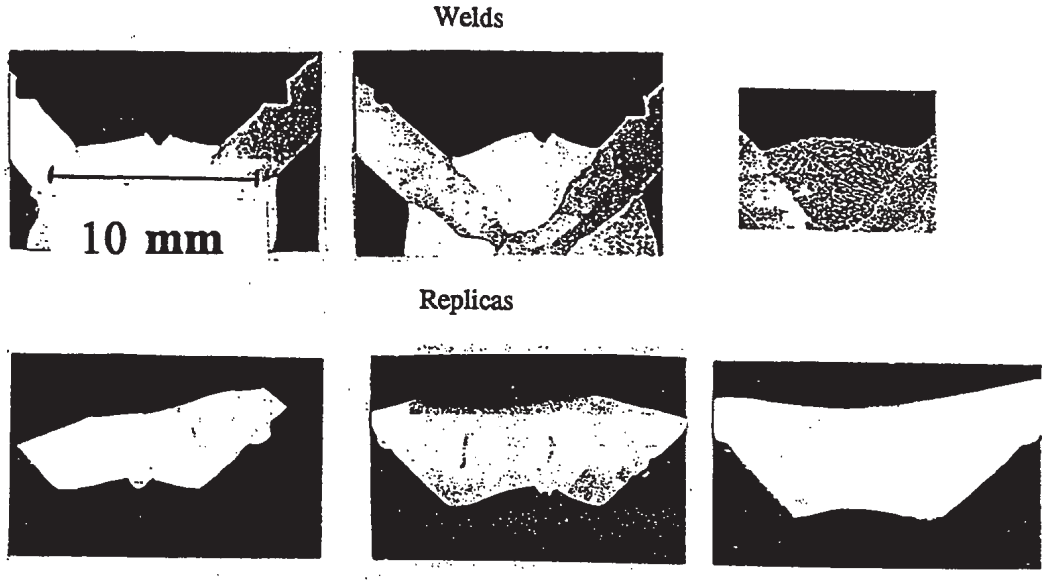

Figure 1 Calibration of the replica technique. Magnification 4.5 for angle measurement.

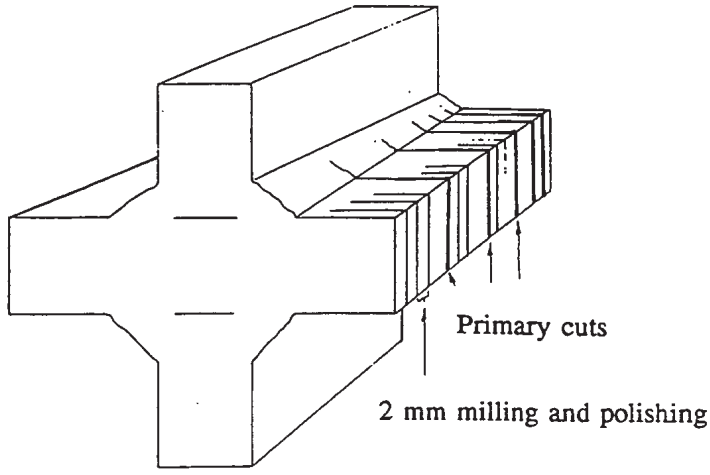

Figure 2 Test coupons for study of weld defects

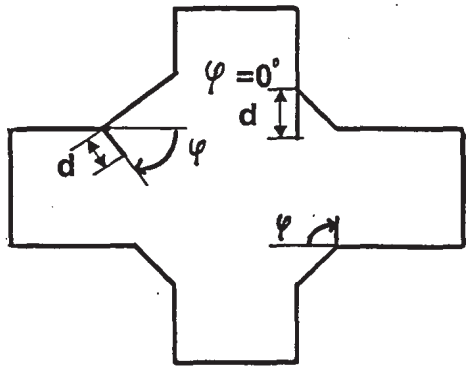

Figure 3 Depth and orientation of weld defects

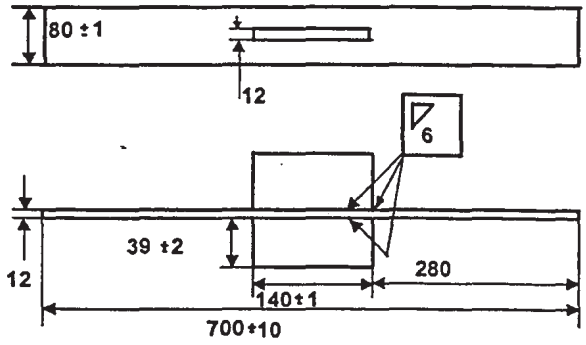

Figure 4 Shape and dimensions of fatigue test specimens.

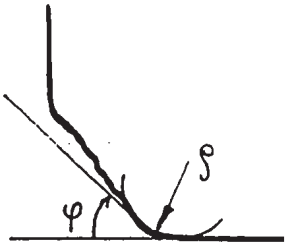

Figure 5 Definition of weld toe angle and weld toe radius.

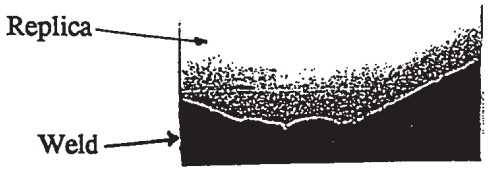

Alternative circle with radius 1

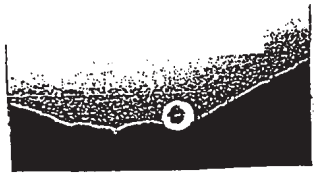

Alternative circle with radius 2

Figure 6 Alternative radius measurements on the same replica

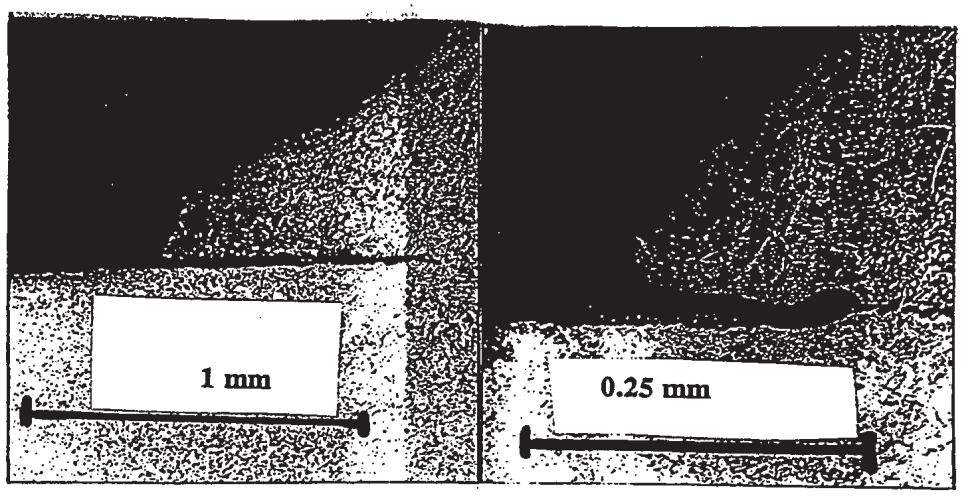

Figure 7 Typical weld defects

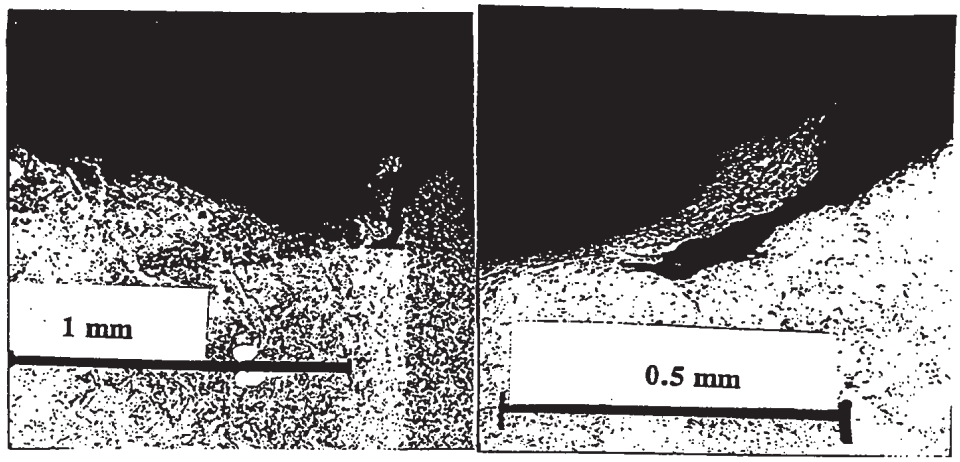

Figure 8 "Unusual" weld defects

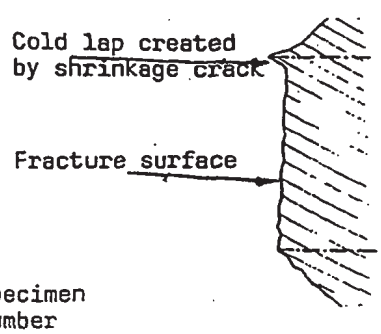

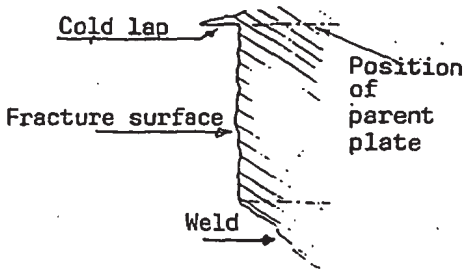

Specimen number

11 Cold lap:

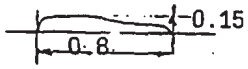

13 Cold lap:

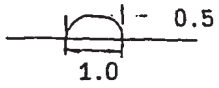

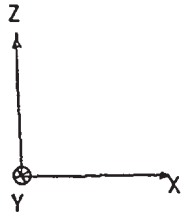

14 No defect. Shape of "early" crack:

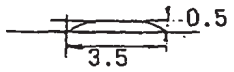

16 Cold lap:

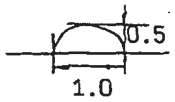

18 Cold lap:

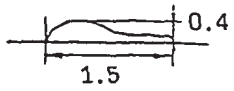

21 Cold lap:

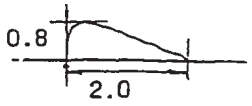

22 Two cold lap defects:

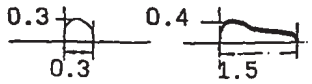

33 Cold lap:
May be starting point, but no visible beach marks.

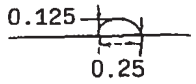

34 No defect? Possibly a long lof with depth <0.05 mm.
43 No defect.
51 No defect.
60 Local pores.

67 Cold lap:

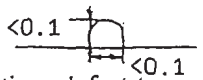

Figure 9 Fracture surface inspection: defect type and orientation.

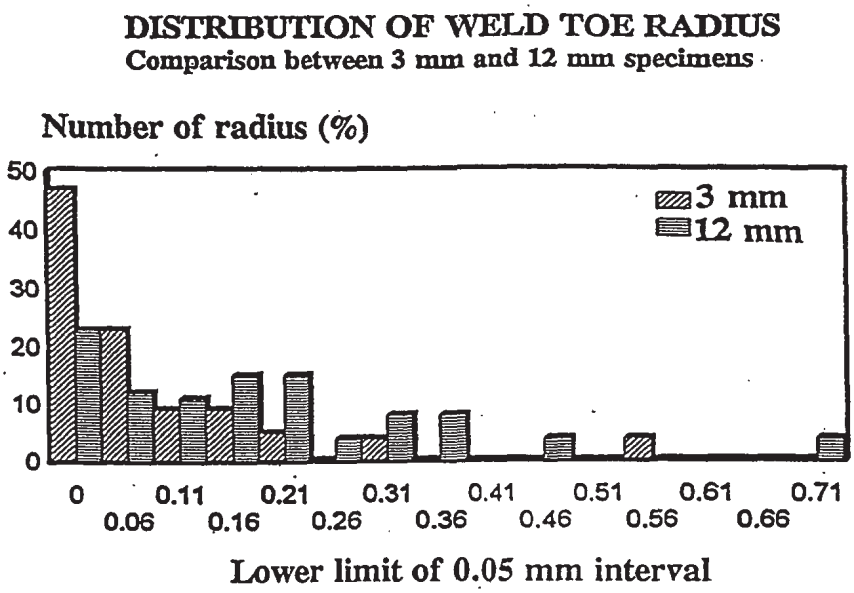

Figure 10 Local weld geometry: weld toe radius distribution.

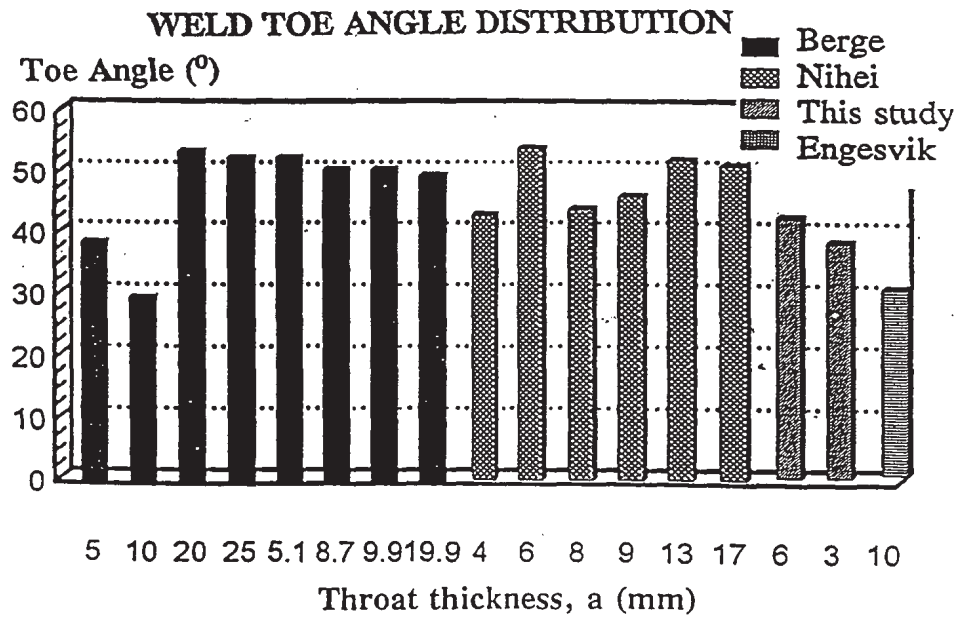

Figure 11 Local weld geometry: weld toe angle.

PAPER B

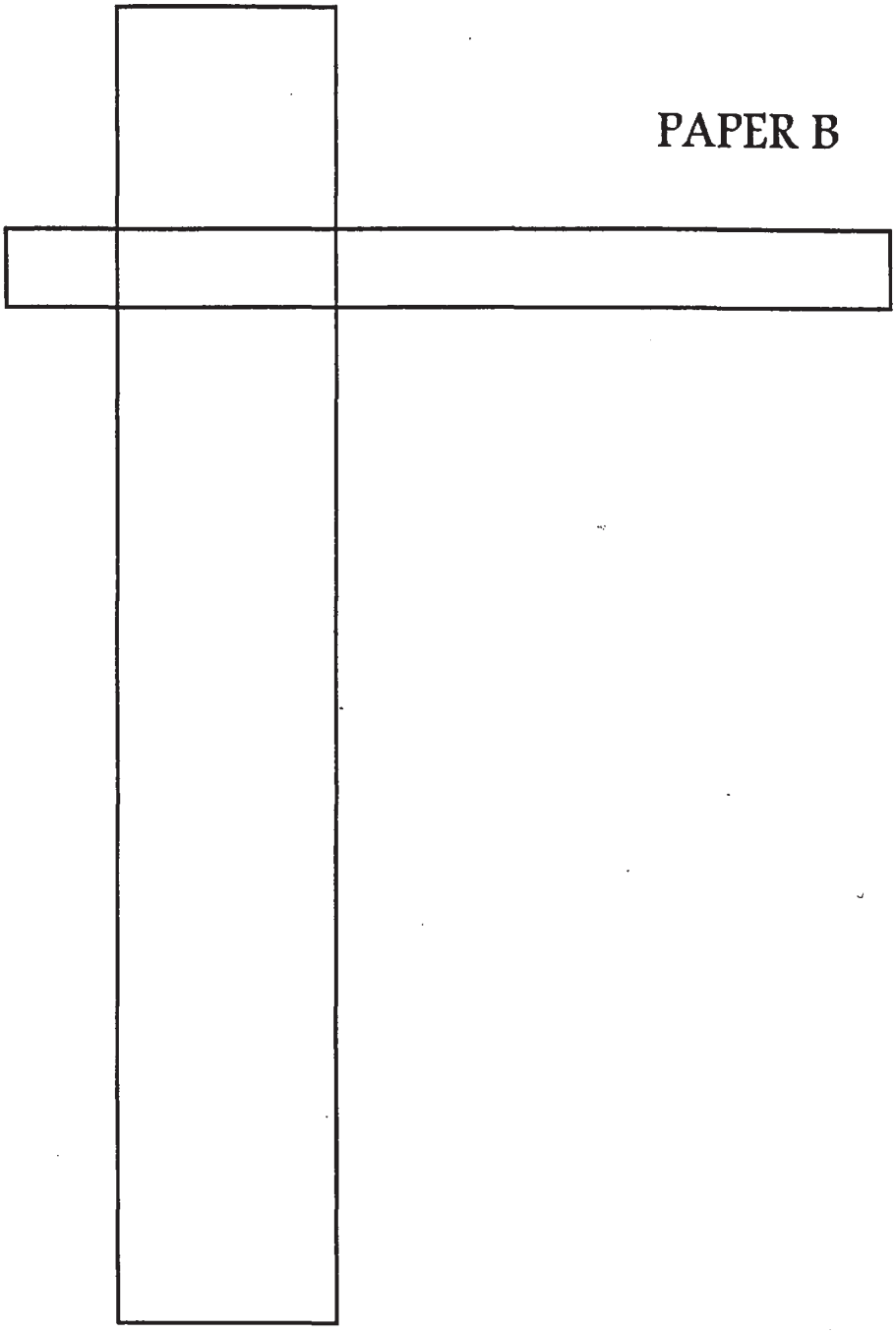

SPECTRUM FATIGUE TESTING AND RESIDUAL STRESS MEASUREMENTS ON NON-LOAD CARRYING FILLET WELDED TEST SPECIMENS

J. Bogren* and L. Lopez Martinez§

The influence of various spectrum parameters on fatigue life and residual stress relaxation has been studied in this investigation. Six spectra have been used. The spectrum parameters that have been varied are stress ratio R and irregularity factor I. The levels of the welding induced residual stresses in the as-welded condition are close to the yield stress of the material. These residual stresses were found to relax very rapidly. Within 8% of the total specimen life 50% or more of the initial stresses are relaxed. Large retardation effects were found for the spectrum with $R = 0$, compared to constant amplitude loading. The only spectrum parameter that had large influence on fatigue life was the stress ratio, R. The other parameter, the irregularity factor I, was of less significance.

INTRODUCTION

The investigation described in this paper is a sub-project within the Nordic project "Spectrum and Environmental Assisted Fatigue", in which more than 15 Nordic companies and institutes participate. This work is part of the Swedish contribution to the project. The purpose of the Nordic project is to improve the knowledge about life predictions under spectrum loading and to obtain more information about fatigue behaviour of welded structures at long lives, i.e. in the range from 10^6 to 10^8 cycles.

The aim of this particular work is to study the influence of various spectrum parameters on fatigue life. These parameters are irregularity factor I and stress ratio R. The influence of the above mentioned parameters on relaxation of welding induced residual stresses during spectrum loading is also studied.

* Structures Department, The Aeronautical Research Institute of Sweden, P.O. Box 11021, S-116 11 Bromma (Sweden)

§ Application Research and Development, SSAB Oxelösund AB, S-613 80 Oxelösund (Sweden)

EXPERIMENTAL PROCEDURES

Material and specimen

The material used for the majority of test specimens is a carbon-manganese steel, DOMEX 350 XP, and has a yield stress σ_y =370 MPa, ultimate tensile stress σ_{UTS} =470 MPa and an area reduction A_5 =28%. The specimens are taken in the rolling direction and the mechanical properties given above are in the same direction. The material is supplied by SSAB Tunnplåt in Borlänge. Mechanical properties of the filler material PZ 6130 are; σ_y =420 MPa, σ_{UTS} =500-570 MPa and A_5 =26%. A few specimens were manufactured using a high strength steel WELDOX 900. The mechanical properties of this material are; σ_y =1005 MPa, σ_{UTS} =1030 MPa and A_5 =14%. These were used for investigating the effect of using high strength steel. The WELDOX 900 material was supplied by SSAB in Oxelösund. More detailed information about the two materials can be found in Lopez Martinez and Korsgren (1).

The test specimen is shown in Figure 1. It has a non-load carrying fillet weld. This geometry has been used in many other investigations, e.g. Blom (2), Eide and Berge (3) and Berge and Eide (4). The geometry has four possible crack initiation sites denoted A, B, C and D, see Figure 1. The specimens used in this project are documented in (1), considering weld classification, geometry and weld defect distribution.

Residual stress measurements

In order to achieve good weld quality the surfaces of the specimens had to be slightly ground before welding. In order to remove the mill scale and to minimise the effect of the grinding, surface removal was done before the residual stress measurements were performed. The surface removal was achieved by electrolytic polishing and the depth of surface removal was between 0.1 - 0.2 mm depending on the condition of the surface.

The method used for measuring residual stresses was X-ray diffraction. The locations of the measurement points are shown in Figure 2. The radiated area was approximately 4x6 mm^2. Due to this the first point is defined to be located 2 mm away from the weld toe, i.e. where the centre of the radiated area was located. The second point was located 5 mm out from the weld toe, and the rest of the points were located 10 mm out from the previous point. In all cases the longitudinal stress component was measured.

Three measurements on five specimens have been performed. The first measurement was carried out in the as-welded condition. The second after a certain number of cycles, varying from 100 000 to 500 000 cycles. The criterion for

interrupting the fatigue test to perform the second residual stress measurement was that at least a load level of 80% of maximum load in the spectrum had been applied. After another 500 000 - 2 000 000 cycles a third measurement was carried out. The number of cycles run before each measurement are summarised in Table 1. An additional measurement was done on a specimen manufactured of the WELDOX 900 material. The purpose was to see the influence from the higher yield stress on the residual stress level in the as-welded condition.

TABLE 1- Number of cycles run before each residual stress measurement.

Max load, MPa	Spectrum	Measurement 1	Measurement 2	Measurement 3
210	SP 1	0	100 000	500 000
210	SP 2	0	100 000	500 000
175	SP 3	0	200 000	500 000
210	SP 4	0	500 000	2 000 000
210	VAMP	0	500 000	2 000 000

The error in the stress calculation method is typically about 10 MPa. The error in the location of the X-ray beam on the sample is approximately 1 mm and the measurements give a stress gradient in the longitudinal direction about 10 MPa/mm. This gives an additional error that is superimposed on the previously mentioned error. Thus a total estimated error for the measurements is about ± 20 MPa. A more thorough description of the residual stress measurements can be found in Bogren et al (5).

Spectrum description

In this investigation six different spectra have been used. As mentioned earlier one of the purposes was to investigate how various spectrum parameters influence fatigue life. The condition that all the spectra must fulfil is to have similar range-pair distribution as the spectrum used by Spennare and Samuelson (6), VAMP. A description of VAMP can be found in Bröndsted et al (7). The spectra constructed and used in the investigation are summarised in Table 2. The spectrum denoted SP 5 is the so-called Case Study spectrum and is derived from measurements on a railway bogie frame running in the Stockholm underground. This spectrum do *not* have the same range-pair distribution as the other five spectra.

TABLE 2 - Spectra used in the investigation.

Spectrum	Mean stress	Stress ratio	p	I	Block length
SP 1	$0.5\sigma_{max}$	0<R<0.9	1/6	0.3	500 000
SP 2	$0.5\sigma_{max}$	0<R<0.9	1/6	1.0	500 000
SP 3	0	R = -1	1/6	1.0	500 000
SP 4	-	R = 0	1/6	1.0	500 000
SP 5	$0.5\sigma_{max}$	0<R<0.9	1/6	0.45	296 346
VAMP	$0.5\sigma_{max}$	0<R<0.75	1/6	1.0	500 000

A randomised sequence was created within each block (SP 1 to SP 5) by employing a draw without replacement routine. The blocks were then repeated without reseed and restart until fracture occurred. This gives an entirely randomised sequence to failure. In the list above I, the irregularity factor, is defined as the number of positive mean crossings divided by the total number of cycles in one block and p is the ratio of minimum load to maximum load in an exceedance distribution according to the Swedish building code, BSK (8). In Figure 3 are the six spectra plotted in the same diagram for comparison.

Fatigue machines and load levels

All testing was conducted at laboratory conditions with servo hydraulic MTS fatigue machines. The maximum load capacity of the machines is ±1000 kN and ±250 kN, respectively. The load was applied in load control with constant displacement rate at an average frequency of 10-12 Hz. The majority of the tests were produced at maximum stresses, σ_{max}=350 MPa and 210 MPa. However, some of the tests were produced at other load levels.

RESULTS AND DISCUSSIONS

Relaxation of residual stresses due to fatigue loading

The measured residual stress levels in the as-welded condition are in the range of the yield stress of the base material, which was also found in (2,4). In Figure 4 individually measured residual stress data, for both materials, are plotted for all the measurements. The shape of the distributions is similar to the one measured in (4).

As mentioned above the relaxation of welding induced residual stresses has been studied on one specimen from each type of spectrum except SP 5, i.e. five specimens have been studied. In Figure 5 a typical relaxation process is shown. As can be seen in Figure 5 most of the relaxation takes place close to the weld toe where the stress concentration is the largest.

Figure 6 shows percentage relaxation of the initial residual stresses as function of percentage of total fatigue life and Figure 7 shows percentage relaxation of the initial residual stresses as function of number of cycles. The reference residual stress level is the level measured in the as-welded condition. Total life was reached when the specimen fractured completely. The data shown in Figures 6 and 7 are calculated from the measured residual stress values at a distance of 5 mm from the weld toe. As can be seen from Figure 6, 50% or more of the initial stress is relaxed within 8% of the total specimen life.

The following remarks can be made about residual stress relaxation and the different spectra. For the same maximum stress level (210 MPa), which also is the

maximum stress range in this case, SP 1 has the largest and fastest relaxation, see Figures 6 and 7. SP 3 that has R = -1 and even a wider maximum stress range ($\Delta\sigma_{max} = 350$ MPa), shows a much lower relaxation rate compared to the other spectra, based on percentage of total life. However, based on number of cycles all five spectra show approximately the same relaxation rate. The influence of the other parameter, irregularity factor I, on the relaxation process is not clear, but it seems to have only a minor influence.

Fatigue lives

The spectrum fatigue results are summarised in Table 3 and Figure 8. A mean regression line is calculated from the CA data in Table 3, assuming a straight $S-N$ line relationship, $\log N + m \log S = \log Const$. Data where $N_f > 2 \cdot 10^6$ are excluded. The two parameters became $Const = 1.398 \cdot 10^{12}$ and $m = 2.99$. The mean regression line with two parallel lines displaced two standard deviations (0.17 in log life) from the mean line are also plotted in Figure 8. In all subsequent calculations m was set equal to $m = 3$. In Table 3 the load intensity value C (Capacity) is calculated as well. This parameter can be calculated in two different ways,

$$C = \sum n_i (\Delta\sigma_i)^m \tag{2}$$

or

$$C = N(\Delta\sigma_{eq})^m \tag{3}$$

In the above equations n_i is the number of cycles at stress range $\Delta\sigma_i$, m is the slope of the SN-curve, $\Delta\sigma_{eq}$ is the equivalent stress range and N is the number of cycles at failure. The equivalent stress range is defined as:

$$\Delta\sigma_{eq} = \left[\frac{1}{N_b}\sum n_i (\Delta\sigma_i)^m\right]^{1/m} \tag{4}$$

where N_b is the block length. In Table 3 C was calculated using equation (3). For further information on the parameter C, see Samuelson (9).

TABLE 3- Summary of test results.

Company	Specimen nr	σ_{max} (MPa)	$\Delta\sigma_{eq}$ (MPa)	Spectrum	$N_f \cdot 10^{-6}$	Capacity $C \cdot 10^{-12}$	Comments
FFA	10	350	83.9	VAMP	2.178	1.286	RR
FFA	2	350	83.9	VAMP	2.330	1.376	RR
FFA	3	350	83.9	VAMP	2.156	1.273	RR
FFA	P336	350	83.9	VAMP	2.165	1.279	WX 900[1]

FFA	P340	350	83.9	VAMP	2.114	1.249	WX 900
FFA	P341	350	83.9	VAMP	2.859	1.688	WX 900
FFA	12	210	50.3	VAMP	9.895	1.259	RR[2]
FFA	20	210	50.3	VAMP	12.11	1.541	RR
FFA	25	210	47.4	VAMP	14.41	1.535	RR
FFA	49	210	50.3	VAMP	13.17	1.676	
FFA	P337	210	50.3	VAMP	13.23	1.684	WX 900
FFA	P338	210	50.3	VAMP	22.13	2.816	WX 900
FFA	P339	210	50.3	VAMP	16.82	2.141	WX 900
FFA	40	350	84.0	SP1	3.312	1.963	
FFA	42	350	84.0	SP1	2.744	1.626	
FFA	56	350	84.0	SP1	1.753	1.039	
FFA	52	210	50.5	SP1	22.79	2.935	
FFA	47	210	50.5	SP1	10.78	1.388	
FFA	24	210	50.5	SP1	9.194	1.184	
FFA	63	350	84.2	SP2	1.361	0.812	
FFA	64	350	84.2	SP2	1.167	0.697	
FFA	68	350	84.2	SP2	1.206	0.720	
FFA	350-14	350	84.2	SP2	1.770	1.057	
FFA	350-15	350	84.2	SP2	1.709	1.020	
FFA	50	210	51.6	SP2	33.01	4.535	
FFA	53	210	51.6	SP2	5.527	0.759	
FFA	61	210	51.6	SP2	10.41	1.430	
FFA	350-16	170	40.9	SP2	34.30	2.347	
FFA	46	350	176.3	SP3	0.216	1.184	
FFA	45	175	84.6	SP3	2.897	1.754	
FFA	62	105	50.9	SP3	65.00	8.572	Run-out
FFA	69	350	83.6	SP4	6.000	3.506	Run-out
FFA	48	210	50.2	SP4	57.19	7.235	
FFA	55	210	50.2	SP4	49.79	6.299	
FFA	350-24	350	49.6	SP5	7.263	0.886	
FFA	350-30	350	49.6	SP5	7.810	0.953	
ABB	37	350	83.9	VAMP	2.091	1.235	RR
ABB	27	350	83.9	VAMP	1.250	0.738	RR
ABB	8	350	83.9	VAMP	1.695	1.001	RR
ABB	17	210	50.3	VAMP	10.02	1.275	RR
ABB	4	210	50.3	VAMP	8.704	1.108	RR
ABB	1	210	50.3	VAMP	10.70	1.362	RR
ABB	26	350	84.1	SP2	1.160	0.690	
ABB	39	350	84.1	SP2	1.740	1.035	
ABB	66	250	60.1	SP2	5.200	1.129	
ABB	65	170	40.9	SP2	82.81	5.666	
ABB	75	170	40.9	SP2	24.00	1.642	
ABB	92-1	170	40.9	SP2	25.80	1.765	
ABB	92-3	170	40.9	SP2	62.00	4.242	
ABB	59	102	24.6	SP2	219.1	3.262	
ABB	350-18	102	24.6	SP2	510.0	7.592	Run-out
ABB	76	204	49.0	SP2	43.30	5.094	PWT[3]
ABB	77	204	49.0	SP2	16.40	1.929	PWT
ABB	78	204	49.0	SP2	32.40	3.812	PWT

ABB	92-4	165	23.2	SP5	73.05	1.819	
ABB	92-2	165	23.2	SP5	78.56	1.956	
ABB	350-17	165	23.2	SP5	68.61	1.708	
SP	9	350	83.9	VAMP	1.480	0.874	RR
SP	31	350	83.9	VAMP	3.210	1.896	RR
SSAB	16	250	250	CA	0.0752	1.175	
SSAB	18	250	250	CA	0.1069	1.670	
SSAB	350-7	250	250	CA	0.0891	1.392	
SSAB	350-8B	250	250	CA	0.0938	1.466	
SSAB	21	175	175	CA	0.2798	1.500	
SSAB	22	175	175	CA	0.2022	1.084	
SSAB	33	175	175	CA	0.2142	1.148	
SSAB	60B	175	175	CA	0.7693	4.123	
SSAB	34	125	125	CA	0.4668	0.912	
SSAB	43	125	125	CA	1.158	2.262	
SSAB	51	125	125	CA	0.6934	1.354	
SSAB	67	125	125	CA	0.7593	1.481	
SSAB	60A	125	125	CA	5.667	11.07	Run-out
SSAB	13	107	107	CA	1.144	1.401	
SSAB	11	107	107	CA	2.713	3.324	
SSAB	14	107	107	CA	4.008	4.910	Run-out
SSAB	350-6	90	90	CA	3.072	2.896	
SSAB	350-7A	90	90	CA	7.000	5.103	Run-out
SSAB	350-8A	90	90	CA	5.000	3.645	Run-out
VTT	5	375	93	VAMP	1.660	1.335	RR
VTT	32	365	90.4	VAMP	1.490	1.101	RR
VTT	7	381	92.7	VAMP	1.760	1.402	RR
VTT	6	337	79.8	VAMP	2.320	1.179	RR
VTT	15	230	46.9	VAMP	15.30	1.578	RR
VTT	30	229	46.3	VAMP	14.80	1.469	RR
NTH	1-S1	390	77.6	VAMP	3.609	1.685	RR
NTH	2-S1	401	74.6	VAMP	3.345	1.389	RR
NTH	3-S1	417	78.7	VAMP	3.162	1.541	RR
NTH	11-S2	244	44.5	VAMP	15.832	1.395	RR
NTH	12-S2	242	44.2	VAMP	11.301	0.976	RR
NTH	13-S2	242	44.2	VAMP	11.969	1.034	RR

[1]WX 900 = WELDOX 900 all other specimens DOMEX 350
[2]RR = Round Robin calibration tests
[3]PWT = Post Weld Heat treatment

The scatter in fatigue lives for the different spectra are not large at the higher stress level. However, at the lower stress level there is a considerable amount of scatter. SP 2 shows the largest amount of scatter within the same type of spectrum. At the lower stress level there is a factor of six in difference between the specimens with the longest and the shortest lives. An explanation to this could be a favourable weld geometry, considering weld toe angle and root radius. SP 4 with $R = 0$ shows the longest lives of the studied spectra. This is in agreement with other investigations, e.g. (2,4). The specimen run at the lowest stress level ($\sigma_{max} = 105$ MPa) with SP 3

shows a surprisingly long life. The reason for this could be a power failure during the test, resulting in some unknown amount of overloading with subsequent retardation effect. The influence on the fatigue life of the other spectrum parameter, the irregularity factor I, is of less significance. The specimens made of the high strength steel did not show any significant increase in fatigue strength compared to the medium strength steel. The influence from the PWT is negligible.

In order to investigate the amount of load interaction in the tests, predictions using the Palmgren-Miner rule has been performed,

$$d = \sum \frac{n_i}{N_i} \tag{5}$$

with the failure criterion $d = 1$. The predictions are based on constant amplitude data given in Table 3. The results from these calculations are given in Table 4. In this table N_t is the test specimen life. N_p and N_{pf} are predicted lives with equation (5) without and with a fatigue limit, respectively. The fatigue limit at constant amplitude testing was set to 60 MPa at $6.6 \cdot 10^6$ cycles, and at this point the slope of the $S-N$-curve changes to $k_2 = 5 = (2m-1)$. These assumptions are the same as in (6). For all cases where more than one specimen was run the logarithmic mean value of N_t is used in the calculations.

TABLE 4 - Life ratios calculated without and with fatigue limit, respectively.

Spectrum	$\Delta\sigma_{max}$, MPa	N_t/N_p	N_t/N_{pf}
SP 1	350	1.02	1.02
SP 1	210	1.19	0.91
SP 2	350	0.59	0.59
SP 2	210	1.80	1.39
SP 2	170	2.09	1.25
SP 2	102	4.09	1.08
SP 3	700	0.45	0.45
SP 3	350	1.17	1.17
SP 3	210	>5.9	>4.6
SP 4	350	>2.4	>2.4
SP 4	210	4.78	3.58
SP 5	350	0.63	0.50
SP 5	165	0.67	0.28
VAMP	350	0.98	0.98
VAMP	210	1.33	1.07

With the exceptions of the highest stress levels for SP 2, SP 3 and both stress levels for SP 5 the Palmgren-Miner rule underestimates the fatigue life under spectrum loading. The life ratios for the lowest level of SP 2 and both levels of SP 4 are very large. For SP 4, is this according to what has been observed elsewhere (2,4). When using a fatigue limit in the calculations, the life ratios tends towards

unity. The highest stress level is not influenced by the fatigue limit, except for spectrum SP 5. Equation (5) gives highly unconservative results for spectrum SP 5.

CONCLUSIONS

From this investigation the following conclusions can be drawn:

Influence on fatigue life of other spectrum parameters than stress ratio are of less importance.

Within 8% of the total specimen life 50% or more of the initial residual stresses, whose magnitude is close to yield stress, are relaxed.

The spectrum with R = -1 shows a slower relaxation rate compared to the other spectra, based on percentage of total life. Based on number of cycles all five spectra show almost the same relaxation rate.

The spectrum with R = 0 shows much more retardation than the other spectra.

Life ratios, tested to predicted life, are in the range of 0.3 - 5.

Post welding heat treatment is probably not cost effective as residual stresses are found to relax very quickly anyhow.

ACKNOWLEDGEMENTS

The authors are indebted to Mrs Torvald Linderoth, Lennart Nystedt and Bengt Wallstenius for performing the fatigue tests and Mr Mats Brunnberg for the residual stress measurements.

REFERENCES

(1) Lopez Martinez, L. and Korsgren, P, "Characterization of Initial Defect Distribution and Weld Geometry in Welded Fatigue Test Specimens", Proceedings of the Conference "Fatigue Under Spectrum Loading and in Corrosive Environment". Edited by A. F. Blom, EMAS Ltd., Warley, England, 1993.

(2) Blom, A. F., "Fatigue Strength of Welded Joints Subjected to Spectrum Loading", Jernkontoret, Stockholm, Report No. 41-02, 1987.

(3) Eide, O. I. and Berge, S., "Cumulative Damage of Longitudinal Non-Load Carrying Fillet Welds", Proceedings of the Conference "Fatigue '84". Edited by C. J. Beevers, EMAS Ltd., Warley, England, 1984.

(4) Berge, S. and Eide, O. I., "Residual Stress and Stress Interaction in Fatigue of Welded Joints", Residual Stress Effects in Fatigue, ASTM STP 776. American Society for Testing and Materials, 1982.

(5) Bogren, J., Lopez Martinez, L and Brunnberg, M., "The Influence of Various Spectrum Parameters on Fatigue Life and Residual Stress Relaxation", The Aeronautical Research Institute of Sweden, Bromma, FFA TN 1991-44.

(6) Spennare, H. and Samuelson, J., "Spectrum Fatigue Testing of a Longitudinal Non-Load Carrying Fillet Weld - A Round Robin Exercise", Jernkontoret, Stockholm, Report 7317/89, 1990.

(7) Bröndsted, P., Slind, T. and Solin, J. P., "Fatigue Testing Using Offshore Load Spectrum", in Steel in Marine Structures. Edited by C. Noordhoek and J. de Back, Elsevier, Amsterdam, 1987.

(8) BSK, Bestämmelser för stålkonstruktioner (Regulations for Steel Structures, part of the Swedish Building Code), Statens Planverk och AB Svensk Byggtjänst (in Swedish), 1987.

(9) Samuelson, J., "Fatigue Design of Vehicle Components: Methodology and Applications", Department of Aeronautical Structures and Materials, The Royal Institute of Technology, Sweden, Report No. 88-23,1988.

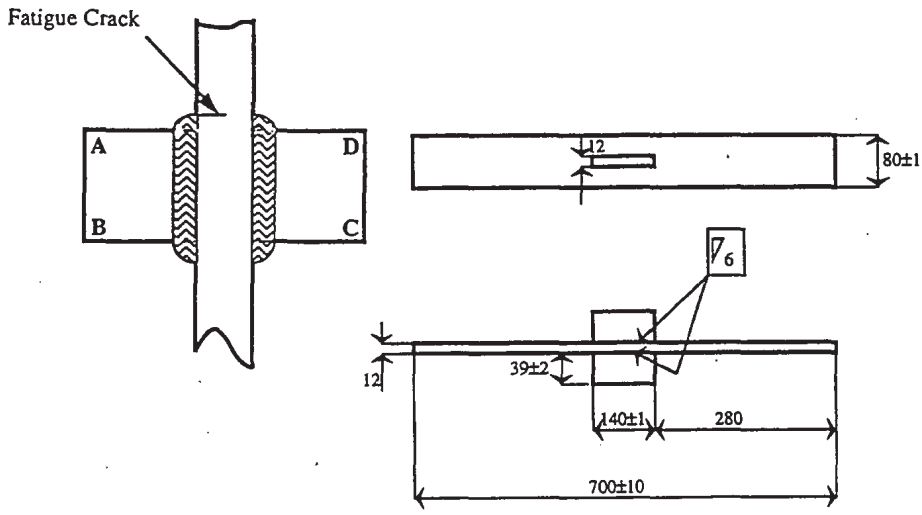

Figure 1 Test specimen and possible crack initiation sites. All dimensions in mm

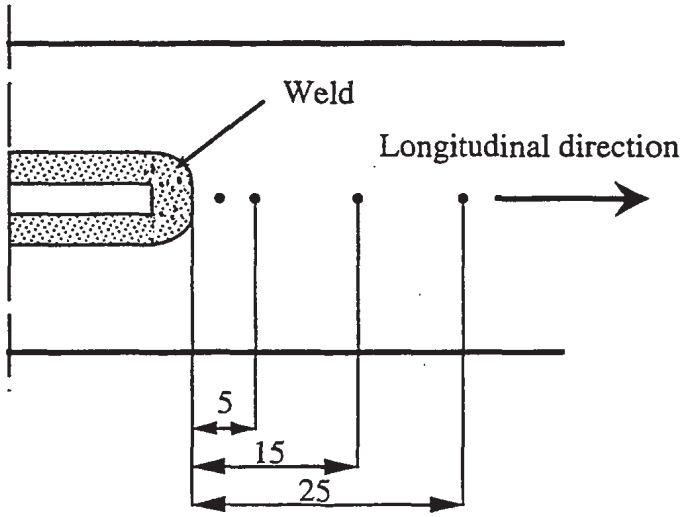

Figure 2 Locations of residual stress measurement points

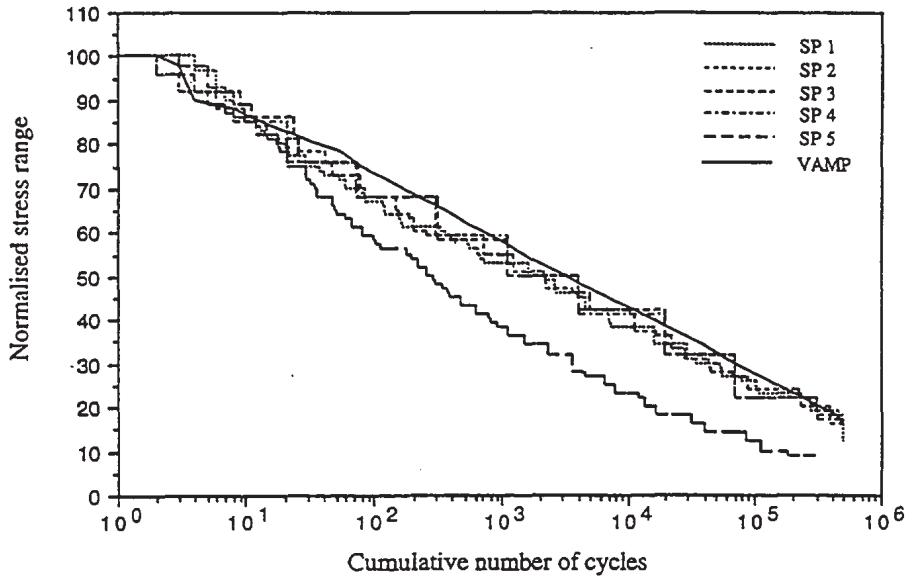

Figure 3 Range-pair distributions for the six spectra used

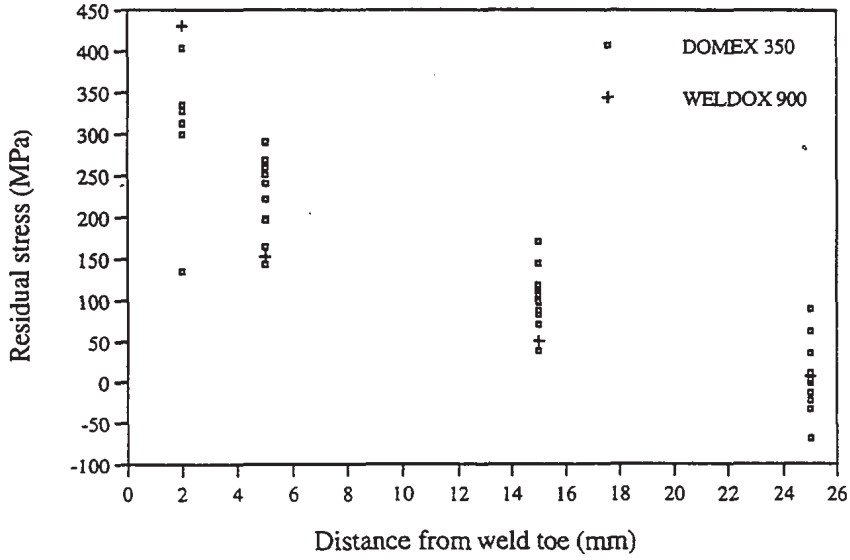

Figure 4 All residual stress data from all specimens. As-welded condition

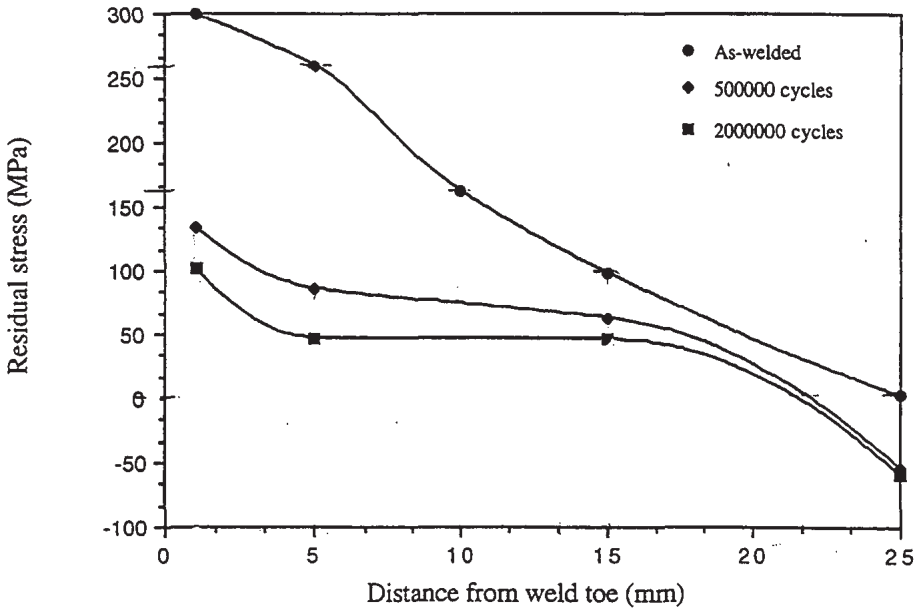

Figure 5 Typical relaxation process. Specimen 48, crack site D

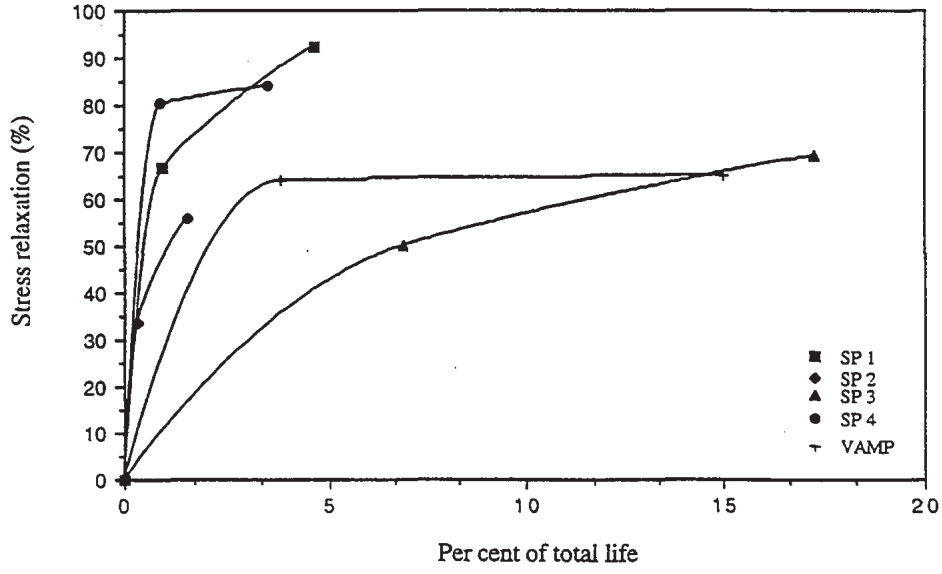

Figure 6 Residual stress relaxation versus percentage of life

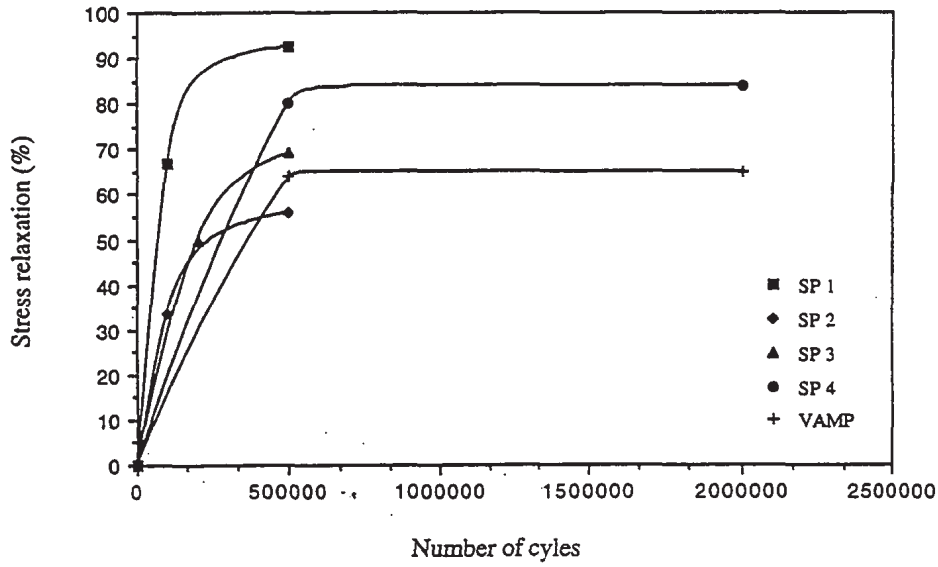

Figure 7 Residual stress relaxation versus number of cycles

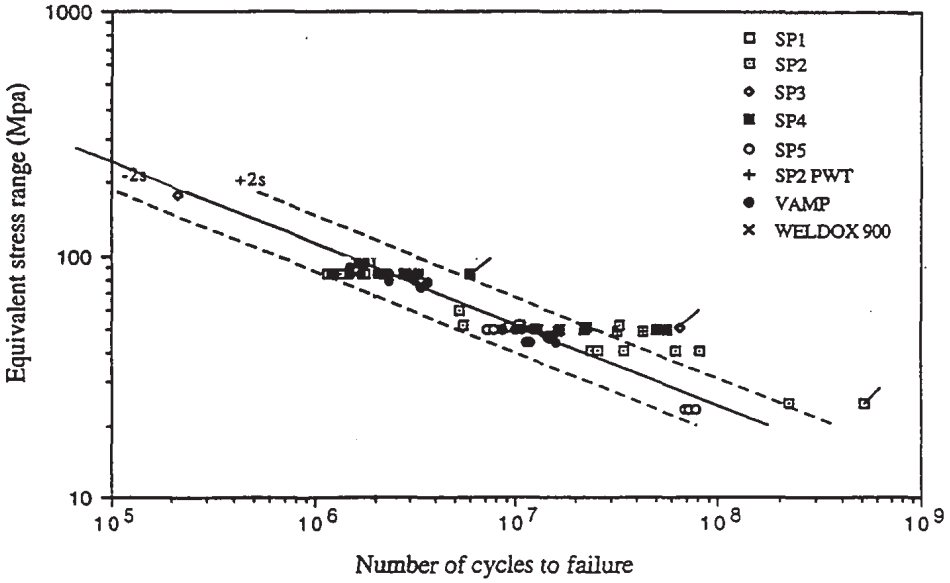

Figure 8 Spectrum test results

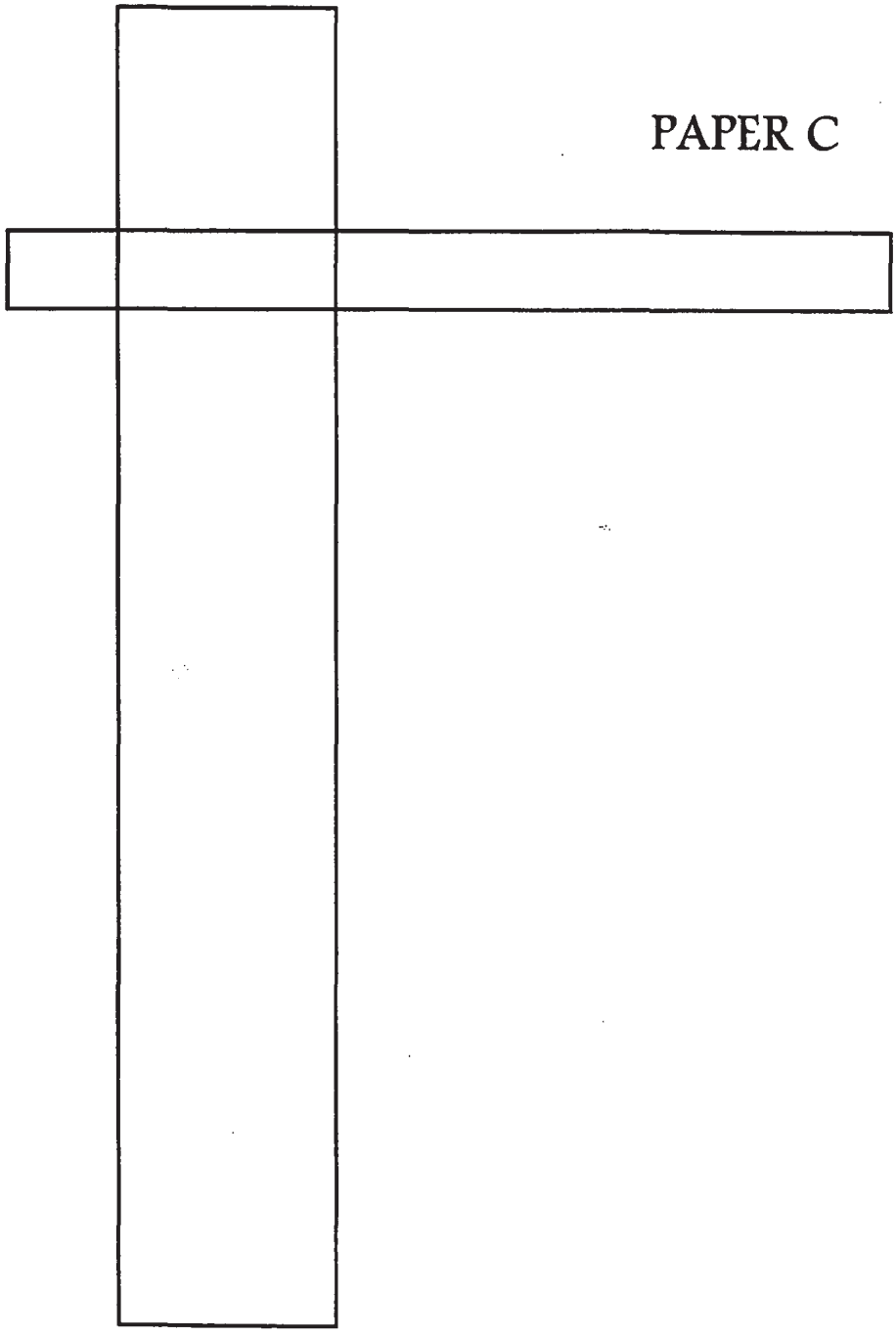

PAPER C

INVESTIGATION OF RESIDUAL STRESSES IN AS-WELDED AND TIG-DRESSED SPECIMENS SUBJECTED TO STATIC/SPECTRUM LOADING

L. Lopez Martinez* , R. Lin**, D. Wang** and A. F. Blom ***

This paper deals with measurements of residual stresses by neutron diffraction in several conditions. Both the as-welded and the TIG-dressed conditions are studied. The relaxation of weld-induced residual stresses is investigated by removing the test specimens and performing measurements during spectrum fatigue loading as function of number of load cycles. Neutron diffraction results are also compared to ultrasonic 3D-measurements as well as to χ-ray diffraction results on the surface.

INTRODUCTION

Together with stress concentrations and weld defects, residual stress fields are one of the determinant parameters controlling the fatigue strength of welded joints (1). In normal fatigue design the level of residual stresses is unknown and therefore it is assumed that this level is in the same order as the yield strength of the filler metal. This fact leads to the assumption that the entire stress range, irrespective of stress ratio, produces fatigue damage. Residual stress distributions are also influenced by other parameters such as metallurgical properties, the welding technique used, and the heat input, Legatt (2).

The change of residual stress distribution through the thickness by relaxation is a main factor influencing fatigue crack growth in welded components. For current fracture mechanics modelling an understanding of relaxation and redistribution of residual stresses is of vital interest.

* SSAB Oxelösund AB, S-613 80 Oxelösund, SWEDEN
** Studsvik Neutron Research Laboratory, S-611 82 Nyköping, SWEDEN
*** FFA, P.O. Box 11021, S-161 11 Bromma, SWEDEN

The present paper deals with residual stresses in welded fatigue test specimens. It is a part of the present Nordic program which aims at improving fatigue design/assessment for high-strength steels. By neutron diffraction and χ-ray diffraction, residual stress distributions in as-welded and TIG-dressed specimens were non-destructively measured. In addition, the effects of both static and spectrum fatigue loading were evaluated. Results are also compared to ultrasonic 3D-measurements.

MATERIALS AND FATIGUE TESTING

The material used in this investigation has strength properties and chemical composition shown in Table 1. For more details, see reference (1).

TABLE 1- Chemical compositions and tensile properties of steel

Chemical composition (wt%)							Yield strength (MPa)	Tensile strength (MPa)	Nominal strength (MPa)
C	Si	Mn	P	S	Al	Nb			
0.09	0.21	1.63	0.11	0.02	0.03	0.024	615	747	590

Spectrum fatigue testing and static loading were performed on specimens with a longitudinal fillet welded attachment also used in other investigations (3), see Fig.1. The spectrum type is the same as used earlier , SP2 (R=0-0.77), which is a straight line range-pair counted spectrum and with I=1.0. The maximum applied stress, σ_{max}, in the test spectrum was chosen to be the same as the selected static load, i.e. 250 MPa. This value was chosen to produce plastic deformation in the vicinity of the weld root. The fatigue tests were carried out at FFA in Stockholm.

The welding procedure was MAG with 1.6 mm electrode, current of 185 Amp (DC), voltage = 23.5 Volt and heat input approximately 1.5 kJ/mm with consumable PZ 6130 (Mison 25), performed without pre-heating. The welds on the sides of the attachments as well as at the corners have been produced in an alternating diagonal sequence in order to limit the interpass temperature (<250° C), as well as specimen distortion.

Since all specimens have been produced in the same way, the residual stress fields should have very similar pattern and, therefore, should be repre-

sentative also for the rest of the specimens tested within the Nordic programme for the same steel.

RESIDUAL STRESS MEASUREMENTS

Neutron diffraction measurements of residual stress were carried out with the REST diffractometer at the R2 reactor in Studsvik. The technique uses atomic interplanar spacing as internal strain gauge and measures changes in the interplanar spacing due to stresses. Strains are then calculated by the following equation:

$$\varepsilon_{hkl} = \frac{d_{hkl} - d^0_{hkl}}{d^0_{hkl}} \qquad (1)$$

where d_{hkl} and d^0_{hkl} are the stressed and the stress-free interplanar spacing, respectively.

If the three principle strain components, ε_i , are obtained, residual stresses can be derived using Hooke's law:

$$\sigma_i = \frac{E_{hkl}}{1+\nu}\left[\varepsilon_i + \frac{\nu}{1-2\nu}\sum \varepsilon_j\right] \qquad (2)$$

where σ_i, i=1 to 3, are the three principle stress components; E_{hkl} and ν are the Young's modulus and Poisson's ratio, for the corresponding crystallographic orientation, respectively. Only longitudinal stresses are presented in this paper as they play a dominant role in fatigue life for the component.

Residual stress distributions were measured in the as-welded and TIG-dressed specimens. The specimens were then subjected to fatigue spectrum loading and residual stress measurements were performed after 500.000 and 2.000.000 cycles. Residual stress distributions were also measured in two other specimens before and after static loading up to 250 MPa.

The locations for stress measurements are shown in Figs 2 and 3. At these locations both the level of residual stresses and subsequent relaxation were expected to be pronounced. The first cross section, indicated by "A", was chosen to be near the weld toe and was 13 mm from the end of the attachment. Fatigue failure was mostly confined to this cross section for the as-welded

specimens. The second cross section, named "B", was prone to fatigue failure for the TIG-dressed specimens. The last cross section "C" was at the mid-width of the plate. Strains parallel to the specimen's natural co-ordinates, i.e. the longitudinal, transverse and normal directions, were obtained and were assumed to be the principle directions. Residual stresses were therefore calculated from the measured strains using Eq.(2), with Young's modulus E_{hkl} =225 Gpa and a Poisson's ratio ν= 0.285. Both were calculated from Fe single crystal elastic constants by the Kröner model.

The specimen geometry indicates a symmetrical stress field about the mid-plane and about the mid-width, which was confirmed by preliminary neutron diffraction measurements and by X-ray diffraction measurements at the surface. Therefore, only through half-thickness stress distributions were mapped. The incident slit, which defines the size of the incoming neutron beam, was 2 mm wide and 2 mm high. With a receiving slit of 2 mm width, the spatial resolution in all the three directions can be approximated to about 2 mm.

The stress-free lattice spacings were obtained by measuring on small coupons cut from different locations in an as-welded plate and an as-welded and TIG-dressed plate. They were cross checked by measuring, in each specimen, a location which was far away from the weld. Standard deviations in strains were typically smaller than $\pm 1 \times 10^{-4}$, calculated from uncertainties in peak fitting. The resulting errors in residual stresses are less than ±25 MPa. These errors are caused from uncertainties in peak fitting, gage volume and metallurgical changes in the heat affected zone.

RESULTS AND DISCUSSIONS

Residual stresses due to welding

Tensile residual stresses were observed in both A and B sections in the as-welded specimen, see Fig. 4. The maximum stress, close to the yield strength of the material, was found near the surface at the weld toe. It decreases with increasing distance from the weld toe and from the surface.

Influence of TIG-dressing on distribution of welding residual stresses

The application of TIG-dressing on the weld toe has a strong effect on the local stress distribution. As is shown by comparing Fig. 4a to Fig. 5a, the tensile

stress peak was shifted from near surface to subsurface and the maximum stress was increased from 556 to 699 MPa. As result, much lower tensile stress was found near the surface. This is consistent with χ-ray diffraction measurements at the surface where tensile stress was decreased from 360 to 256 MPa by the TIG-dressing operation. These results confirm the hypotheses that TIG-dressing increases fatigue resistance not only by improving weld geometry, i.e reducing the stress concentration factor, but also by reducing the tensile residual stress near the surface.

At the TIG-dressed edge, the tensile stress was increased near the surface while the compressive stress near the specimen edge became larger, compare Fig. 5b and Fig. 4b.

Relaxation by static load

As the weld toe, where max. stress concentration is found, is already at the yield point of the weld metal, σ_{ywm}, static tensile loading, σ_{max}, would cause local plastic deformation and the stresses in the weld remains at yield level, σ_{ywm}, while the surrounding stress field changes to accommodate the applied load. When the applied load is removed, the residual stress distribution was altered to the level shown in Fig. 6 for the as-welded condition and in Fig. 7 for the TIG-dressed condition. The maximum residual stress was decreased by 200 MPa for the as-welded specimen and 130 MPa for the TIG-dressed specimen.

Relaxation under variable amplitude fatigue testing

It follows , therefore, that if σ_{max} is repeatedly applied, i.e. fatigue loading ranging from zero to σ_{max}, the actual stress will cycle between a minimum value of $\sigma_{ywm} - \sigma_{max}$ and a maximum value of σ_{max}. i.e. at a range equal to the nominal range applied, but with a mean value different from that calculated from $\sigma_{max}/2$. In the case of variable amplitude fatigue testing we are not cycling from 0 to σ_{max} every cycle so the situation changes drastically. Only a few times the σ_{max} is applied at every block of $5x10^5$ cycles so the change of residual stresses in the surrounding field to accommodate the applied load is mostly influenced by the level of σ_{max} on each block. In Fig 8 we present the results for relaxation studies in the as-welded condition and in Fig. 9 for TIG-dressed conditions. Most of the relaxation occurs early during the fatigue load sequence. For the following fatigue load intervals we can see that relaxation occurs as redistribution of the residual stress field.

Correlation with χ-ray diffraction measurements

Residual stresses in the surface of the as-welded and the TIG-dressed specimens were also measured by χ-ray diffraction. The results are presented in Fig. 10 and 11, together with measurements done by neutron diffraction at 1 mm depth. It should be noted that the χ-ray measurements reveal stresses in a very thin surface layer while the neutron diffraction measurements show average stress in a 2^3 mm^3 gauge volume, thus they are not directly comparable.

Correlation with acoustic diffraction measurements

The results from neutron diffraction measurements at A-location for the longitudinal stress at mid-thickness can only be correlated to measurements carried out by acoustic diffraction, ultrasonic waves. Such measurements are presented in detail by Kudriavtsev et al (4). However, these measurements were performed on DOMEX 350 steel, so a direct comparison is not possible. Yet, it is interesting to note that both these 3D techniques present similar trends in the shape of the mid-plane residual stress distribution, see Figs 12 and 13. More work is needed to fully understand the total complex 3D residual stress fields.

CONCLUSIONS

Large longitudinal tensile stresses in the order of yield levels were found at the surface close to the weld toe. TIG-dressing was shown to shift the tensile stress peak into the depth of the specimens.

Relaxation studies have shown that a static load applied did relax residual stresses as expected. The applied variable amplitude loading did show the same degree of relaxation as the static load case. This relaxation occurs early during the fatigue loading and is correlated to the occurrence of maximum load in the spectrum.

Good agreement in residual stress shape was been found for the measurement methods studied. However, the magnitudes were found to be different for different methods. The exact reason for this is not yet fully understood, but is probably due to several factors.

It is interesting to notice that the different results from the three methods were obtained by very well known laboratories (Studsvik Neutron Research Laboratory for neutron diffraction, Linköping Institute of Technology for χ-ray diffraction, and Paton Electric Welding Institute, Kiev, for ultrasonic

measurements). Yet, the mentioned difference still exists. Thus, any data interpretation should be somewhat cautious until a more complete understanding is obtained.

ACKNOWLEDGEMENTS

This work was financially supported by NI (Nordic Industrial Foundation), NUTEK (Swedish National Board for Industrial and Technical Development), SSAB, and FFA. The authors are indebted to Mr. Bengt Wahlstenius (FFA) for performing the fatigue tests and Mr Tommy Linden (SSAB Oxelösund AB) for performing welding and TIG-dressing.

REFERENCES

(1) Lopez Martinez, L. and Blom A.F. "Influence of life improvement techniques on different steel grades under fatigue loading", Fatigue Design 95 Proceedings, Espoo, Finland, Edited by G. Marquis, 1995.

(2) Legatt, R. "Welding Residual Stresses", ICRS 5, June 16-18, 1997, Linköping, Sweden.

(3) Bogren, J., Lopez Martinez, L. "Spectrum fatigue testing and residual stress measurements on non-load carrying fillet welded test specimens" Proceedings of the Nordic Conference on Fatigue. Edited by A.F. Blom, EMAS Publishers, West Midlands, England, 1993.

(4) Kudriavtsev, Y. et al "Measurement of residual stresses in welded specimens containing non-load-carrying fillet welds in as-welded condition and after TIG-dressing", Test report 201/3, Kiev 1996.

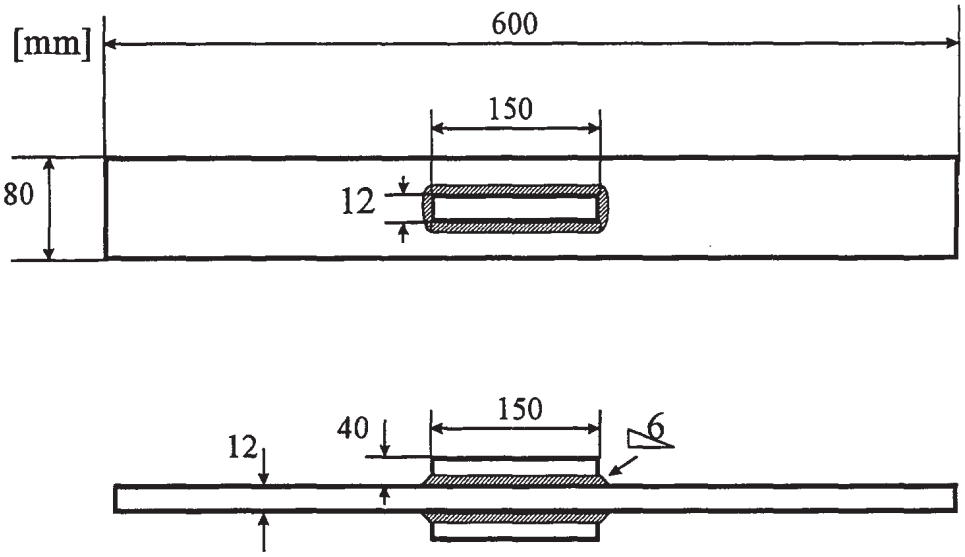

Figure 1 Fatigue test specimen

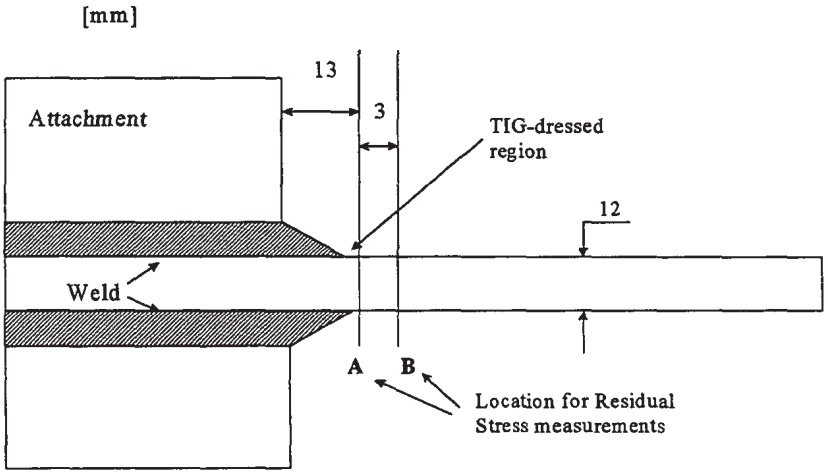

Figure 2 Specimen mid-section showing location for residual stress measurements

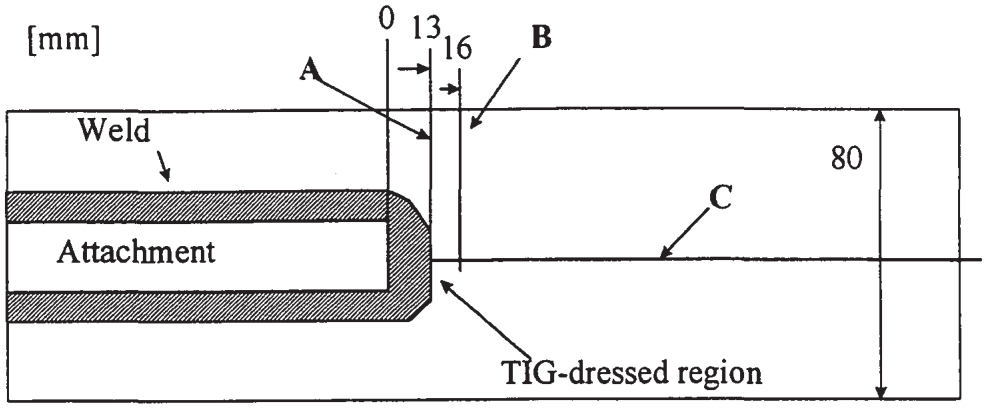

Figure 3 Upper view showing fatigue test specimen with locations for residual stress measurements

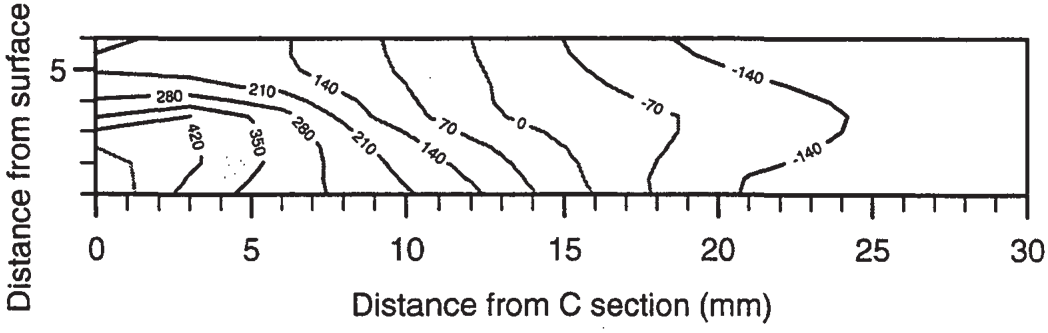

Figure 4a Longitudinal residual stress distribution in A-section of as-welded specimen

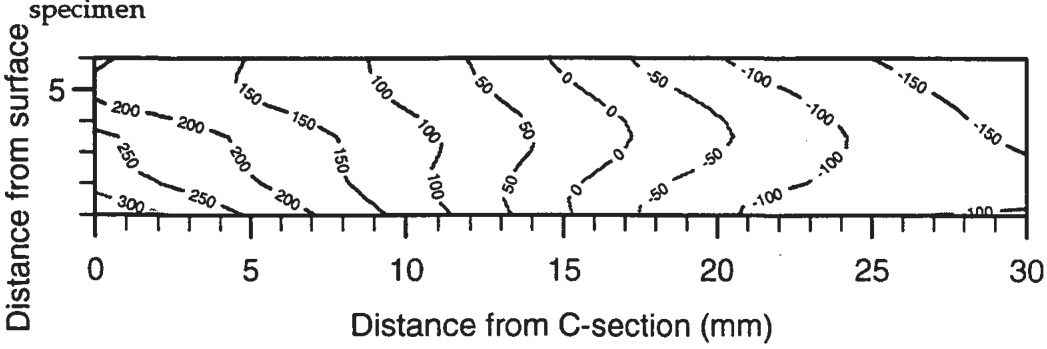

Figure 4b Longitudinal residual stress distribution in B-section of as-welded specimen

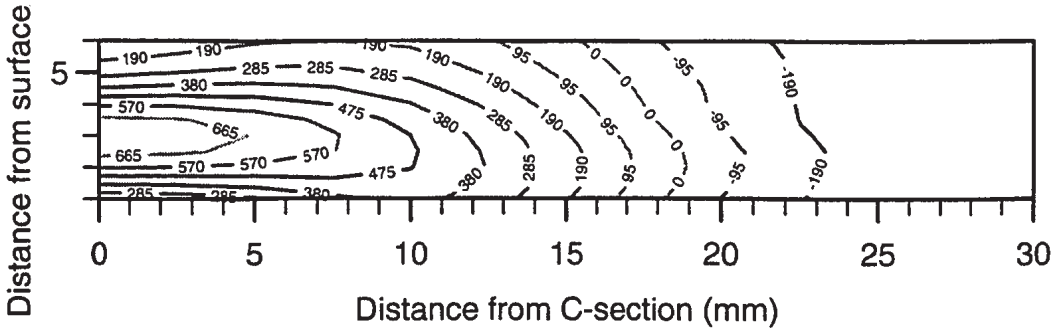

Figure 5a Longitudinal residual stress distribution in A-section of TIG-dressed specimen

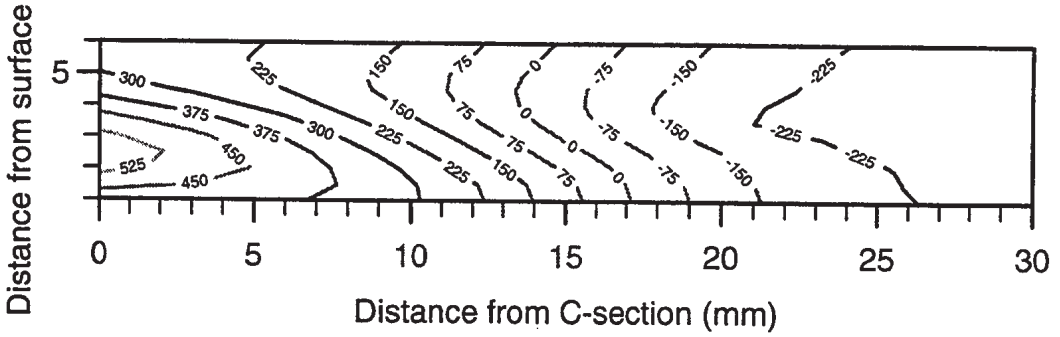

Figure 5b Longitudinal residual stress distribution in B-section of TIG-dressed specimen

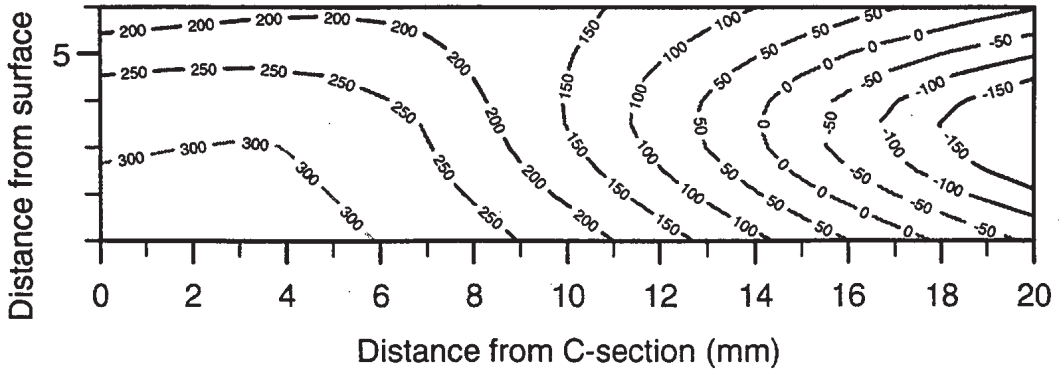

Figure 6 Longitudinal residual stress distribution in A-section of as-welded specimen following static loading

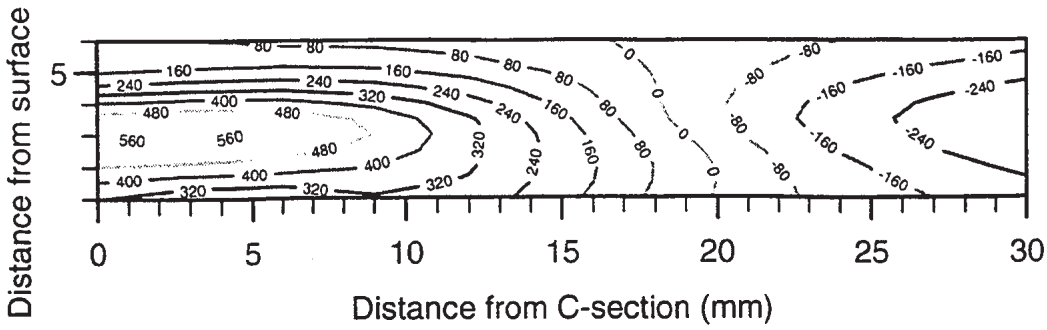

Figure 7 Longitudinal residual stress distribution in A-section of TIG-dressed specimen following static loading

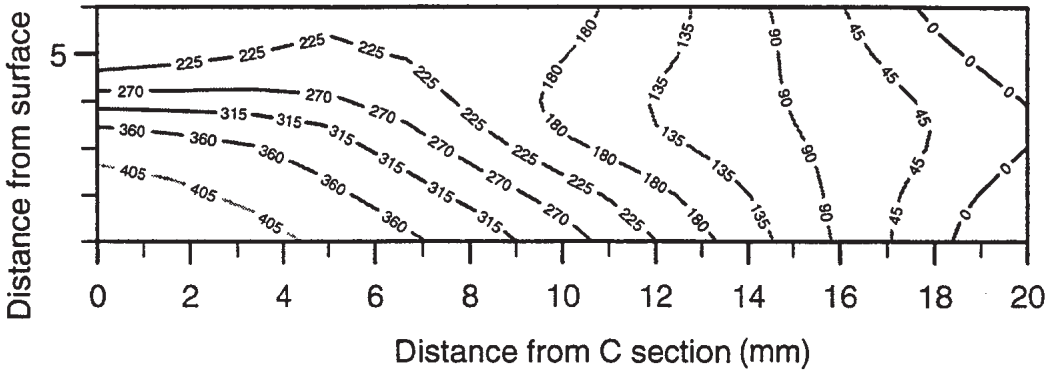

Figure 8a Longitudinal residual stress distribution in A-section of as-welded specimen after 500.000 cycles of spectrum loading

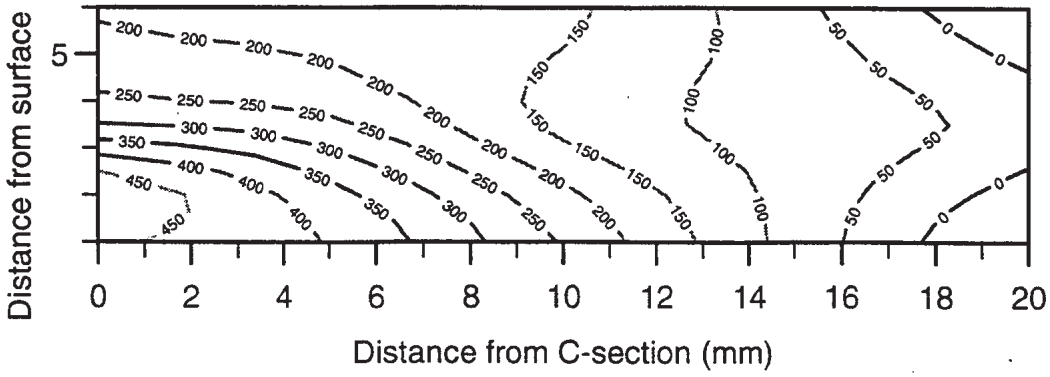

Figure 8b Longitudinal residual stress distribution in A-section of as-welded specimen after 2 million cycles of spectrum loading

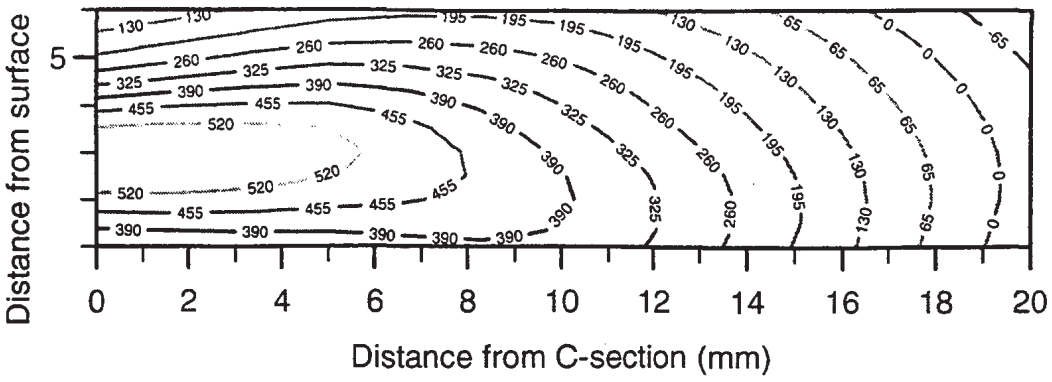

Figure 9a Longitudinal residual stress distribution in A-section of TIG-dressed specimen after 500.000 cycles of spectrum loading

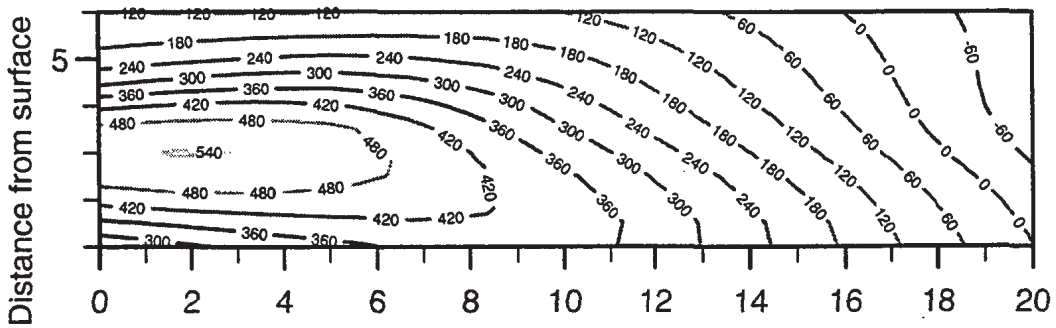

Figure 9b Longitudinal residual stress distribution in A-section of TIG-dressed specimen after 2 million cycles of spectrum loading

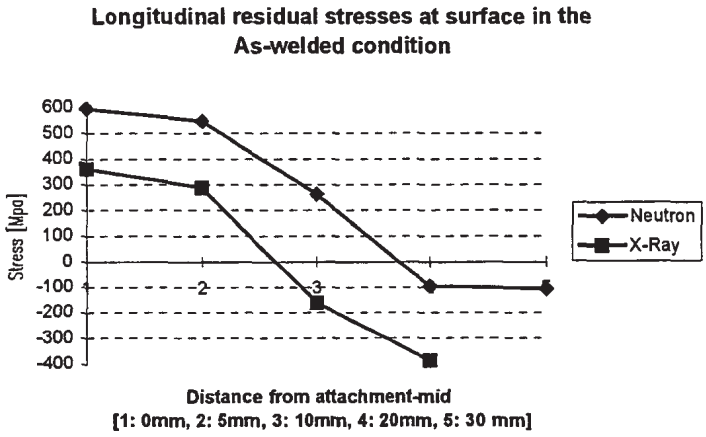

Figure 10 Measurement results at near surface: Neutron diffraction at 1 mm depth and χ-Ray diffraction at 10μ depth .

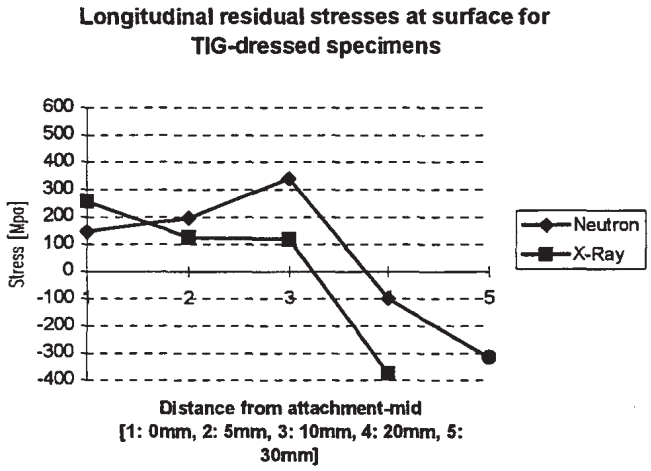

Figure 11 Measurement results for the TIG-dressed condition

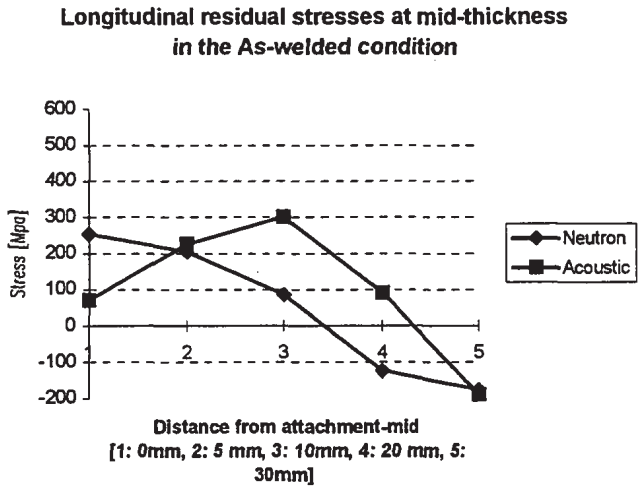

Figure 12 Measurements at mid-thickness: as-welded condition. Neutron diffraction data for 590 steel, ultrasonic data for 350 steel

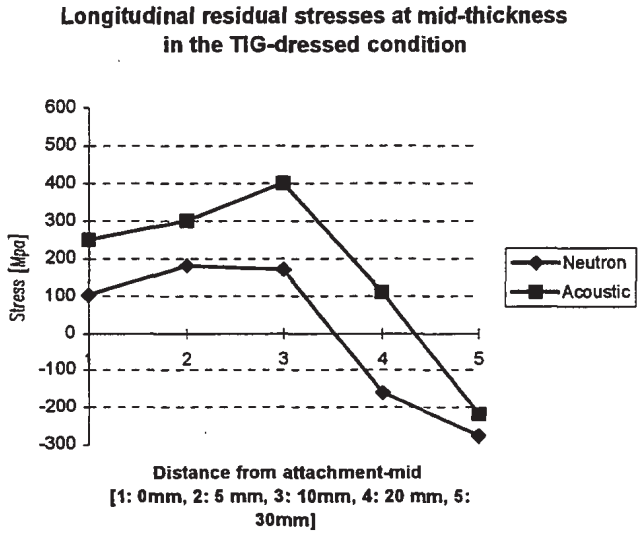

Figure 13 Measurements at mid-thickness: TIG-dressed condition. Neutron diffraction data for 590 steel, ultrasonic data for 350 steel

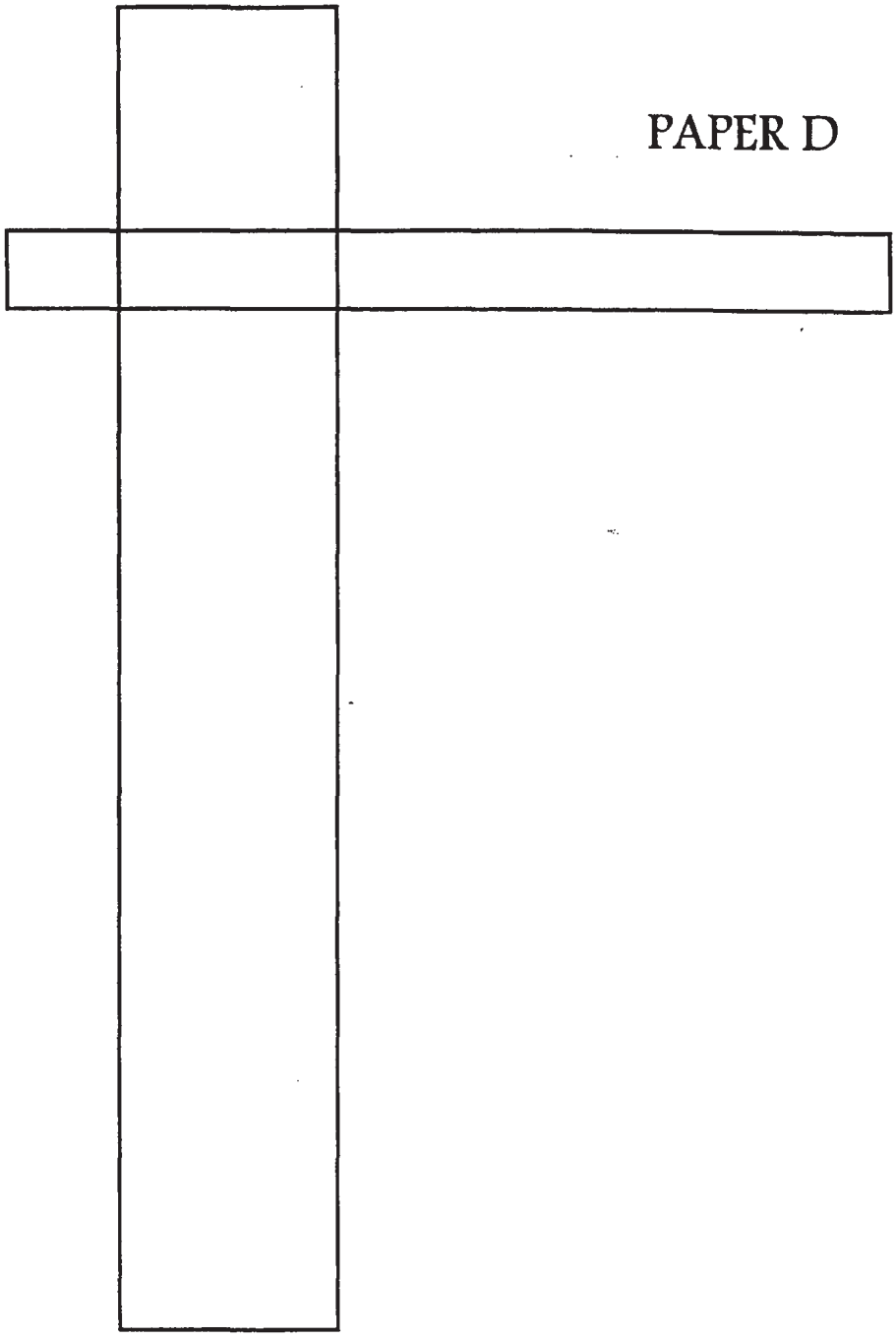

PAPER D

FATIGUE BEHAVIOUR OF STEELS WITH STRENGTH LEVELS BETWEEN 350 AND 900 MPa- INFLUENCE OF POST WELD TREATMENT UNDER SPECTRUM LOADING

L. Lopez Martinez* , A. F. Blom**, H. Trogen*** and T. Dahle****

The object of this paper is to summarize experimental results from an inter-Nordic project concerning spectrum fatigue of improved welded components. Steels with strength levels of 350 - 900 MPa were used both for constant amplitude and spectrum loading. Improvement techniques included shot peening, hammer peening, ultrasonic peening and TIG-dressing. Mean life improvements were obtained up to a factor of two in terms of applied stress.

INTRODUCTION

Two Nordic projects carried out under the last decade have produced a considerable number of fatigue test results under both constant amplitude and spectrum loading. The second of these projects, summarised in the current proceedings, include results for several parent plate strength levels as well as different fatigue life improvement techniques and combinations thereof for certain parent plate qualities.

Fatigue life improvement techniques studied and presented in the archival literature have shown a considerable degree of improvement on the fatigue strength of welded joints. Most, in fact almost all, of these investigations have been performed under constant amplitude loading where an effect of parent plate yield strength has been observed. Higher strength steels would

* SSAB Oxelösund AB, S-613 80 Oxelösund, SWEDEN
** FFA, P.O. Box 11021, S-161 11 Bromma, SWEDEN
*** SSAB Tunnplåt AB, S-781 84 Borlänge, SWEDEN
**** ABB Corporate Research, S-721 83 Västerås, SWEDEN

normally show better fatigue life improvement, largely due to the larger magnitude of compressive stresses possible to introduce in these steels. However, under realistic service conditions the loading, for the vast majority of load carrying structural components, is not constant amplitude. Since spectrum loading necessarily will cause redistribution of the residual stress fields once the nominal stress times the local stress concentration factor at the root of the weld will exceed yielding, see Ref. (1) for details, it is not at all obvious that the effects of post weld treatment seen under constant amplitude loading can be transferred to the case of real service conditions.

Three categories of improvements techniques exist, i.e. those which impose beneficial compressive stresses at the weld hot spot, those which improve the geometrical shape of the weld toe and combinations of these two. Also, several of these methods will also reduce the size of the local flaw population.

In the present paper we present fatigue data for a range of materials, obtained both underconstant amplitude loading as well as under different types of load spectra. It is shown that the use of improvement techniques on welds subjected to spectrum loading may allow an increase in admissible stresses (=design stresses). This increase is found to be larger for higher strength steels. Hence, even under spectrum loading it may become possible to utilise higher strength steels, if the proper post weld treatment is carried out. The tolerance boxes for such procedures need to be further defined within a larger cooperative effort, preferably of international level. Hence, the data shown below should not be taken as design data even if the trends shown certainly are expected to be accurate.

MATERIALS AND TESTING

The materials used in this investigation have yield strengths 350, 590, 700 and 900 MPa. These steel grades include two (HSLA-steels) cold forming DOMEX 350YP and 590XPE and two quenched and tempered steels WELDOX 700 and 900. Their strength properties and chemical compositions are shown in Table 1. For further details, see Ref. (2).

Fatigue testing was performed on a specimen with a longitudinal fillet welded attachment, Lopez Martinez and Blom (2), which was also used in former investigations by Blom (3) and Bogren and Lopez Martinez (4). Both constant amplitude and variable amplitude testing were carried out. The spectrum type is the same as used earlier (5), SP2 (R=0-0.9) and SP3 (R=-1),

TABLE 1- Chemical compositions and tensile properties of steels

Chemical composition (wt%)							Yield strength (MPa)	Tensile strength (MPa)	Nominal strength (MPa)
C	Si	Mn	P	S	Al	Nb			
0.06	0.02	0.62	0.009	0.01	0.042	0.014	398	503	350
0.09	0.21	1.63	0.11	0.02	0.03	0.024	615	747	590
0.15	0.44	1.32	0.012	0.002	0.099	0.060	780	850	700
0.17	0.22	1.40	0.020	0.003	0.060	0.030	900	1010	900

which is a straight line range-pair counted spectrum and with irregularity factor I=1.0. The block length is 500 000 load cycles. The spectrum tests were carried out at ABB Corporate Research, The Aeronautical Research Institute of Sweden (FFA) and the Royal Institute of Technology (KTH) (Dept of Lightweight Structures) while the constant amplitude tests were performed at SSAB (Borlänge).

The thickness of the specimens was 12 mm, width 80 mm and length 650 mm. The attachment was 12 mm thick, 50 mm high and had 150 mm length. This specimen is classified as FAT 71 according to IIW Recommendations (6).

WELDING PROCEDURES AND IMPROVEMENT TECHNIQUES

Weld parameters

The welding procedure was the same for all steels tested, i.e. MAG with 1.6 mm electrode, current 185 Amp (DC), voltage 23.5 and heat input approximately 1.5 kJ/mm with consumable PZ 6130 (Mison 25) without preheating. The welds on the sides of the stiffeners as well as at the corners have been produced in an alternating diagonal sequence in order to limit the interpass temperature (<250° C). The same welder has manufactured all test specimens. No root treatment or weld preparation for the series has been utilised except for the hammer peening series where full penetration welds were used to get the same failure mode as for the rest of the series. As the same filler metal has been used for all steels tested, a degree of mismatch may be present as far as residual stresses are concerned. This may influence the fatigue results, especially the tests run with constant amplitude, but would probably be of minor influence for tests run with variable amplitude.

TIG-dressing parameters

The parameters used for the TIG-dressing technique are based on earlier experience within SSAB (Oxelösund) and the IIW Recommendations, Haagensen and Maddox (7). The angle of application of the TIG-electrode was 90° and distance to the plate material was held at 2-2.5 mm during remelting and the distance to the weld toe was max 1.5 mm, see Lopez Martinez and Blom (2). The diameter of the electrode was 2.4 mm and the gas (Argon) flow rate 12 l/min, the current 156 Amp and voltage 14.8 Volts giving a heat input of 1.4 kJ/mm.

Hammer peening parameters

The hammer peening was performed at TWI, United Kingdom. All specimens were hammer peened using a lightweigth pneumatic hammer, 'Atlas Copco RRD57' normally sold as a chipping tool. A round-tipped tool with 6 mm diameter was used throughout. The hammer and the particular tool used in the present project are shown in Manteghi (8). The tool is normally sold as a descaling chisel, but its tip was blunted to produce a round tip of the required diameter for use in hammer peening. The hammer peening equipment was capable of delivering 31 blows per second and needed air supply of 620 kPa. The air consumption was 9.5 lit/sec. The angle and position of the tool relative to the weld toe were as illustrated in Ref. (8). The majority of specimens received four passes of hammer peening. This is the number of passes adopted in most known previous investigations. However, lighter, vibration damped hammer guns should facilitate slower travel speeds, and hence more thorough treatment per pass. Indeed, the equipment used in the present project was much lighter, weighing 3.4 kg only, and thus easier to handle than the pneumatic or electrical rotary hammers normally used.

Shot peening parameters

The shot peening was performed at the industrial blast cleaning facility at Volvo Construction Equipment Eskilstuna plant. The Almen intensity for this equipment corresponds to 8-10. The equipment uses cut-wire as cleaning medium. The cut-wire is continuously replaced, so that always at least 60% of the used cut-wire is sharp enough to obtain an acceptable cleaning result in the stipulated time. The normal time for such blast cleaning process is approx. 5-10 minutes which gives a plastically deformed layer of 1/5 to 1/3 mm thickness. This is depending of the steel yield level as well as variation in Almen intensity.

Ultrasonic peening parameters

The ultrasonic shot peening was performed at Paton Electric Welding Institute, Ukraine. A compact hand tool with a multicomponent working element is employed for ultrasonic impact treatment. The tool comprises a magnetostriction transducer, a wave guide and a holder with striking needles. A semiconducting ultrasonic generator is used as a power supply for the tool. The treatment deforms the surface in the region of interest (i.e. weld toe) by the needles oscillating at ultrasonic frequencies.

TABLE 2- Specifications for ultrasonic impact treatment , Ref. (9)

Tool for Ultrasonic impact treatment	
Rated watt consumption	600-900W
Operation frequency of oscillation system	25-28 kHz
Bias current	15A
Oscillation amplitude of wave guide edge	25-30 mkm
Treatment speed in manual mode	0,3-0,7 m/min
Overall dimensions of manual tool	455x180x75 mm
Manual tool's weight	3,5 kg
Tool's axial clamping force	20-40 N
Cooling	Liquid
Needle diameter	2-5 mm
Ultrasonic generator	
Output power	600-1200 V
Main voltage	220, 380 V
Supply frequency	50 Hz
Operational frequency range	25-30 Hz

RESULTS

Evaluation of equivalent stress

One way to compare constant and variable amplitude fatigue test results is to represent the stress range in the spectrum by an equivalent stress. For as-welded (AW) joints it has been demonstrated in many investigations that this stress can be calculated using the Palmgren-Miner fatigue damage accumulation rule and a linear Basquin type of S-N curve with slope m. For AW condition the slope m is determined to be 3 based on regression analysis of constant amplitude tests. However, for improved welds a steeper slope (m>3) is to be expected due to the increased period of crack initiation and the residual stresses. For all improved test series in this investigation, the equivalent stress is determined with exponent m=3, and the results are plotted as equivalent stress range as function of number of cycles to complete fracture of the specimen. Further, the regression analyses have been performed with all data (including run-outs) due to few data. This is still a conservativeapproach.

Evaluation of degree of improvement

The data sets are presented both graphically and numerically by calculation of improvement effect by comparing each data point with that of the mean regression curve shown on the graphs which is based on the AW condition of the 350-steel tested with constant amplitude and not on the regression line from each series. The motivation is that fatigue data of the AW condition for any steel is assumed to lie within that scatter band and any other tendency is due to randomness of the data. Also, any effect of the treatment of parent plate before welding is supposed to disappear by the improvement technique itself. We concentrate here on the effect of fatigue life improvement only for the variable amplitude tests as these have most original value.

Fatigue test results for As-welded condition

Figure 1 shows the as-welded data from the current investigation compared to data from the literature. The parallel straight lines shown in this graph is from regression analysis of constant amplitude tests on 350-steel, the mean line and the lower and upper lines with -2σ to $+2\sigma$ [σ=standard deviation] from the mean line.

It is seen that some of the data, especially the 590-data all lie at the lower limit whereas the data for the 700 and 900-steels lie on the upper limit of the

scatter band. The reason for this is not clearly understood but in the 590-steel it has been confirmed that the mill scale induces additional weld defects which are detrimental to the fatigue strength. This is shown in Figure 2 where 590-data are compared for specimens including the mill scale versus specimens that were blast cleaned.

DOMEX 350 steel TIG improved

Figure 3 shows results from TIG-dressed specimens, both CA and VA tests. The estimated regression line parameters for TIG (CA) are : log C=14.35 and m=3.66. The calculated improvement is only performed for the lower data points due to the large scatter and are shown in Table 3.

TABLE 3- Calculated improvement for TIG-remelted DOMEX 350 steel

Stress range (MPa)	Failure cycles	Calculated improvement
175.1	3.936E+05	1.147
175.1	3.322E+05	1.084
175.1	4.435E+05	1.194
87.6	3.840E+06	1.226
87.6	4.991E+06	1.338
62.5	1.252E+07	1.298
48.5	1.676E+07	1.109
48.5	1.552E+07	1.081
Mean improvement		1.185

DOMEX 590 steel TIG improved

Figure 4 shows results from TIG-dressed specimens, both CA and VA tests. The calculated improvement is shown in Table 4. Note the increase of the calculated improvement for this steel.

WELDOX 700 steel TIG improved

Figure 5 shows results from TIG-dressed specimens, both CA and VA tests. The calculated improvements are shown in Table 5.

TABLE 4- Calculated improvement for TIG-dressed DOMEX 590 steel

Stress range (MPa)	Failure cycles	Calculated improvement
129.8	1.812E+06	1.415
129.8	2.059E+06	1.477
110.3	5.486E+06	1.740
110.3	2.829E+06	1.395
90.9	1.213E+07	1.867
90.9	1.695E+06	0.969
64.9	9.637E+06	1.235
64.9	1.111E+07	1.295
Mean improvement		1.424

TABLE 5 - Calculated improvement for TIG-dressed WELDOX 700 steel

Stress range (MPa)	Failure cycles	Calculated improvement
133.1	3.827E+06	1.862
133.1	3.829E+06	1.862
113.1	1.309E+07	2.384
113.1	3.234E+07	1.496
93.2	4.249E+06	1.349
66.6	3.790E+07	1.999
66.6	9.272E+06	1.250
66.6	1.496E+07	1.466
66.0	8.830E+06	1.220
66.0	5.220E+07	2.206
55.9	5.317E+07	1.880
Mean improvement		1.725

WELDOX 900 steel TIG-dressed

Figure 6 shows results from TIG remelted specimens, both CA and VA tests. The calculated improvements are shown in Table 6.

TABLE 6- Calculated improvement for TIG-dressed WELDOX 900 steel

Stress range (MPa)	Failure cycles	Calculated improvement
169.3	1.585E+06	1.765
169.3	1.518E+06	1.740
112.9	5.050E+06	1.731
112.9	6.340E+06	1.868
112.9	8.640E+06	2.071
112.9	7.380E+06	1.965
112.9	6.170E+06	1.851
90.2	1.220E+07	1.857
90.2	2.884E+07	2.474
Mean improvement		1.893

Effect of shot peening

The effect of shot peening on specimens run with constant amplitude is illustrated in Figure 7. Shot peening has not given any significant effect on the fatigue strength for steels 350, 590 and 700.

Effect of hammer peening

The effect of hammer peening is also shown in Figure 7 for 350 and 700 steels. Too few data for the 350 steel were obtained until now. The effect measured as above for the 700 steel is a mean improvement of 1.714.

Effect of ultrasonic peening and the combination TIG and ultrasonic peening

The effect of ultrasonic peening is shown for steels 350 and 700 in Figure 8 and in Tables 7 and 8, respectively. The effect of the combination TIG and ultrasonic peening is shown for 900 steel in Figure 8 and in Table 9.

TABLE 7- Calculated improvement for ultrasonic peening for DOMEX 350

Stress range (MPa)	Failure cycles	Calculated improvement
360.0	9.610E+04	1.474
340.0	5.642E+04	1.166
290.0	4.100E+05	1.926
278.0	4.885E+05	1.958
190.0	2.000E+06	2.140
Mean improvement		1.733

TABLE 8- Calculated improvement for ultrasonic peening for WELDOX 700

Stress range (MPa)	Failure cycles	Calculated improvement
294.0	2.052E+05	1.550
247.0	4.030E+05	1.631
241.0	6.350E+05	1.851
225.0	6.530E+05	1.745
211.0	1.050E+06	1.918
200.0	1.405E+06	2.003
162.0	2.000E+06	1.825
Mean improvement		1.789

TABLE 9- Improvement for TIG and ultrasonic peening for WELDOX 900

Stress range (MPa)	Failure cycles	Calculated improvement
410	1.171E+05	1.793
375	1.540E+05	1.797
363	1.516E+05	1.731
330	3.500E+05	2.079
325	2.912E+05	1.926
303	5.510E+05	2.221
275	5.200E+05	1.977
259	8.241E+05	2.171
234	1.335E+06	2.304
220	1.830E+06	2.406
Mean improvement		2.041

DISCUSSION AND CONCLUSIONS

Influence of mill scale on fatigue properties

It was shown that non-removal of the mill scale for the 590 steel led to significantly worse fatigue properties than when a blast cleaning process was used to remove the mill scale. Similar results have also been obtained for other steels. It appears that the detrimental effect of mill scale is general and connected to the prevalence of more and/or larger initial flaws.

The effect of parent plate strength level for TIG-dressed specimens

The general effect of TIG-dressing is to improve the fatigue life of all tested specimens, both under constant amplitude and spectrum loading. This beneficial effect becomes larger for lower applied stress levels, i.e. at longer fatigue lives as well as for higher yield strength for parent plate.

The calculated improvement for 350 MPa steel is a 20% improvement both for CA and VA, for 590 MPa steel is 40% improvement, for 700 MPa steel the improvement is 70% and for 900 MPa steel the improvement is 90%. This shows a clear influence of parent plate yield strength. This is due to the improved weld shape, lower stress concentration and lower residual stress level after TIG-dressing.

Effect of different improvement tecniques

- Shot peening gave no or marginal effect for all steels studied.

- Hammer peening gave a mean improvement of 1.7 for the 700 steel.

- Ultrasonic peening gave a mean improvements of 1.7 and 1.8 for the 350 and the 700 steel, respectively.

- Ultrasonic peening combined with TIG-dressing gave a mean improvement of 2.0 for the 900 steel.

ACKNOWLEDGEMENT

This work was financially supported by NI (Nordic Industrial Foundation), NUTEK (Swedish National Board for Industrial and Technical Development, SSAB, ABB and FFA. The authors are indebted to Mr. Bengt Wahlstenius (FFA) and Mr. Sune Bodin (KTH) for performing the fatigue tests and Mr Tommy Linden (SSAB Oxelösund AB) for performing welding and TIG-dressing.

REFERENCES

(1) Lopez Martinez, L., Lin R., Wang, D. and Blom A. F. "Invstigation of Re sidual Stresses in As-Welded and TIG-dressed Specimens subjected to Static/Spectrum Loading" This Conference.

(2) Lopez Martinez, L., Blom A. F. "Influence of spectrum loading on the fatigue strength of improved weldments", To be presented at the Int. Conf. Performance of dynamically loaded welded structures, 1997, 14-15 July, San Francisco, Am. Welding Society.

(3) Blom, A.F. "Fatigue strength of welded joints subjected to spectrum loading", Scand. J. Metall. 1979, 18, pp. 181-184.

(4) Bogren, J., Lopez Martinez, L. "Spectrum fatigue testing and residual stress measurements on non-load carrying fillet welded test specimens, in Blom, A.F. (ed.), "Fatigue under Spectrum Loading and in Corrosive Environments", EMAS Ltd, Warley, UK, 1993, pp 77-90.

(5) Blom, A. F. "Spectrum Fatigue Behaviour of Welded Joints", Int. J. Fa tigue, 1995, 17, pp. 485-491.

(6) Hobbacher A., Fatigue design of welded joints and components, IIW Doc. XIII-1539-96/XV-845-96, Abington Publishing, Abington Hall, Abington, Cambridge CB1 6AH, England.

(7) Haagensen P.J. and Maddox S.J., Specifications for weld toe Improve ment by Burr Grinding, TIG-dressing and Hammer Peening for trans verse Welds, IIW, Doc. No. XIII-WG2-46-95.

(8) Manteghi S., "The Application of Fatigue Life Improvement Tech niques". TWI Report 5635/5A/96.

(9) Statnikov E. Sh., Trufyakov V.I., Mikheev P.P. and Kudryavtsev Y.F., Specifications for Weld toe Improvement by Ultrasonic Impact Treat ment, IIW Doc. XIII-1617-96

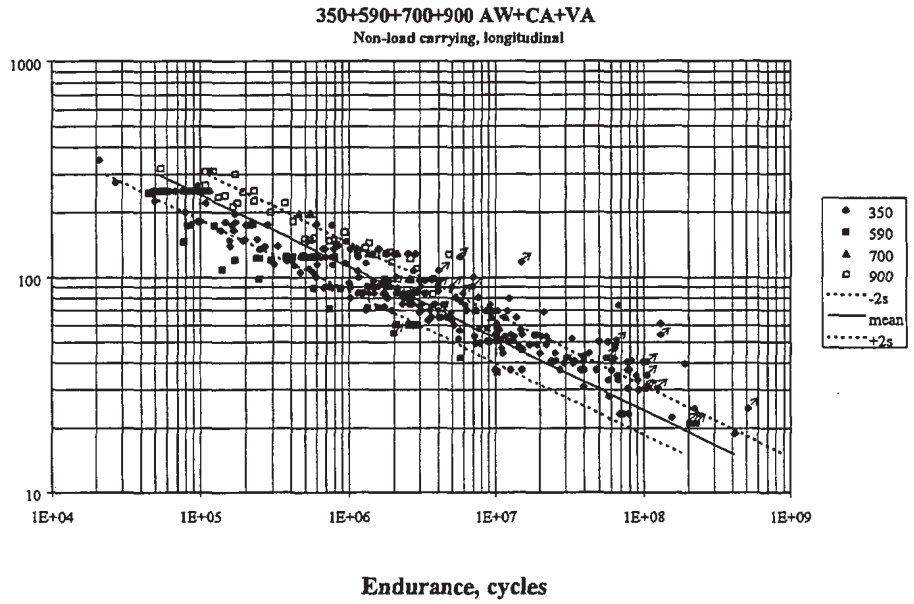

Figure 1 Summary of CA and VA tests on as welded non-load carrying, longitudi nally stiffened welded joint specimen, current data compared to literature

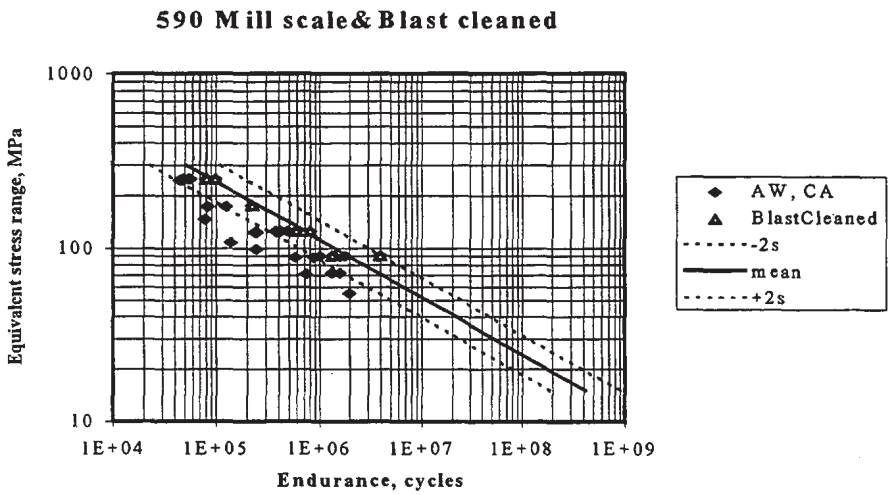

Figure 2 Effect of pre-treatment (sand-blasting) on fatigue behaviour of 590 steel

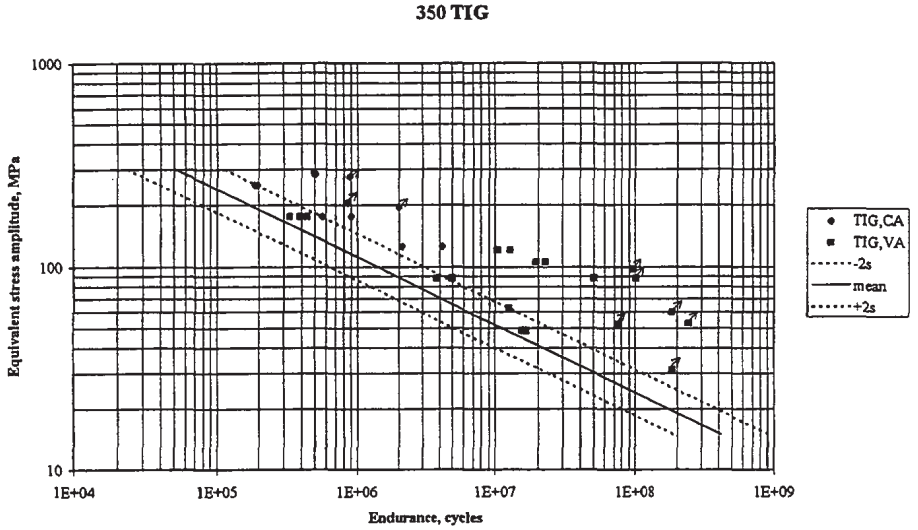

Figure 3 TIG remelted 350 steel results, constant amplitude and variable amplitude tests compared to the reference scatter band

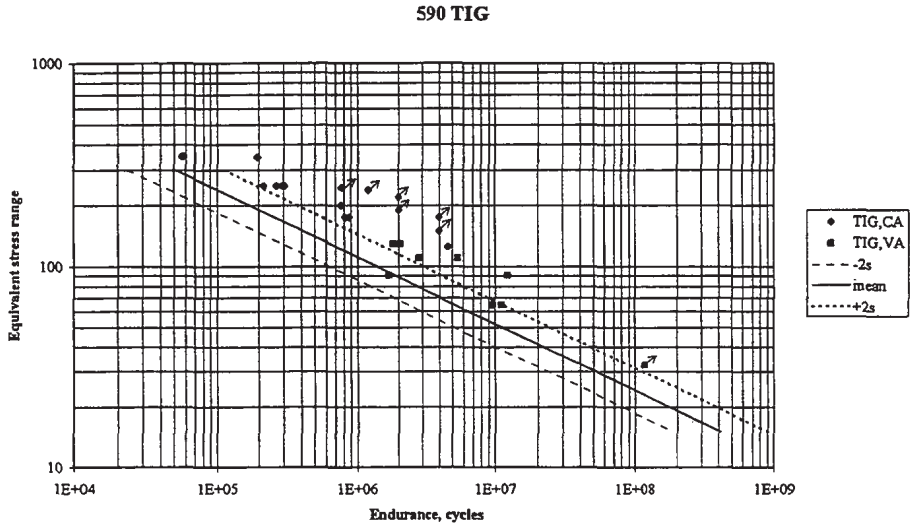

Figure 4 TIG remelted 590 steel results, constant amplitude and variable amplitude tests compared to the reference scatter band

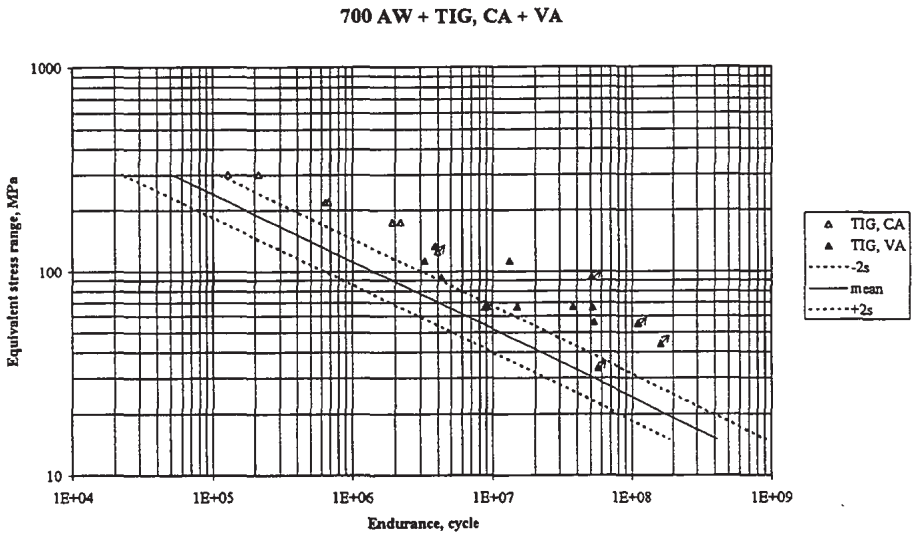

Figure 5 TIG remelted 700 steel results, constant amplitude and variable am plitude tests compared to the reference scatter band

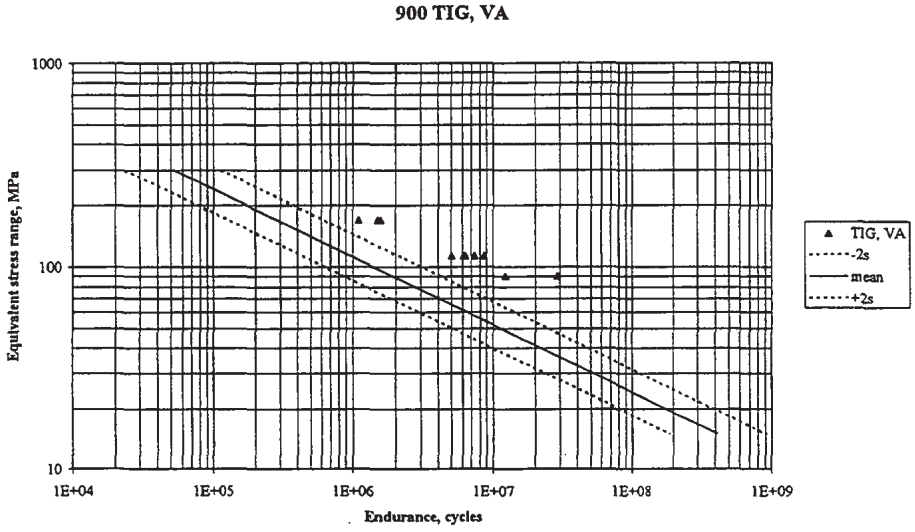

Figure 6 TIG remelted 900 steel results, constant amplitude and variable am plitude tests compared to the reference scatter band

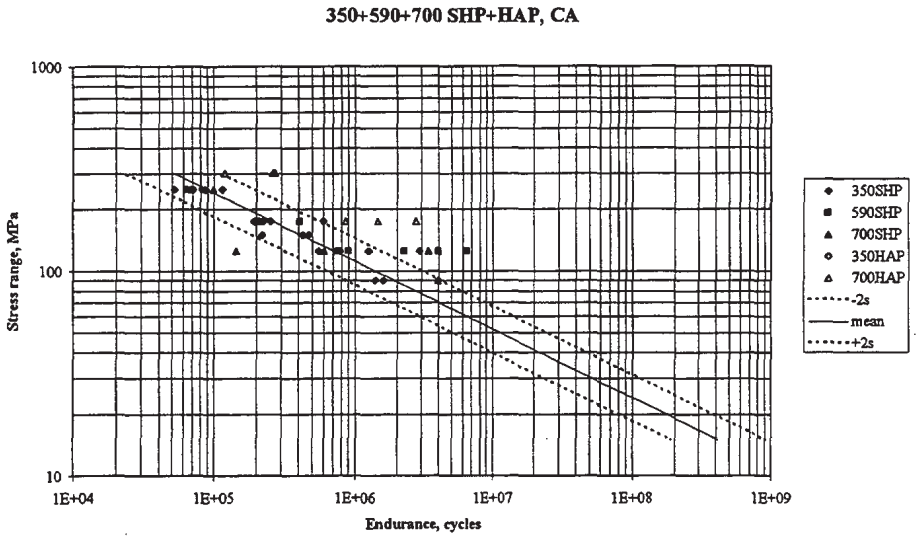

Figure 7 Effect of shot peening and hammer peening on steels 350, 590, 700 and 900 on specimens run at constant amplitude

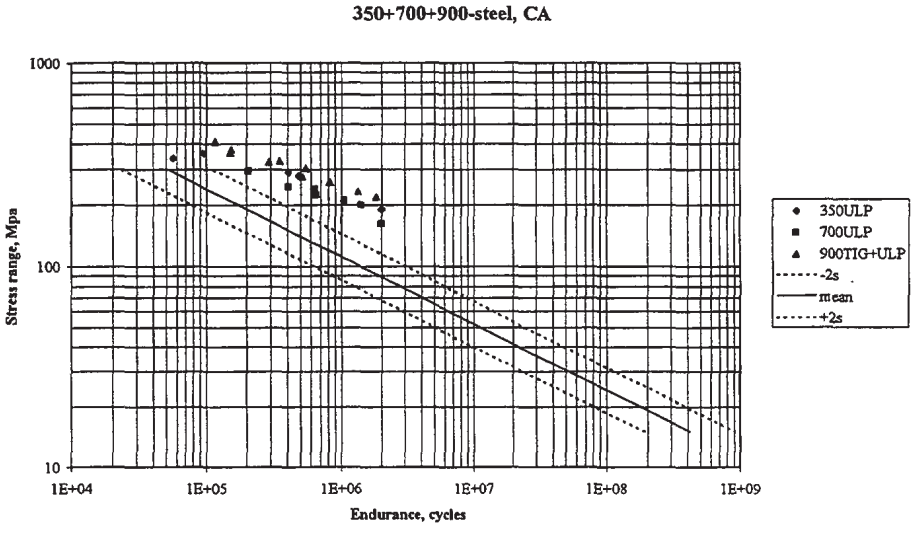

Figure 8 The effect of ultrasonic peening on steels 350, 700 and the combination of TIG and ultrasonic peening on 900 steel on specimens run with con stant amplitude

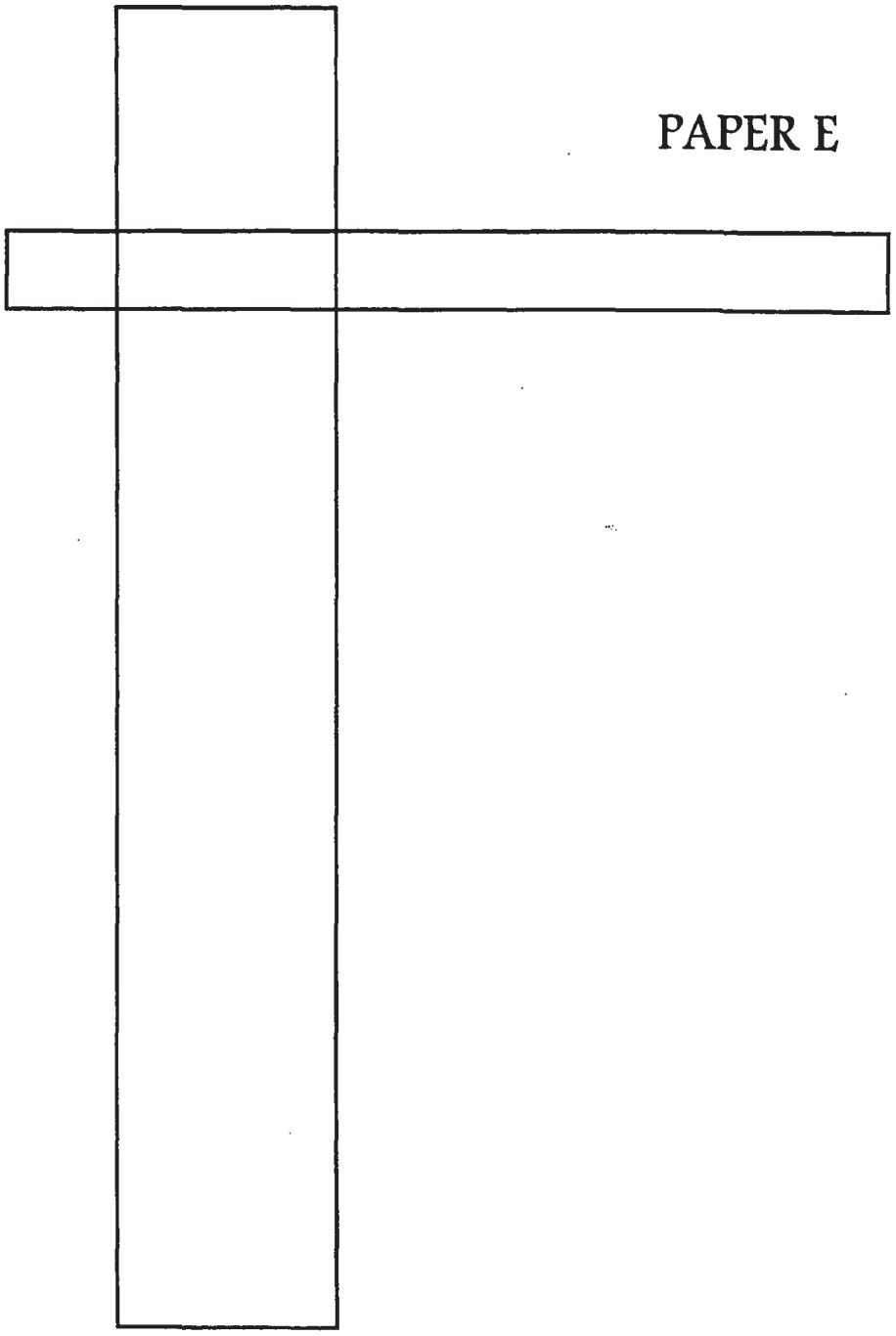

PAPER E

FRACTURE MECHANICS MODELLING OF FCG IN WELDED JOINTS

G. S. WANG[1], A. F. BLOM[1,2], and L. LOPEZ MARTINEZ[2,3]

This paper summarises the fatigue crack growth analysis part of a larger investigation on spectrum fatigue behaviour of non-load carrying fillet weldments of different strengths. The fatigue crack growth analysis is based on the weight function technique and the strip yield crack growth method so that the fatigue crack growth in the complex joint configuration can be analysed when the effect of residual stress is considered. The total test programme is aimed at assessing the influence of weld quality with related defects, material strength, thickness, load spectrum variation and residual stress relaxation on the overall fatigue behaviour of the welded test specimens. Here, we present results obtained on two high strength steels in both the as-welded and TIG-dressed conditions. These results are then compared to experimental results under both constant and spectrum load conditions.

INTRODUCTION

Fatigue of welded joints is basically regulated by various codes. Still, these codes treat neither spectrum loading nor post weld treatments in any detail. Yet, almost all engineering components and structures are subjected to spectrum loading during their service lives. There is currently a strong demand for utilising higher strength steels in many welded applications because of static strength requirements. However, welding always introduces initial defects removing the time for crack initiation. Fatigue crack growth is essentially independent of material strength and therefore there is no beneficial effect of using high strength steels in fatigue loaded applications. The only remedy to this is to apply post weld treatments in order to increase the fatigue lives of high strength steels. The main challenge is currently to combine such beneficial post weld treatment with general spectrum loading.

This paper summarises the crack growth analysis part of the fatigue testing programme being performed in the present inter-Nordic study. Experimental

[1]The Aeronautical Research Institute of Sweden (FFA)
P.O. Box 11021, S-16111 Bromma, Sweden
[2]The Royal Institute of Technology; S-100 44 Stockholm, Sweden
[3]SSAB Oxelösund AB, S-613 80 Oxelösund, Sweden

results are shown for DOMEX 590XPE, a cold forming HSLA-steel, both in the as-welded and the TIG-dressed conditions, and an even higher strength steel WELDOX 700, also in as-welded and TIG dressed conditions. Testing was performed both under constant amplitude and spectrum loading. Residual stress measurements were systematically performed by means of X-ray diffraction and neutron diffraction methods to determine initial distributions and their relaxation on both the surface of specimens and in the thickness under both static load and after various periods of spectrum loading. Specifically, this paper addresses fracture mechanics modelling of certain chosen experimental combinations of the parameters involved. This modelling is done in order to quantify the influence of the various parameters involved on the overall fatigue behaviour under complex loading. The model accounts for local stress concentration, residual stress distributions, residual stress relaxation, applied stress levels, spectrum shape and the weld-induced defect distribution.

EXPERIMENTAL PROCEDURE AND TEST RESULTS

Material and Test Specimens

The mechanical properties of DOMEX 590XPE are: R_{eh} = 615 MPa, R_m = 747 MPa, A_5 = 31%. The mechanical properties of WELDOX 700 are : R_{eh} = 780 MPa, R_m = 850 MPa. Chemical composition and further information of these two materials have already been presented [1, 2].

All experimental results presented in this paper are obtained on non-load carrying fillet weld fatigue test specimens. These are shaped as a plate, 80x700 mm, containing a flange on each side, 140x40 mm, MAG-welded by a one pass fillet weld, with no weld preparation. In this study we consider only the as-welded and the TIG-dressed conditions. The same welder has manufactured all the test specimens for all the test series at SSAB Oxelösund AB Laboratories, in order to keep the scatter of weld- and TIG-dressing quality under a controlled level. Weld- and TIG-parameters are given in Refs [1, 2].

Fatigue Testing

Fatigue testing includes constant amplitude and spectrum loading. The spectrum is a randomised sequence created within each block of 500 000 cycles by employing a draw without replacement routine. The blocks were repeated without reseed until fracture occurred. This gives an entirely randomised sequence until failure. The spectrum used, SP2, was previously used for similar testing together with other spectra with similar but different parameters [3]. SP2 is shown in Figure 1 and has a mean stress equal to 0.5 σ_{max}, a stress ratio $0<R<0.9$ and an irregularity factor equal to one.

Residual Stress Measurements

Both X-ray diffraction and neutron diffraction methods have been used to measure the residual stresses at the toe of the weldment. The technique used for measuring residual stresses on the surface of the specimen was X-ray diffraction while the residual stress in depth is measured using the neutron diffraction method. For the neutron diffraction measurement, the incident slit which defines the size of incoming neutron beam was 2 mm wide and 2 mm high. With a receiving slit of 2 mm wide, spatial resolutions in all three directions are approximately 2 mm. The locations of measurement are basically determined by the experimental crack initiation locations which are usually at the fusion line. In the case of the TIG-dressed specimens it is very difficult to define the exact location of the fusion line. Therefore we have decided to measure the distance from the flange end. The locations of longitudinal measurement points were in the symmetry plane at 13 mm (estimated weld toe region), 23 mm, 33 mm and 63 mm from the flange.

Measurements across the specimen width were all located 13 mm ahead of the flange. They were performed at 0 mm, 6 mm, 12 mm and 24 mm in the transverse direction on each side of the symmetry line. The radiated area was approximately 4x6 mm. In all cases the longitudinal stress component was measured. In order to study residual stress relaxation, testing was interrupted at various predetermined no. of load cycles at which the specimens were removed and subjected to X-ray diffraction and neutron diffraction measurements before testing was continued. This was done several times during the fatigue loading of each specimen. In addition, one specimen for each material has been statically loaded to the maximum load level that occurs in the spectrum load to investigate its effect on the residual stress relaxation and compare to the residual stress relaxation due to fatigue loading. Experimental results are shown below together with computed results.

Results of Fatigue Testing

The results of fatigue testing are presented in Figures 2 and 3. Constant amplitude data include as-welded conditions (mill scale and blast cleaned plate surface) as well as TIG-dressed condition, always with mill scale. In Figure 3 fatigue lives are plotted both versus maximum stress in the load spectrum and also versus equivalent stress. For definition of equivalent stress, see e.g. Ref. [3]. Spectrum data show the beneficial effect of TIG-dressing. Also shown in Figs 2 and 3 are computed model predictions (designated CMP in the figues). These are further discussed below.

NUMERICAL MODELLING

The present modelling of welding induced residual stress fields is mainly based on the finite element stress analysis, the residual stress measurement, the baseline fatigue crack growth rate data for standardised specimens under constant amplitude loading, and an elastic-plastic crack closure fatigue crack propagation

analysis model [4, 5]. The influence of the residual stress fields on fatigue crack growth is accounted for by a residual stress intensity factor concept. Such stress intensity factors are determined by the residual stress distributions at the crack site using a 3D weight function method [6] based on the residual stress in the crack growth planes.

The analysis involves not only the residual stresses for as-welded or the TIG dressed condition. It involves also the relaxation due to the fatigue loading. In the analysis of the fatigue crack growth, the residual stress intensity factor represents the influence of residual stress fields on the crack growth quantitatively, and will be added to the stress intensity factors caused by the cyclic loading. The redistribution of residual stress fields is accounted for by the procedure of calculating the residual stress intensity factors using the superposition principle of linear elasticity under elastic considerations [7]. Crack tip plastic deformation under both applied load and residual stress is accounted for in the elastic-plastic crack growth analysis model.

The numerical model used to predict fatigue crack propagation is a strip yield model based on Dugdale-Barenblatt assumptions but extended to leave plastically deformed material in the wake of the extending crack tip due to both fatigue crack growth and the weld induced residual stresses. This model was previously developed and was shown to be applicable both for plane stress and plane strain conditions by incorporating a variable constraint factor [4]. A constraint factor $\alpha = 2$ was used for the material of steels in the crack growth analysis model, based on comparison with elastic-plastic FEM calculations [8], to account for the three dimensional effect at the crack tip essentially leading to plain strain conditions.

Elastic Stress Distributions

Finite element 3D solid models have been created both for the as-welded specimen and the TIG- dressed specimen to analyse the stress distributions in the weld toe region. 20 noded isoparametric brick elements were used to achieve good accuracy in the stress results. One eighth of the specimen has been modelled due to the symmetry. Very small elements were created near the toe of the weld to account for the dramatic stress concentrations, especially for the as-welded specimens. The finite element models are shown in Fig.4.

The weld toe radii were obtained from measurements on several specimens and average values of 0.14 mm obtained for the as-weld specimens, and 7.0 mm for the TIG dressed specimens, respectively. The finite element analysis is based on linear elasticity. The computations reveal such high local stresses that plastic deformation will occur for most of the load levels applied in the testing, especially for the specimens in the as-welded condition.

For the fatigue crack growth analysis, the most critical location is at the stress concentrations where the crack can be initiated under cyclic loading. The finite element stress analysis shows consistently good agreement between the

highest stress concentration locations and the experimental crack initiation locations, see the insert shown in Fig.5. The finite element analysis shows that the local stress concentration for the crack is very high at the toe, with a stress concentration factor of around 5.8. The stress concentration, however, decreases rapidly in depth, see the open square symbols shown in Fig.5. There is, however, a significant area on the surface of the specimen near the toe with the high stress concentration, indicating a possibility of multiple crack initiations in a relatively large area.

This particular stress distribution shows that considerable error may be introduced in the analysis of fatigue life if a surface stress based methodology such as the "hot spot method" is used to analyse the fatigue life since the stress concentration is basically on the surface. Cracks can be rapidly initiated in such a high stress concentration area so that the main fatigue life may be determined by the crack growth life. Only the crack growth based methodology can be used to reasonably analyse the fatigue life of such joints. It is therefore considered that the fracture mechanics based crack growth analysis methods may be the best way to analyse the fatigue life of the welded joints.

The stress concentration can be effectively reduced by the TIG dressing technique as the finite element analysis results in Fig.5 show. The stress concentration has been dramatically reduced from 5.8 to about 1.6 after the TIG dressing treatment. In addition, the change of stress through the thickness becomes much more smooth, see the results shown in Fig.5b. The reduction in the stress concentration for the TIG dressed specimen is mainly due the change of configuration at the toe with a now much larger radius on the fusion line along the weldment near the global stress concentration area.

Residual Stress Distributions

Normally, it is assumed that weld induced residual stresses in fillet weldment reach yield stress levels at the actual weld toe. The X-ray diffraction measurements along the longitudinal line are shown in Fig.6 as triangles for as-welded specimens. The longitudinal residual stress increases near the toe (the left side of the figure). The results shown in the figure are for as-welded specimens of DOMEX 590XPE with a yield stress of 615 MPa. The trend shown in the figure indicates that the maximum residual stress in the as-welded state may reach or come close to the yield stress of the material at the fusion line.

The maximum measured residual stress is about 300 MPa at a distance of 13 mm from the flange. Experimental results reveal high values, albeit less than yield. This is probably due to the inability of the experimental technique to measure very close to the weld toe. As already mentioned, the local elastic stress concentration is high enough to cause local yielding under most of the fatigue loading. Together with residual stresses a plastic deformation will occur under applied load that leads to a redistribution of the initial residual stresses when the structure is unloaded.

Fig.6 shows also the X-ray diffraction measurements after various cycles of fatigue loading for the specimen with a maximum load of 180 MPa. The measurements are made before crack initiation so that the residual stress results represent the relaxation mainly due to the cyclic fatigue load instead of the crack growth process. The relaxation occurs mainly near the highest initial residual stress region which is close to the weld toe. There appears to be no major difference between the residual stress distributions after 100,000 and 500,000 cycles of fatigue load although they are quite different from the initial residual stress distribution.

A simple computation of residual stress relaxation can be made by assuming an elastic perfectly-plastic material constitutive behaviour with a flow stress of the average of the ultimate stress and yield stress, and that the plastic deformation changes only the local stress distribution. Together with the finite element analysis and the measurement of the initial residual stress, the relaxation of the residual stress can be computed based on the cyclic material behaviour shown on the left side of Fig.6. The analytical result is shown as a solid line in the right hand side of Fig.6. The analytical result shows a good agreement with the experimental result. The meaning of this comparison is very clear. The relaxation of residual stress under fatigue loading is mainly due to the plastic deformation under the peak fatigue load. Therefore, different stress levels may create different relaxation of residual stress for the same welded configuration.

Residual stresses through the thickness of the specimens are taken from ref. (9). In Figure 7, the longitudinal through-the-thickness distribution is shown at 13 mm away from the flange in the symmetrical plane. This location is the most possible place that a crack may be initiated. The stress in this location will be used in the fatigue crack growth analysis.

Within the range of accuracy for the neutron diffraction measurements, the results shown in Fig.7 indicate that stress relaxation occurs more strongly near the surface than in the interior of the specimen. 500,000 cycles create more stress relaxation than 200,000 cycles. For a depth of more than 2 mm, there is basically no difference in the residual stress for various load cycles and the initial condition. Therefore, the residual stress relaxation is a near surface phenomenon for the as welded specimens. Since significant fatigue life of the joints is consumed in the small crack growth region, the residual stress near the surface region should be analysed in detail.

As mentioned above, the relaxation of residual stress depends on the level of load. An example will be discussed based on the simple solution demonstrated in the results shown in Fig.6 for the residual stress on the surface of the specimen. The peak stress level is 250 MPa which is the same stress level as used in the spectrum loading. Fig. 8 shows the normal stress variation through the depth at the same position as in Fig. 7. The residual stress on the surface is an estimated value equal to the yield stress of the material. When the specimen is loaded, a high stress region appears near the surface. Using a perfect elastic plastic deformation relation to approximate the material constitutive relation schematically, as shown

in the left side of Fig.6, the residual stress relaxation following unloading can be computed. The result is shown in Fig. 9.

In this figure, the analytical results show that there is a significant relaxation of residual stress near the surface. Even after one single peak load only, the residual stress on the surface becomes compressive with a level near the compressive yield stress. Such a dramatic change of residual stress is due to the high stress concentration for the as-welded specimen. The results also indicate inefficiency in using mild surface treatments such as shot peening in improving the spectrum fatigue quality of the joint since their beneficial residual stress on the surface is meaningless for a residual stress already approaching the yield stress. The only beneficial effect of the shotpeening technique may be the improvement in the surface condition and the possible increase in the root radius at the weld toe which may somewhat reduce the local stress concentration at the toe. The analytical results compare favourably to the measurements for depths larger than 2 mm, confirming the reliability in the simple evaluation of the residual stress relaxation. The analytical result will be used in the analysis of fatigue crack growth and fatigue life of the as-welded joints.

For TIG-dressed specimens the residual stress distributions are quite different from those of the as-welded specimen, Ref. (9). In particular, the residual stress near the surface is rather low. There is almost no residual stress relaxation near the surface after either static load or fatigue loading up to 500,000 cycles.

Nevertheless, there is some extent of relaxation taking place in the region of about a quarter through the thickness due to the initial high residual stress in this region. The relaxation for the static load is still quite close to the relaxation of residual stress after 500,000 cycles, indicating that the relaxation of residual stress is still mainly due to the plastic deformation of the material. The plastic deformation now occurs beneath the surface of the specimen instead of on the surface like for the as-welded specimens, Ref. (9).

Using the finite element results shown in Fig.5 and the residual stress distribution for the initial condition, the longitudinal normal stress distribution is computed and shown in Fig.10. Under a load level of 250 MPa, the stress on the surface at the toe is about 400 MPa, which is lower than the yield stress. Therefore, there is no plastic deformation on the surface under this load. At a depth of between 2 mm to 4 mm, the normal stress level is higher than the yield stress under the load of 250 MPa, indicating that plastic deformation will occur in this region. The residual stress will consequently be considerably relaxed following unloading.

Again, the simple method discussed above is used to compute the stress relaxation and the numerical results are shown in Fig.11 together with the neutron diffraction measurements for both the static load and fatigue loading after different numer of cycles. The measurements show that the residual stress relaxation is a gradual process. The longer the specimen is subjected to fatigue load, the more the residual stress will be relaxed. The relaxation due to the static load is very close to the stabilised residual stress state after 200,000 load cycles.

The result from the simple model evaluation of residual stress is also quite close to the stabilised residual stress state.

The gradual relaxation of the residual stress may be explained by the rate of the application of the peak load. Under rapid loading, the material reaction is different from that of the slow static load, usually resulting in an increased yield stress. There needs to be many cycles of fatigue peak load before the material reaction is stabilised. The measured results show that the stabilised residual stress relaxation is rather close to the relaxation due to the static load. Very close estimation of the residual stress relaxation can be made even from the simple consideration of the plastic deformation due to the combined effect of applied stress and the initial residual stress distribution. Therefore, it is possible to analyse the fatigue crack growth in the joint under different load levels based on the finite element stress results and the initial residual stress results for both the as-welded and the TIG-dressed specimens. The numerical results will be presented in the following sections.

Computed Fatigue Crack Propagation

With the numerical model described above, fatigue crack growth is analysed for both constant amplitude and spectrum loading. The fatigue crack growth is based on the finite element stress analysis results, the residual stress measurements on the initial condition for both the as-welded specimens and the TIG-dressed specimens, and the residual stress relaxation based on the simple plastic deformation consideration for different stress levels. The fatigue crack growth analysis for WELDOX 700 is based on an effective crack growth Paris relation with the data based on constant amplitude loading with a high stress ratio. The crack growth rate is expressed as $da/dN = 8.97083 \times 10^{-12} \left(\Delta K_{eff}\right)^{2.882}$ $m/cycle$. ΔK_{eff} is Elber's effective stress intensity factor in MPa $\sqrt{m}$. The fatigue crack growth rate for DX 590 is expressed in tabulated form in Table I below:

Table I The crack growth rate for DOMEX 590

da/dN m/cycle	ΔKeff, MPa √m
9e-10	4.30
6.6e-9	9.10
2.6e-8	14.30
1.3e-7	21.13
6.3e-7	35.50

The crack growth analysis is firstly performed for the constant amplitude loading, with a stress ratio of R=0, for both the as-welded specimens and the TIG-dressed specimens of both WELDOX 700 and DOMEX 590 steels. The computations were started with an initial flaw size of 0.15 mm in depth with an aspect ratio of 1. This initial flaw size is in the order of the average experimentally observed initial flaws at the weld toe . The analytical results are shown in Fig.2 as piece-wise lines in the plot of experimental S-N curves.

The analytical results agrees rather well with the experimental results. The computations show that WELDOX 700 steel has a slightly better fatigue life than DOMEX 590 steel for the as-welded condition. However, this is not obvious from the experimental results. For high stress levels, the WELDOX 700 steel has generally slightly better fatigue life than the DOMEX 590 steel although it has a non-proportional higher static strength. However, for low stress levels and in the TIG-dressed specimens, both the experimental data and the numerical predictions show that DOMEX 590 steel have better fatigue life than WELDOX 700 steel. This change of fatigue life behaviour is probably mainly due to the better crack growth properties in the near-threshold region for the DOMEX 590 steel.

Despite of the compressive residual stress present on the surface at the weld toe after residual stress relaxation as shown in Fig. 9 for as-welded specimens, their fatigue lives are still significantly lower than those for the TIG-dressed specimens, revealing the importance of stress concentration on the fatigue lives. The fatigue life is mainly related to the range of stress, rather than the maximum value, at the crack concentration. The range is not effectively reduced by the compressive residual stress that can only reduce the stress ratio. For both WELDOX 700 and DOMEX 590, however, the crack growth rate seems not to be very much affected by the stress ratio. Therefore, a major means to increase fatigue life of welded joints seems to be by reducing the stress concentration at the weld toe.

Both the experimental results and the analytical/numerical results show quantitatively the same improvement for the TIG-dressed specimens for both steels. The analytical results show better agreement for DOMEX 590 steel than for WELDOX 700 steel, compared to the experimental results. This might be due to the much better baseline crack growth data used for the DOMEX 590 steel, shown in Table I, than the simple Paris type of crack growth rate relation used for WELDOX 700 steel. This is particularly important in the near-threshold area. Re-evaluation of data for WELDOX 700 steel may be needed in the future when better and more complete baseline crack growth data are available.

For more realistic situations involving both spectrum loading and various initial flaw size distributions, the fatigue life may vary significantly depending on both the load spectrum and the initial flaw. Analyses are therefore performed for the actual spectrum load with different initial flaw sizes. One example is shown in Fig.12 for the computed fatigue life of the TIG-dressed specimen under the load spectrum shown in Fig.1, SP2, and a similar spectrum used in previous investigations, e.g.Ref. [10], SP3, with a stress ratio R=-1 under the same peak stress level of 350 MPa. The fatigue life is shown as function of both the initial flaw size in the range of 0.1 to 1 mm, and the type of spectrum. This result shows that the fatigue life is less sensitive to the initial flaw size for the tension/compression spectrum while a significant dependence of the initial flaw size on the fatigue life is observed for the tensile dominated spectrum discussed in the present paper.

When comparing the fatigue life for both as-welded and TIG-dressed specimens under the present load spectrum , SP2, analytical results are shown in Fig.13 as function of initial flaw sizes in the range of 0.1 mm to 1 mm under a

lower stress level of 250 MPa. The fatigue life for the TIG-dressed specimens show much better fatigue life than the as-welded specimens. However, TIG-dressed specimens are much more sensitive to the initial flaw size than as-welded specimens. This is mainly due to the fact that a larger part of fatigue life is consumed within the smaller part of the crack size region. Such behaviour must be recognised when post weld treatment is to be used for applications.

A final comparison of predicted spectrum behaviour, SP2, is shown in Figure 14 for both as-welded and TIG-dressed specimens under two different stress levels. The most significant improvement in the fatigue life of TIG-dressed specimens is for small initial crack sizes. In this region the fatigue life curves, for as-welded versus TIG-dressed specimens, diverge. This is the same behaviour as already observed in the experimental fatigue life results shown in Figure 3. This clearly confirms the notion that life improvement by TIG-dressing is particularly relevant in the long life regime, where also the need may be most prevalent. We have earlier confirmed that initial flaw sizes become substantially smaller following TIG-dressing [1, 2].

DISCUSSION AND CONCLUSIONS

The general effect of TIG-dressing is to improve the fatigue life of all tested specimens, both under constant amplitude and spectrum loading. This beneficial effect becomes larger for lower applied stress levels, i.e. at longer fatigue lives.

Based on results from numerical modelling of fatigue crack propagation it is concluded that the largest effect of TIG-dressing is to significantly reduce the elastic stress concentration.

Since a significant initiation period appers to be prevalent after TIG-dressing an effect of material strength is becoming apparent even in the case of welded specimens, which is normally not the case.

Influence of residual stresses is quite large under constant amplitude loading, but rather insignificant under spectrum loading due to relaxation following large loads.

Initial flaw sizes were shown to not influence fatigue life strongly for a rather wide range of flaw sizes under constant amplitude loading, especially for as welded specimens. This may be confirmed from the rather small scatter in observed test results. However, for small flaw sizes under spectrum loading there is a strong effect, especially for the TIG dressed specimens. This effect becomes most obvious under low applied loads, i.e. at long fatigue lives. Again, this predicted result is confirmed from experimental results where the fatigue life curves for as-welded and TIG-dressed specimens diverge.

Since the fatigue life for TIG-dressed specimens under spectrum loading at low stress levels is very sensitive to the initial flaw size, it appears that any post weld treatment aimed for such conditions need to be very carefully applied.

ACKNOWLEDGEMENTS

Financial support from both NI, the Nordic Industrial Fund, and NUTEK, the Swedish National Board for Industrial and Technical Development is gratefully acknowledged.

REFERENCES

[1] Lopez Martinez, L. and Blom, A. F., Influence of life improvement techniques on different steel grades under fatigue loading, in Fatigue Design 95, Espoo, Finland, 1995.

[2] Lopez Martinez, L., Blom, A. F. and Wang, G. S., Fatigue behaviour of TIG improved welds, in Fatigue '96, Berlin, Germany, 1996.

[3] Blom, A. F., Spectrum fatigue behaviour of welded joints, Int. J. Fatigue, Vol. 17, No. 7, pp. 485-491, 1995.

[4] Wang, G. S. and Blom, A. F., A strip model for fatigue crack growth predictions under general load conditions, Engng. Fracture Mech. Vol. 40, No. 3, pp. 507-533, 1991.

[5] Wang, G. S., The plasticity aspect of fatigue crack growth, Engng. Fracture Mech. Vol. 46, No., pp. 909-930, 1993.

[6] Wang, G. S., A generalised WF solution for mode I 2D part-elliptical cracks, Engng. Frac. Mech. Vol. 45, No. 2, pp. 177-208, 1993.

[7] Wang, G. S. and Blom, A. F., Fatigue crack propagation in residual stress fields, 6th Int. Conf. on Mech. Behaviour of Materials, Vol. 4, pp. 627-632, Pergamon Press, 1991.

[8] Blom, A. F., Wang, G. S. and Chermahini, R. G., Comparison of crack closure results obtained by 3D elastic-plastic FEM and modified Dugdale model, in Localised Damage, Computational Mechanics Publications, Springerverlag, Berlin, 1990, Vol.2, pp. 57-68.

[9] Lopez Martinez, L., Lin, R., Wang, D., and Blom, A. F., Investigation of residual stresses in as-welded and TIG-dressed specimens subjected to static/spectrum loading, in these proceedings.

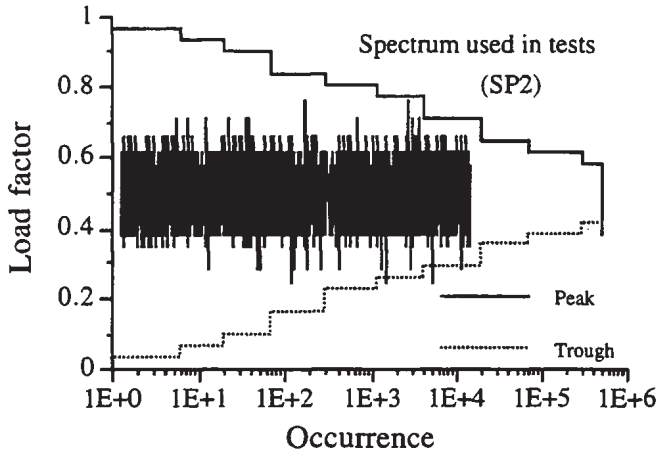

Fig. 1 Load spectrum exceedance distribution.

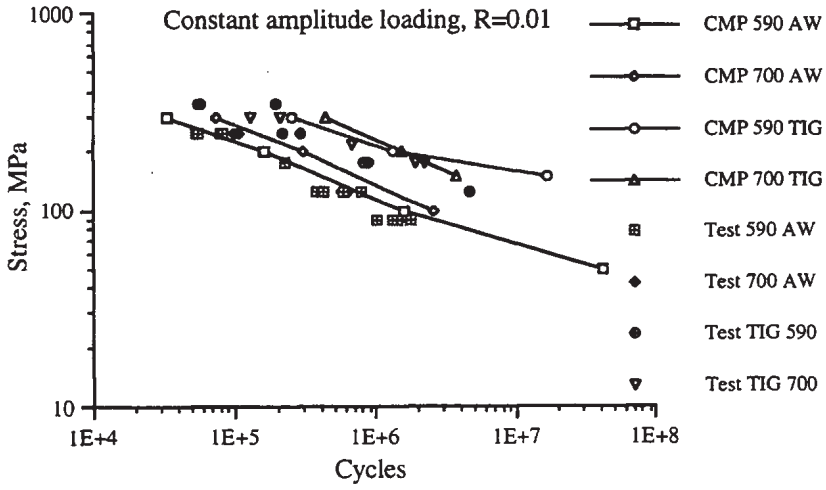

Fig. 2 Constant amplitude fatigue test results and computed model predictions (CMP)

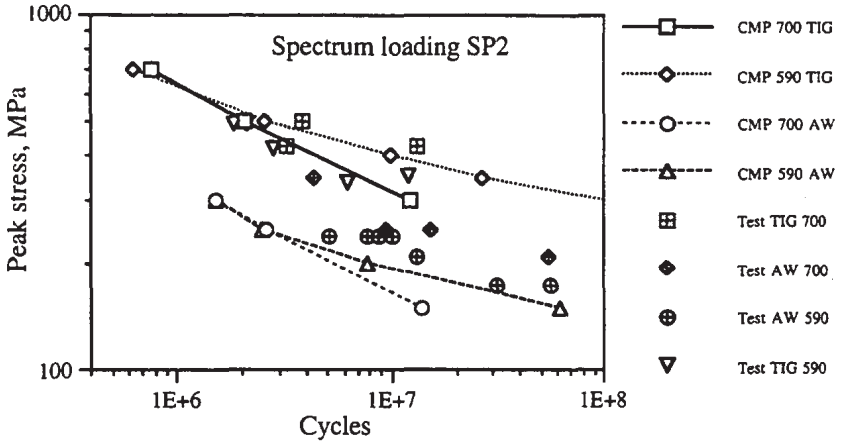

Fig. 3 Spectrum fatigue test results and computed model predictions (CMP)

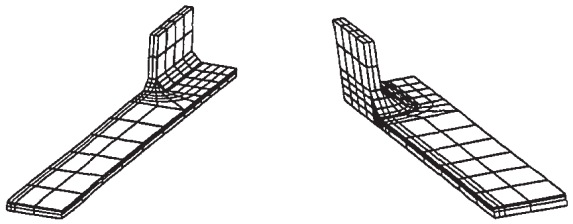

Fig.4 FEM model for as-welded and TIG-dressed specimens

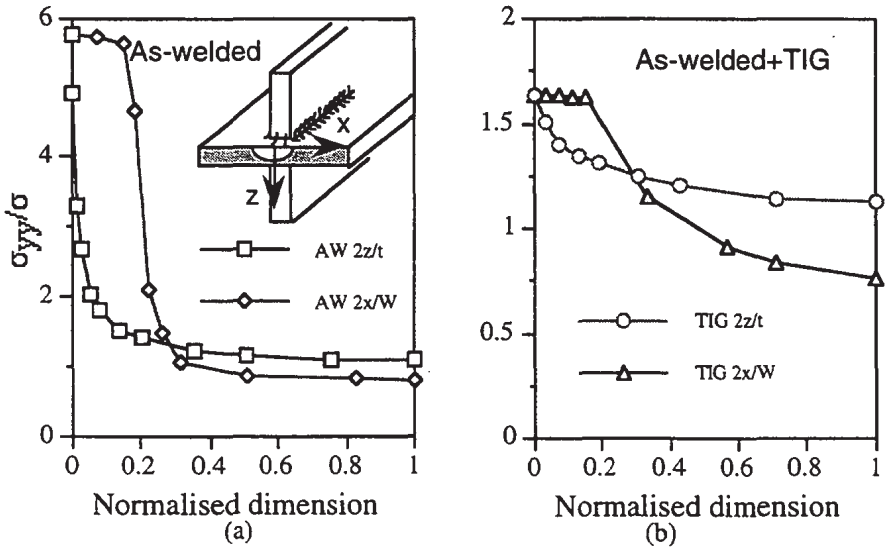

Fig.5 Finite element normal stress results at the crack growth plane

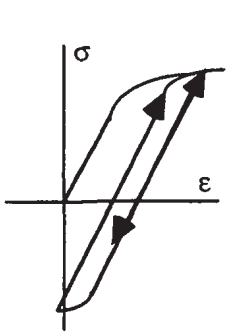

σ–ε Relation

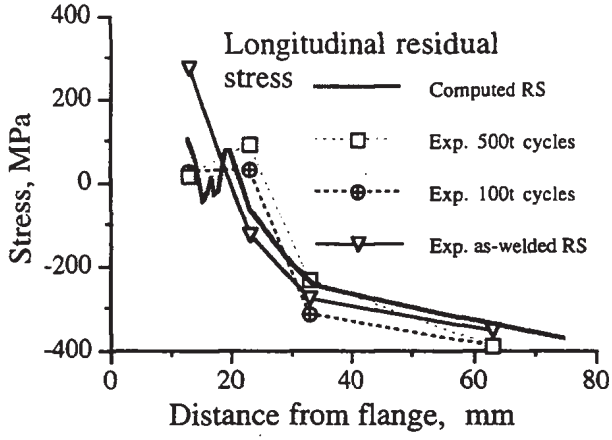

Fig. 6 Residual longitudinal normal stress in centre line ahead of flange. Comparison of measured results and computed redistributed stresses

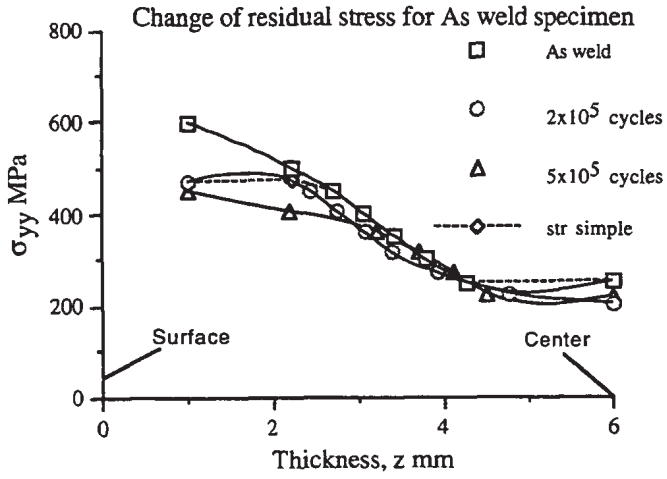

Fig.7 Through-the-thickness residual stresses for as-welded specimen

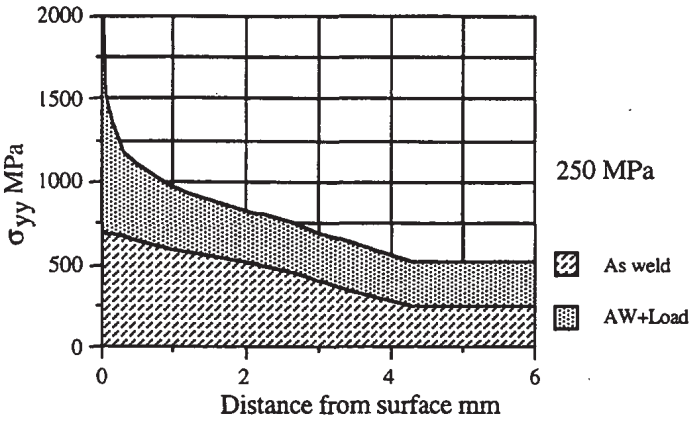

Fig. 8 Normal stress variation through the depth before and after applied load causing plastic deformation in as-welded specimen

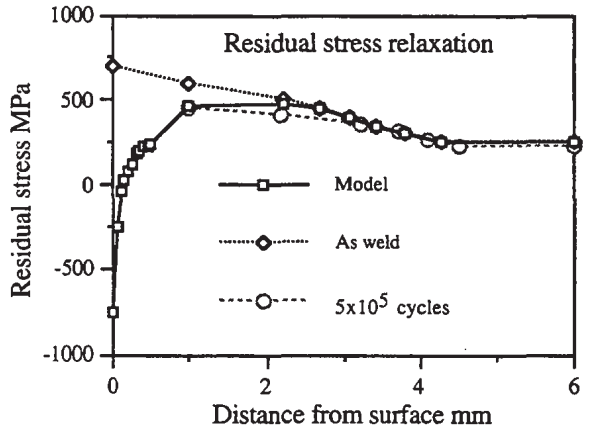

Fig. 9 Relaxation of residual stress due to applied load

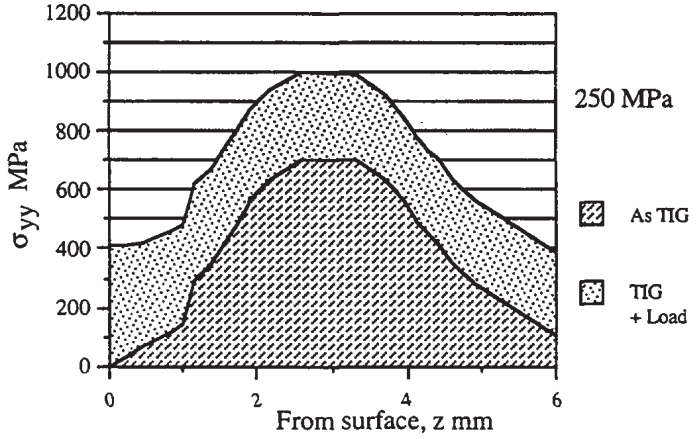

Fig.10 Normal stress variation through the depth before and after applied load causing plastic deformation in TIG-dressed specimen

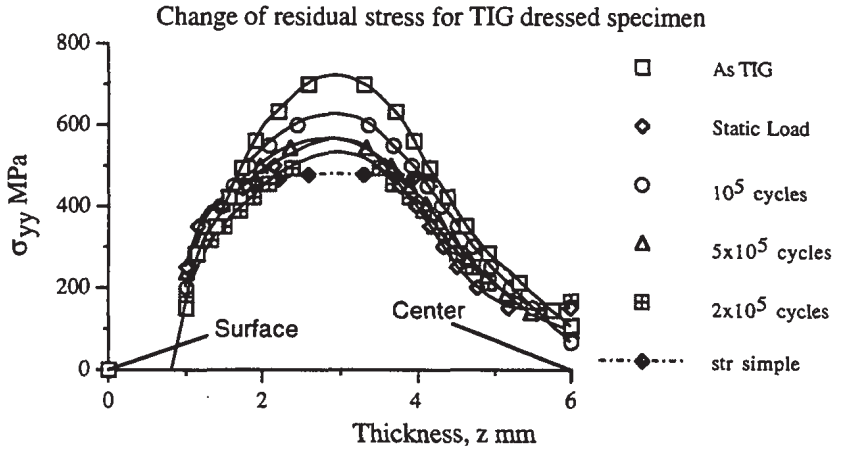

Fig.11 Comparison of through-the-thickness residual stresses for different conditions

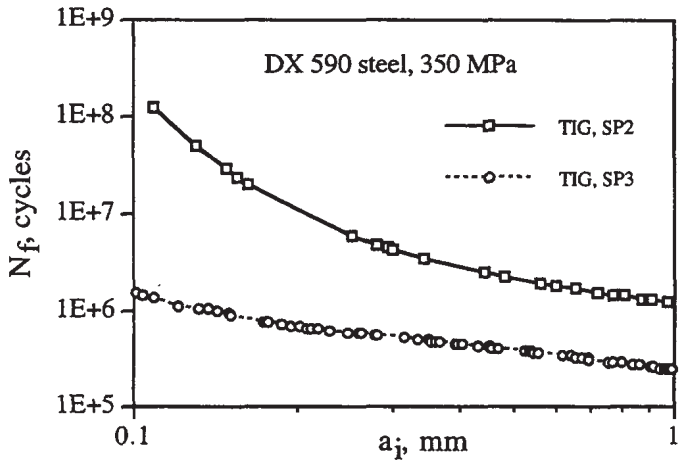

Fig.12 Influence of initial crack length on fatigue life of TIG-dressed specimens made of DOMEX 590 steel under different load spectra

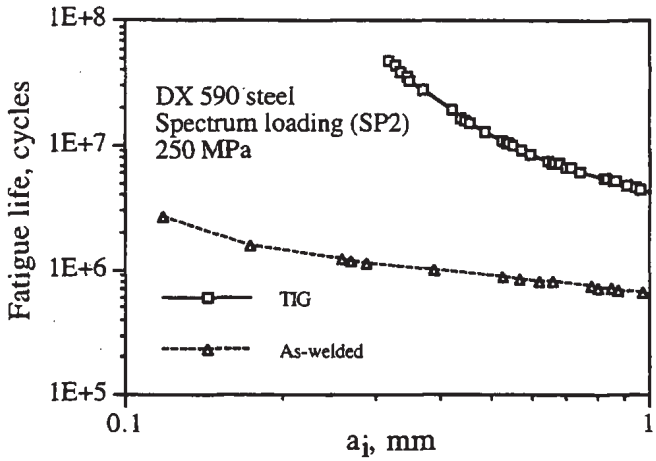

Fig.13 Fatigue life as a function of initial flaw sizes for as-welded and TIG-dressed specimens of DOMEX 590 steel

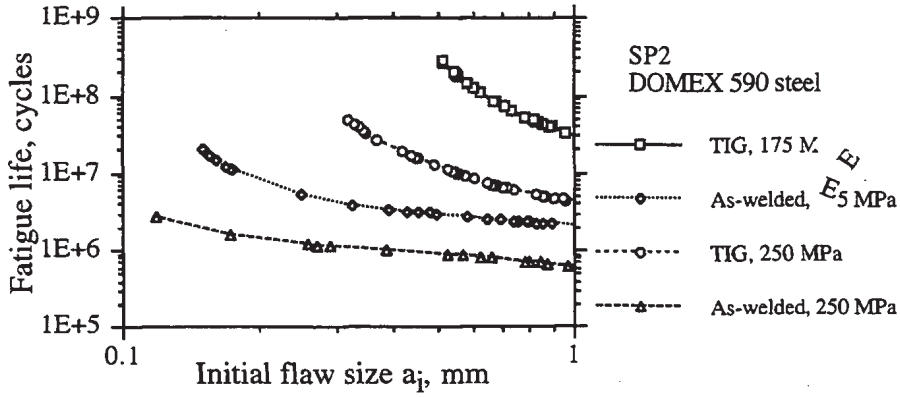

Fig. 14 Predicted spectrum crack growth life of DOMEX 590 under different load levels in both as-welded and TIG-dressed conditions